SCAFFOLDS WITH INTEGRATED PROPERTIES AND APPLICATIONS IN CELL TRANSPLANTATION

A Dissertation
Presented to
The Academic Faculty

by

Jinyang Wang

In Partial Fulfillment
of the Requirements for the Degree
Doctor of Philosophy in the
Department of Biomedical Engineering

Georgia Institute of Technology
Emory University
Peking University
August 2017

SCAFFOLDS WITH INTEGRATED PROPERTIES AND APPLICATIONS IN CELL TRANSPLANTATION

Approved by:

Prof. Ying Luo, Advisor
Department of Biomedical Engineering
Peking University

Prof. W. Robert Taylor
Department of Biomedical Engineering
Georgia Institute of Technology

Prof. Huaiqiu Zhu
Department of Biomedical Engineering
Peking University

Prof. Jincai Luo
Institute of Molecular Medicine
Peking University

Prof. Changhui Li
Department of Biomedical Engineering
Peking University

Date Approved: June 8, 2017

ACKNOWLEDGEMENTS

I would like to express my sincere thanks to my advisors Dr. Ying Luo and Dr. W. Robert Taylor for their guidance and help during my journey of pursuing the Ph.D. degree. They broadened my vision and taught me a lot not only in science, but in all aspects.

I would like to especially thank my mother, father and grandmother. They are my biggest support through these years.

I would like to thank Dr. Haifeng Chen in sharing us with electrospinning technique and PLGA polymers. I would like to thank Dr. Song Li for micropatterning techniques and PU polymers. I would like to thank Lili Du for her assistance in BLI experiments. I would also like to thank Dongwei Ma in assisting with the histology.

I would like to thank all my colleagues from both Beijing and Atlanta. I would like to thank Xiaopeng Liu, Jie liu, Bing Lv, Warran D. Gray, Liyang Jiang, Kai Wang, Ni Su, Fang Wang, Xi Wang, Penglai Gao, Wenda Hou and Yaoyao Hao from Luo lab; Alicia Lyle, Anita Saraf, Christa Ceasar, Daiana Weiss, Giji Joseph, Jane Titterington, Kiyoko Takemiya, Lizz Iffrig and Yanbo Liu from Atlanta. They offered me great help in the six years. I am gratitude to work with you.

I would like to thank my thesis committee members: Dr. Huaiqiu Zhu, Dr. Changhui Li and Dr. Jincai Luo for their time and advice, which help me a lot in finishing this thesis.

I would like to thank Dr. Cheng Zhu for setting up and running the joint program and Jialei Luo and Shannon Sullivan for their administrative contribution.

TABLE OF CONTENTS

LIST OF TABLES

LIST OF FIGURES

LIST OF SYMBOLS AND ABBREVIATIONS

RAFT	Reversible Additive Fragment Transfer
PEG	Polyethylene glycol
SMC	Smooth muscle cell
PCL	Polycaprolactone
MSC	Mesenchymal stem cell
ECM	Extracellular matrix
ESC	Embryonic stem cell
iPSC	Induced pluripotent stem cell
LV	Left ventricle
PLGA	Poly(lactic-co-glycolic acid)
PDMS	Polydimethylsiloxane
CTA	Chain transfer agent
NHS	N-hydroxysuccinimide
DMF	PEGDA
PEGDA	Polyethylene glycol diacrylate
AFM	Atomic force microscope
SEM	Scanning electron microscope
IACUC	Institutional Animal Care and Use Committees
FTIR	Fourier transform infrared spectroscopy
STD	Standard deviation
ADSC	Adipose tissue derived stem cells
FBGC	Foreign body giant cell
THF	Tetrahydrofuran
TPU	Thermoplastic silicone polycarbonate urethane

PCR	Polymerase chain reaction
HLI	Hind limb ischemia
DPBS	Dulbecco's phosphate-buffered saline
LDPI	Laser Doppler perfusion imaging
VEGF	Vascular endothelial growth factor
HGF	Hepatocyte growth factor
b-FGF	b-Fibroblast growth factor
BLI	Bioluminescence imaging
PES	Polyethersulfone
PVP	Polyvinylpyrrolidone
DMAC	Dimethylacetamide

SUMMARY

Scaffolds are biomaterials serve as substrates for cell attachment and provide microenvironments for cell growth. Though they were initially designed for *in vitro* tissue growing applications, they are gaining increasing importance in cell therapy, where they serve as delivery vehicles of cells to overcome the low cell retention and survival resulted from delivering cells alone. An ideal scaffold for cell therapy should be optimized in multiple properties, including mechanical property, biocompatibility and 3D structures. However, traditional scaffolds were limited by their materials and fabrication techniques that they can hardly optimize multiple properties at once. Therefore, in this dissertation① three novel scaffolds with integrated properties were represented and their applications in cell delivery were demonstrated.

Polyester microfibers and hydrogels are two most studied type of scaffolds. Polyester microfibers are hydrophobic. They have good mechanical property and fibrous porous structure. Hydrogels are water absorbable and usually have good compatibility. However, their application is often limited by weak mechanical strength. In the first part of this dissertation, a surface RAFT polymerization technique was developed and for the first time achieved nano-thin PEG hydrogel coating on PCL micro-fiber surface. This composite scaffold showed good macro-mechanical property and fibrous, porous structure like microfibers. Meanwhile, after integration of hydrogel, the hydrophobic scaffold became water-absorbable like hydrogels and showed improved biocompatibility. The method applied in this study could be transformed to other polyester scaffolds as well to make integrated materials.

Microtissues are more likely than single cells to undergo hypoxia induced necrosis and

apoptosis caused by clumping. Therefore, scaffolds for delivering microtissues should have the ability to regulate their spatial distribution. However, traditional scaffolds are usually designed to regulate cell microenvironments in nano to micro scale, such as electrospun fibers and hydrogels, and lack the ability of spatial regulation in higher magnitudes. Therefore, in the second part of this dissertation, a novel method for microtissue transplantation was demonstrated. Microwell patterns were introduced on surface of electrospun fibers through microfabrication technique. This microwell patterned electrospun fibers regulated the spatial distribution of MSC spheroids and maintained their improved paracrine function. MSC spheroids loaded microwell patterned scaffolds were further transplanted in mice with hind limb ischemia. Results showed that the microwell patterned scaffolds increased MSCs' retention and survival and improved the vascularization of ischemic tissues.

The interaction between host tissue and transplanted cells can be controlled by careful design of the scaffold structure and pore size. In the third part of this dissertation, a pore size controllable spherical hollow scaffold was designed for cell transplantation. Comparing with hydrogel beads, this novel spherical scaffold has a double layer spherical structure, better mechanical property and a wider control in pore size. MSCs can be injected inside the hollow core of scaffold for transplantation. The scaffold could improve MSCs' paracrine function and MSCs' retention could be controlled be different pore size of the scaffold surface.

CHAPTER 1. INTRODUCTION

1.1 Aims

Scaffolds are the biomaterials used in tissue engineering, where they function as substrates for cell attachment and provide biochemical and physical cues to establish microenvironments to support cell growth, differentiation and other functions[1-3]. With the rapid development in stem cell technology, besides the initial purpose of growing tissues, scaffolds have found new applications in cell therapy, where they serve as platforms for cell delivery with focusing on improving cell retention and survival[4, 5].

The *in vivo* performance of scaffold is dependent on various characteristics including mechanical properties, biocompatibility and micro, macro-architectures[6]. However, traditional scaffolds often have limited optimization of different properties, which limited their function and final application. Therefore, to fulfill the diverse requirements of scaffolds, integrative designs must be adopted.

The central hypothesis of this dissertation is that the judicious designs is able to develop scaffolds with integrated properties and functions, and the scaffolds with integrated properties could benefit cell retention and survival in cell transplantation. The central hypothesis was studied following three specific aims.

1.1.1 Specific aim 1

Development of scaffolds with integration of hydrogel on surface of polyester microfiber

Hydrophobic plastic polymers, which are mechanically tough and stable, can be conveniently fabricated with pre-defined structures and shapes. These properties make the

polymer-based materials handy to maneuver and useful in a wide range of medical devices [7-9]. Hydrogels made of hydrophilic networks are capable of absorbing water and the hydrated systems often show superior biocompatibility in comparison to hydrophobic polymers by reducing the protein adsorption and displaying tissue-like elasticity [10]. However, hydrogels often exhibit relatively weak mechanical strength, and the materials may deform easily under pressured or water-vaporization conditions. I hypothesized that with integration of hydrogels on polyester microfiber surface could take the advantage of both scaffolds and overcome their limits. Surface RAFT polymerization technique was used to coat hydrogel on PCL electrospun fibers and characterized the chemical, mechanical, *in vitro* cell attachment and *in vivo* biocompatibility of the scaffold with hybrid structure.

1.1.2 *Specific aim 2*

Development of scaffolds with microwell patterning on electrospun fibers for MSC spheroids transplantation

To better mimic the natural ECM structure, classic scaffolds such as electrospun fibers are designed to have architectures in micro-scale. Such micro-architectures have the ability to regulate cells on cellular/subcellular level by modulating the local biochemical and physical microenvironment. With the rapid advancement in stem cell technologies, different microscale tissues or organoids have been produced through scalable processes [11, 12]. These microtissues often exhibit superior therapeutic functions to single cells. To successfully transplant those microtissues, scaffolds should have the ability to not only control local microenvironments on cellular/subcellular level, but also manipulate their spatial distribution on a larger scale (hundreds of microns to a few millimeters) to ensure efficient vascularization and prohibit hypoxia and insufficient nutrient supply caused by random cell

clumping. In this specific aim, I hypothesized that the introduction of microwell patterns on electrospun fibers could control the spatial distribution of MSC spheroids and benefit MSC spheroids transplantation *in vivo*. Microwell patterned electrospun fibers were fabricated and the *in vivo* performance was characterized by transplanting MSC spheroids loaded scaffolds in mice model of hind limb ischemia.

1.1.3 *Specific aim 3*

Development of hollow spherical scaffolds with controllable pore size for MSC transplantation

Cell adhesion and migration, tissue ingrowth and vascularization are strongly related to pore size. In this specific aim, I hypothesized that the pore size controllable hollow spherical scaffold could have the ability to control over the cell retention and survival after cell transplantation. The hollow spherical scaffolds were fabricated through phase separation technique. The mechanical property, mass transfer efficiency and *in vitro* cell function of scaffolds were characterized with different pore size. The *in vivo* performance of scaffolds was further investigated in MSC transplantation.

1.2 Backgrounds

1.2.1 Tissue scaffolds and their properties

Many tissues such as myocardium, nerves, bones and cartilage can hardly regenerate, which made damages to these tissues irreversible. One possible solution is tissue/organ transplantation. However, the donors are too few to meet the demand. Tissue engineering is an alternative method to treat damage to those tissues. The idea of tissue engineering is to regenerate and replace damaged tissue by a material and cells combined method. For

example, Keiji et al. seeded vascular SMCs on PCLA patches and found that the cell-seeded grafts could improve LV function of rats after myocardial infarction [13]. The materials used in tissue engineering are called scaffolds, which serve as the substrates for cell attachment and provide specific environments for tissue growth. Currently two types of scaffolds: premade porous scaffold **Figure 1.1 (A-C)** and *in situ* formed hydrogels **Figure 1.1 (D)** are most applied. With the rapid development in stem cell technology, besides the initial purpose of growing tissues, scaffolds have found new applications in cell therapy, where they serve as platforms for cell delivery with focusing on improving cell retention and survival, as demonstrated later in this chapter.

The *in vivo* capacity of scaffold in determined by multiple properties and can be classified into mechanical property, biocompatibility and geometric property. During implantation, scaffolds often have to encounter compressive forces while handling from tweezers or shear stress from injections. After implantation, scaffolds also need to resist compressive and hydro-static forces in host tissue. Therefore, the scaffold should possess sufficient mechanical property to remain integrity during and after transplantation. It is generally accepted that an ideal scaffold should have similar mechanical property as the tissue to be regenerated. In addition, mechanical property also affects the processablity of scaffold. Materials with too strong or too weak mechanical ability can be hardly fabricated into versatile architecture. Furthermore, mechanical properties can affect cell functions

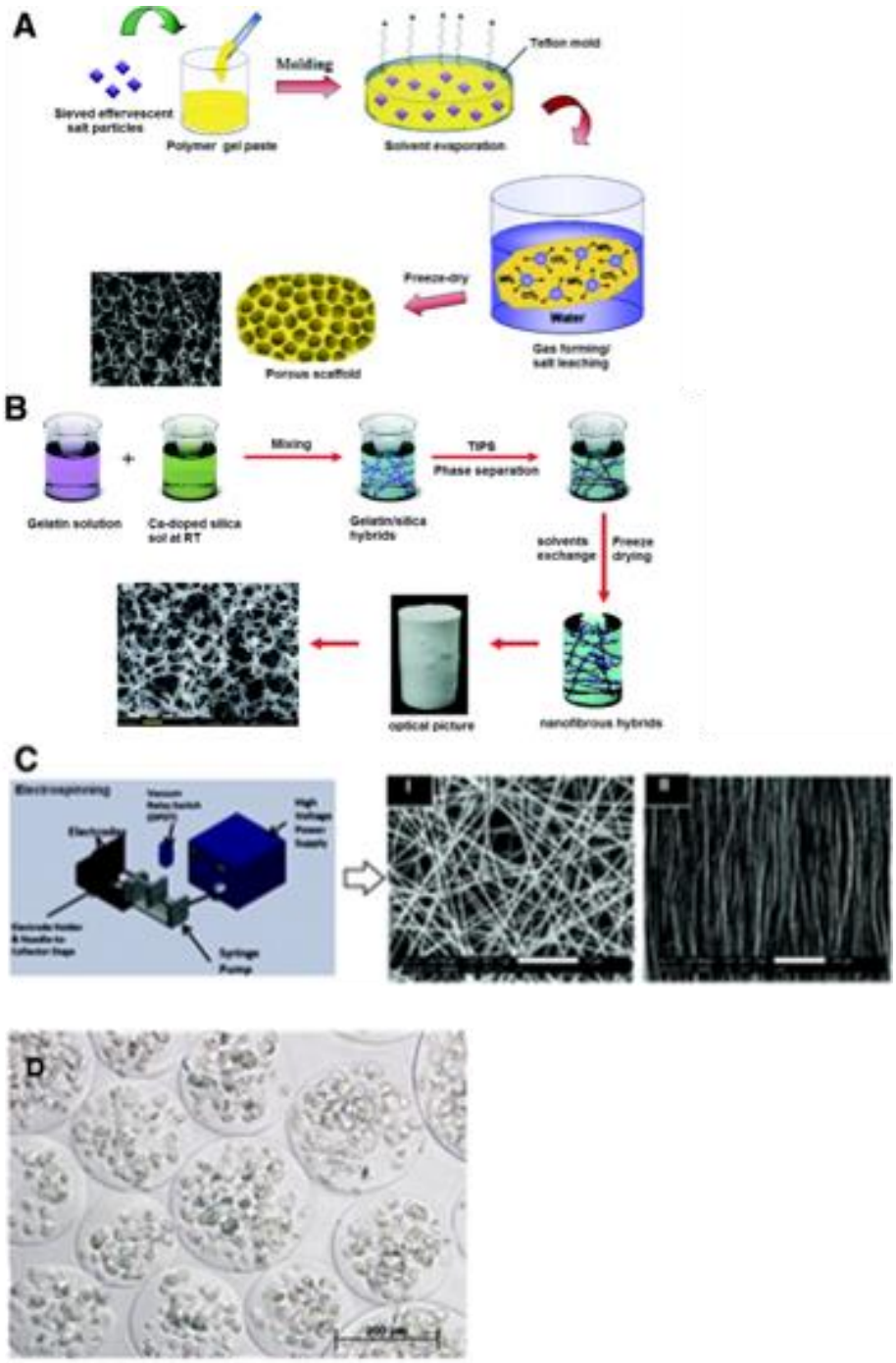

Figure 3.1 Scaffold fabricated by (A) gas foaming, (B) phase separation, (C) electrospinning and (D) *in situ* formed hydrogels (Qiu Li Loh et al. *Tissue Engineering Part B: Reviews.* 2013, 19(6): 485-502, Landázuri, Natalia, et al *Journal of tissue engineering and regenerative medicine* 2012)

directly as well. For example, studies showed that MSC differentiated into different lineage on substrate with different stiffness [14].

The basic requirement in biocompatibility is that the material should not be cytotoxic. The scaffold and its degradation product should not harm the transplanted cells and host tissue. In addition, good biocompatibility also requires a minimal triggering of foreign body reaction. Otherwise the scaffold will be surrounded with a thick layer of fibrotic tissue and the transplanted cells will start necrosis and apoptosis due to hypoxia. The factors that determines scaffold's biocompatibility includes materials' chemical composition, structure,

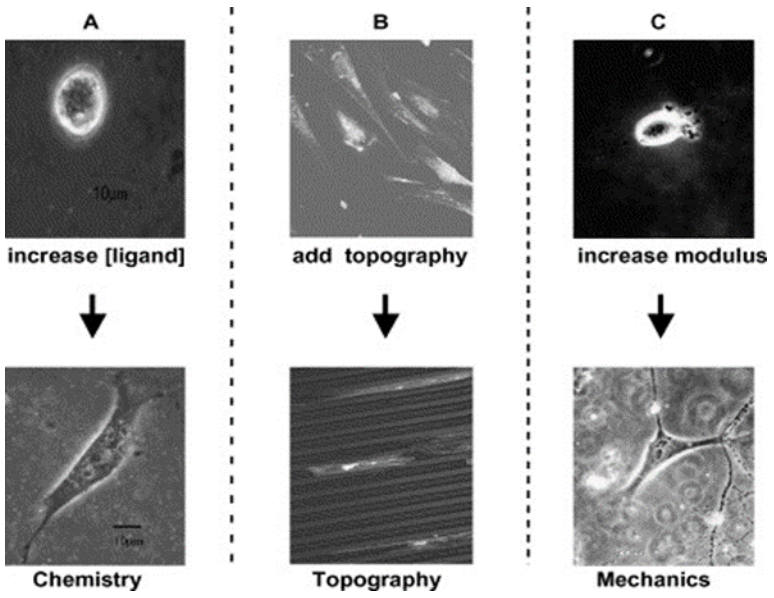

Figure 1.2 Cell response is dependent on multiple properties of scaffolds. (Joyce et al. , Surface Science, 2004)

and their morphology and also their sterilization conditions. Wettability and hydrophilicity are often related to biocompatibility. It is generally considered that materials with higher water content are more biocompatible, such as hydrogels.

Geometric properties include the scaffolds' shape, topology, porosity, pore size and interconnectivity. Scaffolds are typically porous structured. The high porosity offers a high surface/volume ratio which facilitates cell attachment. The interconnected network of pores is essential for the diffusion of nutrient and cellular waste. Pore size controls the permeability of molecules as well as cells. Relatively, larger pore size (>1 μm) is designed to facilitate cell migration (in and out) and blood vessel ingrowth and smaller pore size (<1μm) is usually designed to prevent cell migration, which is often used in immunoisolation devices. Topology has been shown to affect cell function. For example, previous studies in our lab has also proved that surface nanotopography could affect the biocompatibility of scaffold that electrospun nanofibers induced only minimal FBRs with indiscernible activation of macrophage cells compared to microfibrous membranes [15]. On a larger scale, as described later in this dissertation, micropatterning on hundreds of microns could facilitated the spatial distribution of microtissues and promote vascularization. On macro-scale level (>a few millimeters), scaffolds can be made into membrane shaped for convenient cell migration or made into capsules to limit host-transplants interaction.

1.2.2 Electrospinning

Electrospinning is a simple and versatile method for fabrication of continuous fibers with nano- to micrometer range diameters and has gained increasing attention in the past decade. A wide range of polymers can be applied for electrospinning including synthetic polymers such as PCL and PLGA[16] and natural derived polymers such as collagens[17]. A typical electrospinning set up is illustrated in Figure 1.2 A. It usually consists of three major components: a high-voltage supply, a syringe pump, and a collector. When a high voltage is applied on spinneret, the extruded polymer droplet will become highly charged. When

electrostatic force exceeds the surface tension, the polymer droplet will erupt from droplet and form continuous stream. During the stream move toward the collector, the solvent evaporates and the stream is elongated and becomes thinner by a whipping process[18]. Usually the fibers collected are random oriented as shown in **Figure 1.2 B**.

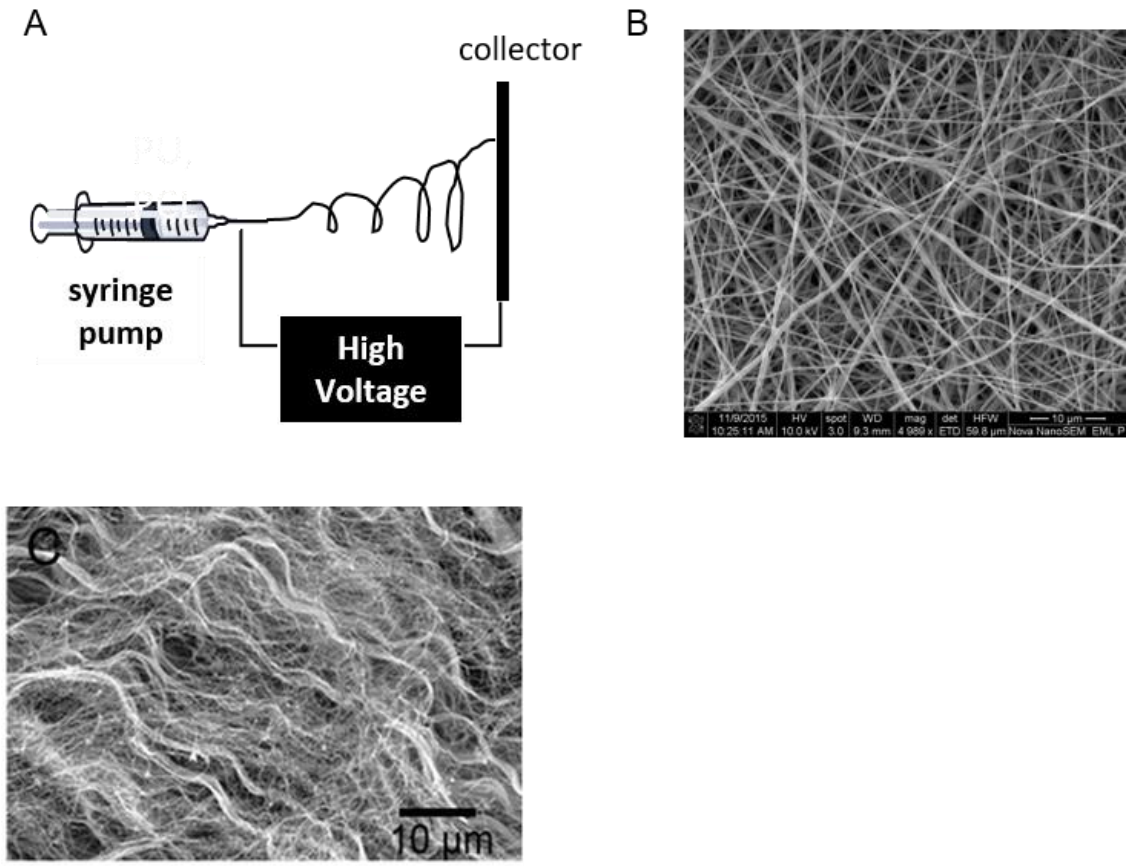

Figure 1.3 (A) Common electrospinning set up (B) Random aligned electrospun PCL fibers (C) Decellularized porcine aortic valve (Ye X, et al. *PLoS ONE*, 2013)

Electrospun fibers have wide biomedical applications, not only due to the versatile materials applied, but also because their fibrous architecture resembles the structure of native ECM. ECM is a collection of polysaccharides such as hyaluronic acid and proteins such as collagen and elastin. They not only offer physical support of surrounding cells, but also have

strong effect in regulating cell adhesion, migration and differentiation [19]. As showed in **Figure 1.2C**, native ECM has fibrous structures with fiber diameter ranging from nanometers to micrometers, very similar to electrospun fibers. One principle of tissue engineering is to mimic natural cells' microenvironment as close as possible. Therefore, the resemblance of electrospun fibers to native ECM made them good candidates for developing desired stem cell niche. In addition, the high surface area could promote cell adhesion and migration, and the high porosity could also facilitate nutrient transfer[19,20].

Electrospun fibers have been widely applied as tissue engineering scaffolds. For example, Peter I. Lelkes et al. fabricated anisotropic scaffolds with electrospinning of polycarbonate-urethane and PLGA. They found the scaffolds could support adhesion and proliferation of cardiac myoblasts and exhibited mechanical properties comparable to those of a human heart[21]. H. Yoshimoto et al. cultured mesenchymal stem cells with osteogenic supplements under dynamic culture conditions and found the cell-polymer constructs were covered with cell multilayers and mineralization and type I collagen were observed at 4 weeks, suggesting that electrospun PCL is a potential candidate scaffold for bone tissue engineering[22]. Changjian Liu et al. developed a tissue-engineered vascular graft with electrospinning a hybrid of chitosan/poly(ε-caprolactone). They seeded endothelial cells on scaffold and implanted *in vivo*. After 3 months, they observed a regeneration of endothelium, and the presence of collagen and elastin, indicating the potential of electrospun fibers in vascular graft applications[23].

1.2.3 Electrospun fiber and hydrogel composite scaffolds

Electrospun fibers and hydrogels are two of the most studied types of materials in the field of tissue engineering. They can both replicate the components of native ECM and

provide desired cell niche for tissue engineering and cell delivery applications [24]. Electrospun fibers, as have been described in last section, usually have good mechanical strength and large surface area. Hydrogels usually have high water content and superior biocompatibility. However, they are usually mechanically weak. Therefore, the integration Electrospun fibers and hydrogels are two of the most studied types of materials in the field of tissue engineering. They can both replicate the components of native ECM and provide desired cell niche for tissue engineering and cell delivery applications [25]. Electrospun fibers, as have been described in last section, usually have good mechanical strength and large surface area. Hydrogels usually have high water content and superior biocompatibility. However, they are usually mechanically weak. Therefore, the integration of electrospun fibers and hydrogel may offer potential to develop superior scaffolds, with a combination of advantages of both materials and overcome their weakness. Meanwhile, the native ECM itself is composed of fibrous proteins and gel like glycosaminoglycans. The integration of electrospun fibers and hydrogels may offer a closer replication of the native ECM.

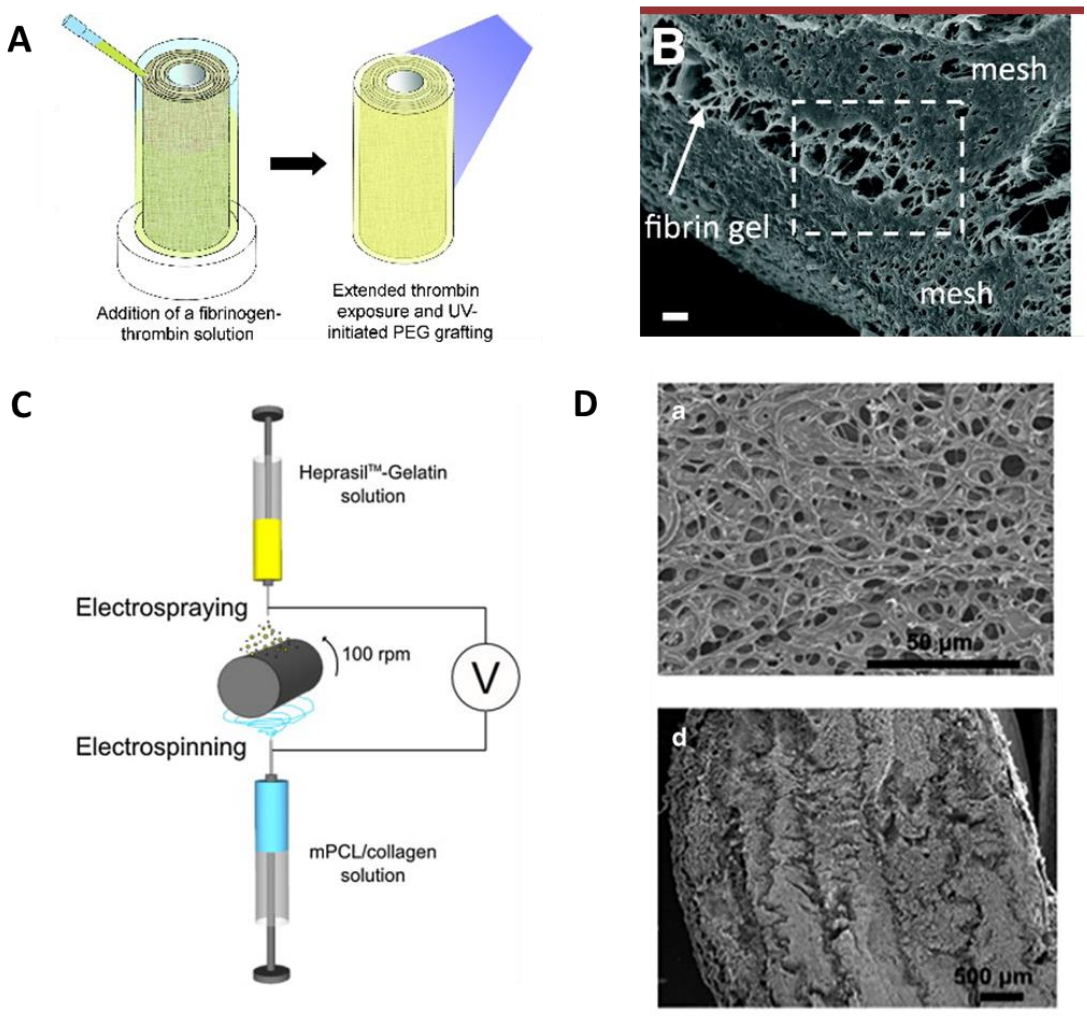

Figure 1.4 Electrospun fiber and hydrogel composite scaffolds. (A, C) Schematic demonstrating encapsulating electrospun fibers in hydrogels and co-electrospinning/electrospraying of fibers and gels (B, D) SEM images of composite scaffolds fabricated by encapsulating electrospun fibers in hydrogels and co-electrospinning/electrospraying of fibers and gels. (A, B: McMahon et al. *Tissue Engineering Part C: Methods,* 2011; C: Bosworth et al. *Nanomedicine: Nanotechnology, Biology and Medicine,* 2013; D: Y. Hong et al. *Biomaterials*, 2011)

There have been some studies investigating electrospun fibers and hydrogels composite scaffolds. Current approaches can be divided into two categories: encapsulating electrospun fibers in hydrogels [26-28]; 2) co-electrospinning/electrospraying of fibers and gels [29,30] (**Figure 1.4 A, D**). In first approach, electrospun fibers are immersed in hydrogel precursor solution, followed by the gelation process. For example, McMahon et al.

fabricated cells seeded hydrogel–electrospun mesh composites for coronary artery bypass grafts. In this study, smooth muscle cells were seeded on electrospun meshes [31]. The cells seeded mesh was wrapped around a tube and incubated in fibrinogen-thrombin solution, followed by immersing in PEGDA solution and polymerization by UV light. They described that the mechanical properties of this composite scaffold mimic those of coronary artery vessels, which electrospun fibers alone cannot achieve. In the co-electrospinning/elecrospraying method, fiber's polymer solution and gel precursor solution was electrospun/elecrosprayed simultaneous on one collector. For example, Ekaputra et al. developed a composite scaffold by electrospinning a mixed solution of poly(ε-caprolactone) and collagen, whilst coinciding with the electrospraying of a hydrogel solution based on glycosaminoglycans on a rotating medrel. They found the pore size of composite material increased significantly that allows cells to infiltrate, where for scaffold with electrospinning alone cells only stayed on surface [32]. In both approaches, the distribution of hydrogels in composite materials is inhomogeneous (**Figure 1.4 B, D**). The composite often showed laminated structure, with hydrogels filling between each layer. The pores of electrospun fibers were also filled with hydrogels randomly.

1.2.4 Micropatterning

The process of fabricating regular micro-scale patterns on surface of material is called micropatterning. Micropatterning technique can easily control the cell and tissue morphology and further affect their function. Different patterns have been designed for different purposes. For example, Mirjam et al. seed cells on the microwell patterned PDMS, phalloidin staining of actin stress fibers showed that the cytoskeleton of cells in microwells was 3D and not limited to the cell–substrate interface [33]. Morgan et al. developed a

micropatterned hydrogel through a micromolding technique. His team seeded HepG2 microtissues in the micropatterned hydrogel and found that the tissues' morphology, distribution and size are dependent on the shape of the molds, but their viability and cytokine secretion are dependent on the seeded cell number [34]. McDevitt' lab used commercialized Aggrewell ™ to produce MSC aggregates. His team found that comparing with single cells, MSC aggregates have more homogenous differentiation [35]. In 2007 and 2010, researchers from University of Korea and MIT cultured ESCs on microwell patterned substrate and achieved embryoid body with homogenous size and shape. They discovered gene expressions of three germ layers from gastrula and found that the size of embryoid body could affect the differentiation into myocardium and nerve. These experiments proved the micropatterning technique's potential in controlling stem cell differentiation and application in regenerative medicine. In addition, the 3-D micropatterning offered a way to control the spatial distribution and sufficient nutrient supply of cells in high density, which are greatly desired in clinical cell transplantation applications.

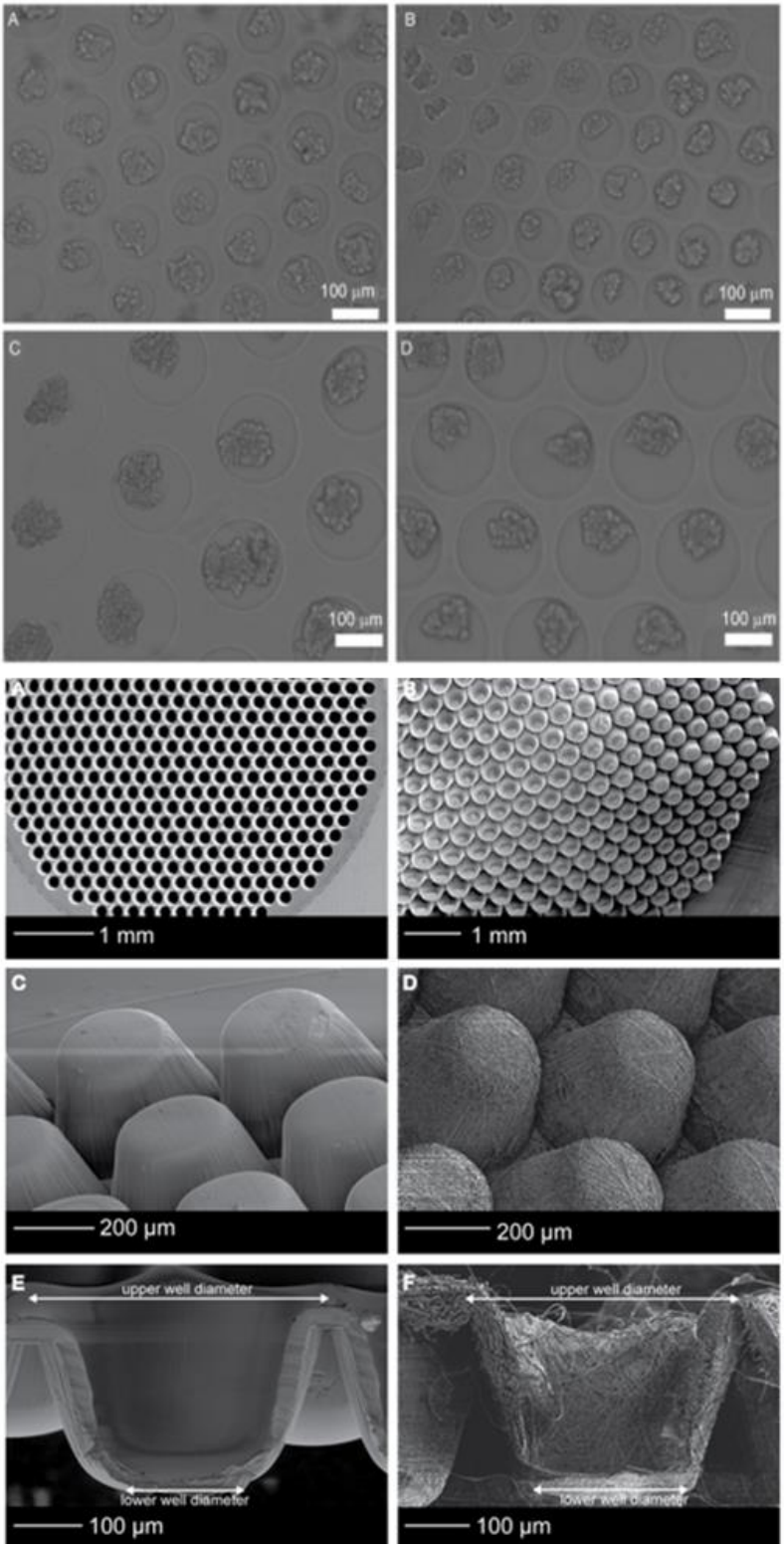

Figure 1.5 Examples of micropatterning technique (left: Jiang LY et al. Sci. China Life Sci., 2014, right: Buitinga M et al. *PloS one*, 2013)

1.2.5 Mesenchymal stem cell transplantation

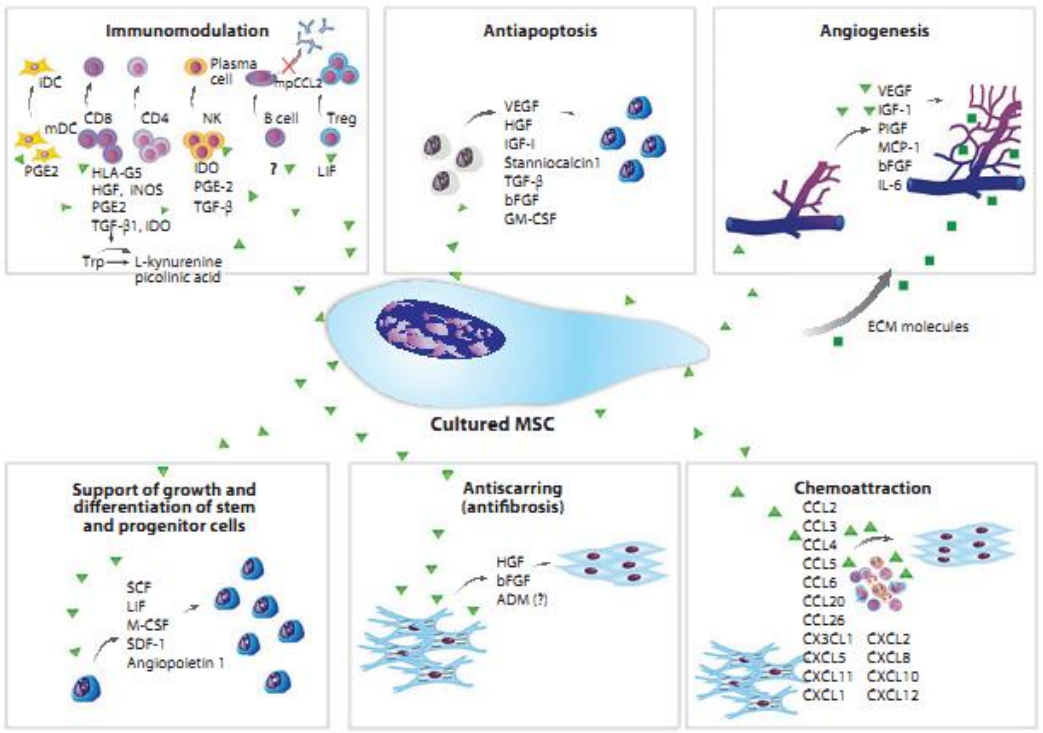

Figure 1.6 Illustration of MSCs' paracrine effects (Singer N G et al. Annual Review of Pathology: Mechanisms of Disease, 2011)

Mesenchymal stem cells (MSCs) are the most studied cell candidates for stem cell therapy[36]. MSCs are adult stromal cells. They were first isolated and characterized from bone marrow in 1980s[37] and later found in almost every tissue: fat, skin, heart, muscle, liver, etc[38]. MSCs are self-renewable. They can be easily expanded in vitro after extraction. MSCs have multi-lineage differentiation potential. They were most known for their osteogenic, chondrogenic and adipogenic differentiation, but they can also differentiate into other mesodermal phenotypes like muscle cells in vitro. Besides their differentiation ability, MSCs are able to secrete a series of biomolecules which can induce tissue regeneration, vascularization, modulate immune function and suppress inflammation. This ability is called MSCs' paracrine function [39], as summarized in **Figure 1.4**. Currently, as little evidence was

found of MSCs integrating with host tissue *in vivo*, it is generally believed that their therapeutic benefits were mainly due to their paracrine function [40].

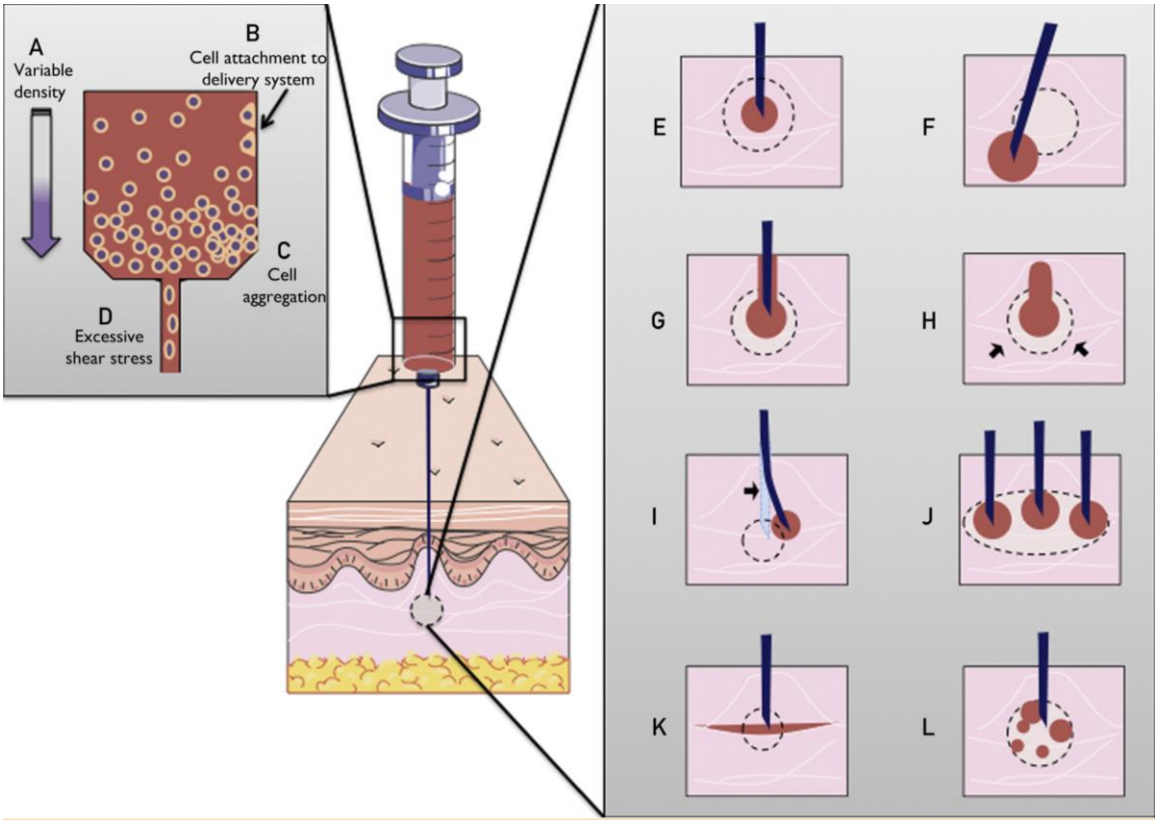

Figure 1.7 Common problems with minimally invasive delivery of cells. (A) Cells in suspension tend to settle, leading to uneven distribution of cells on delivery. (B) Cells may attach to the delivery system. (C) Cells tend to form aggregates that might impair their function and ease of administration. (D) Cell health will depend on the viscosity of the injected fluid, the cell size, the inner diameter and surface roughness of the needle, the ratio of needle diameter to reservoir (syringe barrel) diameter, the rate of infusion, etc. (E), Underdosing. Blind insertion can (F) miss the target site or (G) lead to backpressure, and leakage during infusion into a closed space could lead to cell damage and poor delivery. (H) Improper sealing of the needle track after delivery can lead to escape of the transplanted cells, particularly in muscle tissue, where compressive forces are higher. (I) Heterogeneous tissue structure may cause needles to deflect in an unpredictable manner away from the target site. (J) A large target site may require multiple injections, increasing invasiveness. (K) The injected fluid tends to travel along the path of least resistance (eg, along the fascia), which could cause cells to be dispersed away from the target site. Furthermore, cells may tend to migrate after delivery. (L) Clumps and inconsistent cell dispersion may result from delivery of a cell scaffold or carrier if the rate of infusion or scaffold gelation is poorly controlled. (O'Cearbhaill, Eoin D., et al Mayo Clinic Proceedings. 2014.)

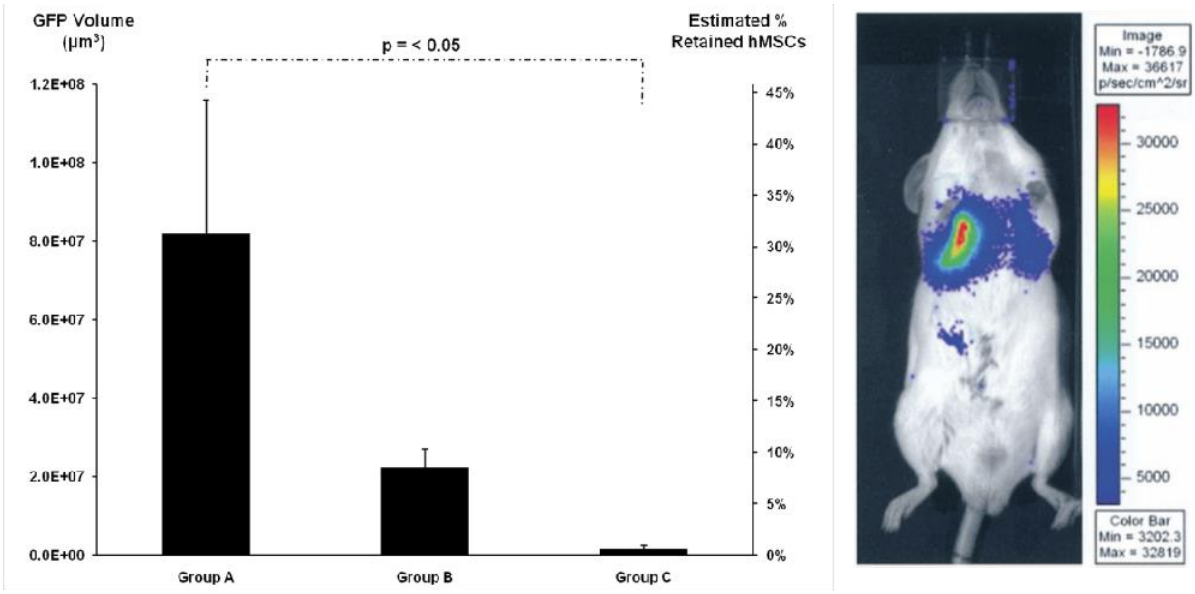

Figure 1.8 Cell retention and engraftment in current studies. (Collins, Maria C., et al. Open Tissue Eng Regen Med J 5 (2012): 17-24.

The results from clinical studies were mixed. Many studies showed promising results in early stage clinical trials, but failed to meet the endpoint in phase III/IV trials. One possible reason for this situation is the low engraftment of MSCs. Currently, in almost all clinical trials, MSCs were administered through intravenous or muscular injection. However, directly injected MSCs usually have very low retention. Studies showed that systemic delivery of MSCs to infarcted hearts yielded only 11% retention at 90 min and 0.6% retention at 24 h. Some problems of direct injection of cells were illustrated in **Figure 1.5**[41]. This huge loss of cells resulted from both physical and biological factors. After administration, cell suspensions were quickly washed out in the in tissue cavities or from the injection hole because of lack of adhesion. Cells that survived acute loss also have to suffer from ischemic and inflammatory environment, which further reduced the cell retention. Such situation restricted the application of MSCs therapy greatly.

Efforts have been made to increase the cell retention of stem cell therapy. For example, researchers have tried to deliver pre-conditioned cells. Ling et al. found that transplantation of hypoxia preconditioning treated BMSCs resulted in better functional recovery after stroke. They found hypoxia preconditioning upregulates pro-survival and pro-regenerative genes in BMSCs [42]. Wang et al. transplanted hypoxia preconditioned ADSCs and found enhanced therapeutic effects in diabetes induced erectile dysfunction rats. They found hypoxia precondition upregulated angiogenesis and neuroprotection genes including VEGF and its receptor FIK-1, angiotensin (Ang-1), bFGF, brain-derived neurotrophic factor (BDNF), glial cell-derived neurotrophic factor (GDNF), stromal derived factor-1 (SDF-1) and its CXC chemokine receptor 4 (CXCR4) [43]. Researchers have also tried genetic modification of MSCs through overexpressing prosurvival genes. For example, Dan et al. engineered MSCs with integrin-linked kinase (ILK), which is a pleiotropic protein critically regulating cell survival, proliferation, differentiation, and angiogenesis. They intracoronary injected ILK engineered MSCs in porcine MI model and found significantly increased functional recovery. They also found increased homing capacity to infarct myocardium with ILK engineered MSCs [44]. Another approach that has been adopted is cell surface modification. For example, Chi et al. incorporated a P-selectin glycoprotein ligand-1 (PSGL-1) mimetic 19Fc[FUT7+] onto surface of MSCs to enhance engraftment of MSCs. Currently they are still working on large animals to prove the efficacy of this method [45].

1.2.6 Scaffolds for MSC transplantation

However, modification of cells alone can hardly reduce the acute loss caused from physical factors. To address this problem, scaffold based delivery strategy was brought forward. In scaffolds based MSCs delivery, MSCs are seeded or encapsulated in scaffolds

before transplantation. Therefore, scaffolds could provide a friendly niche like native ECM with pre-established adhesion, preventing cell loss due to mechanical distribution. They can be classified into injectable scaffolds and cell patch according to their delivery approach.

Injectable scaffolds can be divided in three categories: (1) hydrogel microencapsulation; (2) attachment with preformed microcarriers; (3) entrapment with *in situ* formed hydrogels after injection. hydrogel microencapsulation was first developed for the immunoisolation of islets 30 years ago [46,47]. In this approach, hydrogels beads of several hundred micrometers were formed *in situ* with cell suspensions. The hydrogel capsules are permeability controllable, which allows the diffusion of oxygen, nutrient and paracrine factors, and protect cells from the attack of immune system. For example, Jiashing et al. encapsulated MSCs in alginate microspheres and injected them in the myocardium of MI rats. They found this approach could lead to the maintenance of LV geometry, preservation of LV function, increase of angiogenesis and improvement of cell survival [48]. In second approach, the preformed microcarriers are usually made of micro-scale porous scaffolds. For example, Yaqian et al. loaded human MSCs in gelatin microcryogels, which are porous scaffold with scale of several hundreds of micrometers. They injected the MSC loaded microcarriers to hind limb ischemic mice and found this strategy had superior therapeutic efficacy and prolonged cell survival [48]. The third approach for injectable scaffolds is through injection of a mixture of pre-gelation liquid and cells. The gelation should start shortly after injection, therefore provide adhesion and microenvironment of cells. For example, Eva et al. designed hydrogel consisting of silanized hydroxypropyl methylcellulose. This hydrogel is able to self-crosslink to form a scaffolding matrix. They intramyocardial injected MSC seeded hydrogel in rat model of MI and found this strategy had improved functional recovery [50]. However, injectable scaffolds can hardly avoid the problems caused

by injection procedure as illustrated in **Figure 1.5**. Meanwhile, hydrogels often show limited ability in cell adhesion and restrict ECM secreting and cell-cell interaction.

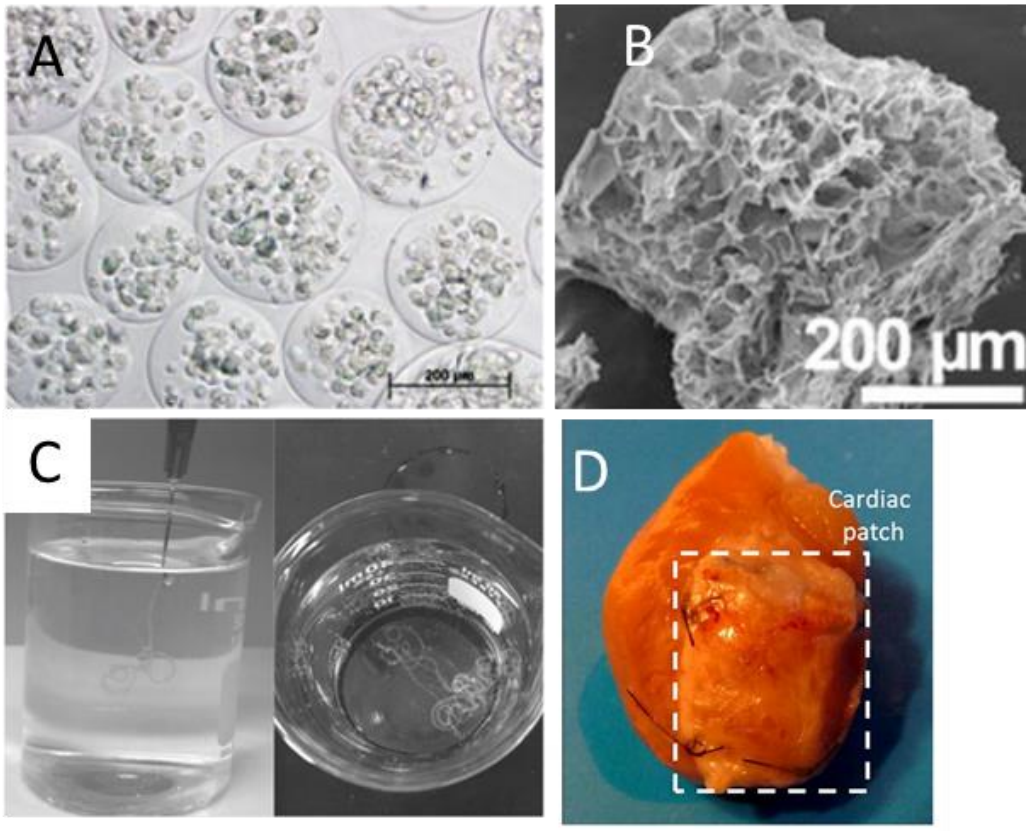

Figure 1.9 Scaffolds for MSCs transplantation. (A)hydrogel microencapsulation, (B)porous microcarrier, (C)*in situ* formed hydrogel, (D)cell patch. (A: Land ázuri, N, et al. *Journal of tissue engineering and regenerative medicine*, 2012; B: Y Li, et al. *Proceedings of the National Academy of Sciences*, 2014; C: Li L, et al. *Advanced Materials*, 2015; D: Kai D, et al. *Acta biomaterialia*, 2014)

Cell patches are usually based on porous scaffolds, which are the most classic type of scaffolds for tissue engineering. Both synthetic and natural materials can be fabricated into porous scaffolds [51,52]. Comparing to injectable scaffolds, cell patches usually have better mechanical strength and could provide better adhesion of cells. The interconnected pores provide large surface area and enable fast mass exchange. In stem cell therapies, cell seeded scaffolds are placed on top of injured areas as shown in **Figure 1.6D**. For example, Dan et al.

loaded MSCs on PCL/gelatin electrospun fibers and implanted on the epicardium of MI rats. They observed restricted expansion of the LV wall, reduced scar size and increased density of the microvessels with this strategy [53]. Juli et al. loaded genetically engineered drug-releasing human MSCs on PLA electrospun fibers and implanted in mouse model of brain cancer glioblastoma surgical resection. They found this strategy had a 5-fold increased MSC retention and 3-fold prolonged persistence over direct injected MSCs. The volume of established glioblastoma xenografts was also reduced in this study [54].

As described above, currently most scaffolds adopted in MSC transplantation are traditional tissue engineering scaffolds like hydrogels or porous scaffolds. They often only display merits of a single material and also show a bulk property [55-58]. For example, hydrogels often show superior *in vivo* biocompatibility due to their high water content [59,60]. However, hydrogels with higher water content also tend to have weaker mechanical strength, which made them hard to remain integrity during preparation and after implantation. Therefore, composite material of hydrogels and porous scaffolds may optimize the biocompatibility and mechanical property and may be a good candidate for cell delivery. Meanwhile, most traditional hydrogels and porous scaffolds often only focus on recapitulating the native ECM on nano- to microscale, while lacking the ability to regulate spatial distribution of cells on larger scale and permeability of seeded cells. Therefore, a hierarchical structure design of scaffolds may offer regulation of cells in more aspects, which might further improve the *in vivo* performance.

CHAPTER 2. DEVELOPMENT OF SCAFFOLDS WITH INTEGRATION OF HYDROGEL ON SURFACE OF POLYESTER MICROFIBER

2.1 Introduction

Biodegradable hydrophobic polymers (e.g. polyesters), or plastics and hydrogels constitute two major categories of materials that have found important applications in fabrication of biomedical devices such as drug carriers, tissue scaffolds and wound dressings [61-66]. The two classes of materials, however, show distinctive characteristics as well as limitations. In particular, hydrophobic plastic polymers, which are mechanically tough and stable, can be conveniently fabricated with predefined structures and shapes. These properties make the polymer-based materials handy to maneuver and useful in a wide range of medical devices [67-69]. Hydrogels made of hydrophilic networks are capable of absorbing water and the hydrated systems often show superior biocompatibility in comparison to hydrophobic polymers by reducing the protein adsorption and displaying tissue-like elasticity [70]. However, hydrogels often exhibit relatively weak mechanical strength, and the materials may deform easily under pressured or water-vaporization conditions. These drawbacks have severely limited the use of hydrogels in design of medical devices.

To address the limitations and develop tough yet bio-compatible materials, developing composite materials by integrating the hydrophobic polymers and hydrogel materials has attracted great interests in recent years [71-73]. In particular, fibrous matrices fabricated

through electrospinning processes not only exhibit high permeability and surface-to-volume ratio but also morphologically mimic the natural fibrous extracellular matrix (ECM). Electrospun fibers therefore have been intensively investigated for use as scaffolds for tissue repair. investigated for use as scaffolds for tissue repair [74-76]. Numerous efforts have been made to fabricate electrospun fiber-hydrogel composite materials [77-87]. Although materials with hydrogels filling up the pore spaces or fiber-hydrogel sandwiches were prepared, the important structural characteristics of fibrous materials—porosity and permeability—could not be maintained in many approaches. Moreover, as plastic fibers and hydrogels of different hydrophobicity are essentially incompatible, physical blending of the two components may result in defection in final matrices.

Table 2.1 Limitation and merits of polyester fibers and hydrogels

	Polyester fibers	Hydrogels
Advantages	mechanically strong morous structure	large water content good biocompatibility
Limitation	hydrophobic	mechanically weak

In this study, a new methodology for creating polyester-hydrogel fibrous hybrid matrices via inducing polymerization of hydrogels on the surface of electrospun fibers was reported. I hypothesized that if the polymerization of the hydrogel component could be localized and controlled at the fiber surface, a stable hydrogel layer ensheathing the fibers can be obtained to render new hybrid structure/properties. To investigate the concept, a trithiocarbonate-based chain transfer agent (CTA) was immobilized onto the surface of poly(ε-caprolactone) (PCL) electro-spun fibers followed by incorporation of poly(ethylene

glycol) (PEG) hydrogel coating layers through surface reversible addition-fragmentation chain transfer (RAFT) polymerization. PEG-PCL hybrid materials of tunable morphologies were obtained. In contrast to the traditional polyester-based electrospun fiber, the matrices with fibers ensheathed in nanothin hydrogels display robust water-absorbing capability, non-deformability, composite mechanical properties and superior biocompatibility. This facile methodology for creating porous plastic polymer-hydrogel hybrids can potentially be exploited to modify different types of porous scaffold materials, and therefore opens the door for fabricating new high-performance materials for biomedical applications.

2.2 Materials and methods

Materials

Water was distilled and deionized using the Gelante Pure Water Equipment (Gelante Pure Water Co., Ltd., Shijiazhuang, China) at 18 M resistance. PCL (Mn ~ 70,000-90,000), polyethylene glycol diacrylate (PEGDA) (Mn ~ 575), N-hydroxylsuccinimide (NHS), NaOH, HCl （ 36% — 38% ） and deuterochloroform were purchased from Sigma-Aldrich (Milwaukee, WI, USA). Solvents including isopropanol， chloroform, dichloromethane, acetone, N,N-dimethylformamide (DMF) and carbon disulfide were from Beijing Chemical Works (Beijing, China). Trioctylmethylammonium chloride (Aliquat 336) and ethanethiol were purchased from TCI Shanghai (Shanghai, China). The suppliers of other chemical and biological reagents are specified in the text below. All ^{1}H NMR experiments were performed with 400 MHz NMR equipment (ARX400, Bruker, Switzerland).

Synthesis of CTA, (S-ethyl-S'-(α,α'-dimethyl-α''-acetic acid) trithiocarbonate) (EDAT)

A trithiocarbonate bearing the carboxylic acid group, S-ethyl-S'-(α,α'-dimethyl-α''-acetic acid)trithiocarbonate (EDAT),The trithiocarbonate CTA was synthesized according to a previously reported method [88]. 1.48 ml ethanethiol (0.020 mol) and 0.323 g Aliquat 336 (0.80 mmol) were sequentially added to the acetone (12.5mL, 0.166 mol) in a round-bottom flask and the mixture was cooled to 10 ℃ under the nitrogen atmosphere. The NaOH solution (50%) (1.68 g, 0.021 mol) was then added dropwise, followed by a carbon disulfide (1.21 mL, 0.020 mol)/acetone (2.6 mL, 0.035 mol) mixture was added over 20 min. After 10 min, chloroform (2.42mL, 0.030 mol) was added in one portion, followed by dropwise addition of 50% sodium hydroxide solution (8.00 g, 0.100 mol) over 30 min. The reaction was then allowed to react overnight under room temperature. To collect the product, the reaction solution was rotary evapora to rid of the acetone. The residue was then redissolved in 25 mL of water, and concentrated HCl was added under vigorously stirring at 5-10 ℃ to neutralize the base in the solution. The aqueous solution was then extracted three times with hexane, concentrated via rotary evaporation, and washed three times with water. The solution was dried by anhydrous sodium sulfate and isolated by column chromatography (silica gel 200-300 mesh) using ethyl acetate:hexane (2:3 v/v) as an eluent. After removal of solvent by rotary evaporation yielded an orange-brownish oil, which was dissolved in a small amount of hexane and washed three times with water. The solution was dried with anhydrous sodium sulfate again and crystallized at -20 ℃. After recrystallization in hexane twice, yellow crystals were achieved as the final product. (1.2 g, yield: 28%) ^{1}H NMR (400 MHz, CDCl3): δ =3.30 (q, 2H), 1.73 (s, 6H), 1.34 (t, 3H).

Synthesis of N-hydroxylsuccinimide (NHS)-activated CTA, EDAT-NHS

EDAT (1.00 g, 4.46 mmol) and the coupling catalyst, N,N'-dicyclohexylcarbodiimide (GL Biochem, Shanghai, China) (1.375 g, 6.67 mmol), were dissolved in 30 mL dichloromethane and cooled to 10 ℃ under nitrogen atmosphere. To this solution was added dropwise NHS (0.768 g, 6.67 mol) dissolved in 20 mL dichloromethane and the mixture was stirred and maintained overnight at room temperature. The solution was then concentrated by rotary evaporation and the EDAT-NHS product was isolated by column chromatography twice (silica gel 200-300 mesh) using ethyl acetate:hexane (3:1 v/v) as an eluent. The crude product, collected upon removal of the eluent, was redissolved in hexane and recrystallized at 4 ℃, and the final pure product obtained as bright yellow powders. (1.12 g, 3.67 mol, yield: 78%) ^{1}H NMR (400 MHz, CDCl3): δ =3.30 (q, 2H), 2.82(s, 4H), 1.73 (s, 6H), 1.34 (t, 3H)

Fabrication of PCL electrospun membrane

The PCL fibers were fabricated using an electrospinning apparatus assembled in the laboratory. First, 1.5 g PCL was completely dissolved in a 10 mL chloroform/DMF (9:1 v/v) binary solvent under vigorous stirring to prepare a 15% (w/v) solution. 1 mL of this solution was then loaded into a 1 mL syringe (Shanghai Zhiyu Medical Material Co., Ltd, Shanghai, China) mounted on a syringe pump (WZS 50-F6，Zhejiang University Medical Instrument Co., Ltd, Hangzhou, China). A blunt-ended 22-gauge stainless-steel needle was installed onto the syringe and then connected with to the positive electrode of a high voltage supply (EST-801A，ESD-China, Beijing, China). The electrospinning was conducted for 2 h with a grounded steel plate was used as collector, and the processing conditions, the flow rate, collection distance, and applied voltage were maintained at 0.5 mL/h, 14 cm, and 12 kV, respectively. After the processing, the final electrospun fibrous membrane was removed

from the collector, cut into defined geometries (typically 7 mm × 7 mm square shape), and stored for further reaction and characterization.

Coupling of trithiocarbonate CTA onto the surface of the PCL fiber

To modify the trithiocarbonate CTA onto the surface of PCL fibers, a 10% (w/v) 1,6-hexanediamine (Alfa-Aesar, Ward Hill, Massachusetts, USA) solution was first prepared by mixing 1.18 mL 1,6-hexanediamine with 8.82 mL isopropanol. PCL electrospun fibres were immersed in the solution and reacted 1h at 37 ℃ in a sealed container. After reaction the PCL electrospun fibres were rinsed thoroughly with deionized water and isopropanol three times each.

The aminated PCL electrospun fibers were soaked in a 4 mg/mL EDAT-NHS solution prepared in isopropanol with 1 μL/mL triethylamine (Xilong Chemical, Guangzhou, China) as catalyst. After incubating 1 h at 37 ℃, the CTA modified PCL electrospun fibers (PCL-EDAT) were washed extensively with deionized water and isopropanol three times each and dried under vacuum.

RAFT polymerization of PEGDA on the surface of the PCL-CTA fiber

Three samples with PEGDA concentration of 5%, 7.5% and 15% (v/v) were synthesized. PEGDA, EDAT and the initiator, 4,4'-azobis[2-(imidazolin-2-yl)propane] dihydrochloride (VA-044) (J&K Chemical Ltd., Beijing, China) were added to a 25 mL round-bottom flask with [PEGDA]:[EDAT]:[Initiator]= 217:1:2. Reactants were dissolved deionized water with a total volume of 5 mL. The CTA-modified PCL matrices were immersed in the solution, the flask was sealed and deoxygenized by nitrogen bubbling for 40 min on ice. Then the flask was transferred to a water bath at 30 ℃ and allowed to react for 1

h. After reaction, PEGDA surface polymerized electrospun fibers (PEG-PCL) were extensively washed by vortex in deionized water and dried in vacuum.

The addition of PEGDA hydrogel was shown by Fourier transform infrared spectroscopy (FTIR) instrument by the attenuated total reflection (ATR) method. (Nicolet 750,USA) Samples were dried overnight under vacuum before testing.

Analysis of the amine content in PCL matrix treated by aminolysis

1 mg of PCL or NH_2- PCL electrospun fibrous sample was added in 4 mL of 2.5 mg/mL ninhydrin DMSO solution. The mixture was heated in water bath at 80 ℃ for 15 min until the polymer dissolved and fully reacted with ninhydrin. The absorbance of the solution at 600 nm was measured by a microplate reader. The NH_2 concentration of PCL or NH_2-PCL samples was calculated from the standard curve and compared.

Microscopic spectroscopic characterization

To obtain the morphological characteristics of different PCL fibers, different PCL membrane samples were gold sputter-coated and examined by the scanning electron microscope (SEM) (S-4800, Hitachi, Japan). ImageJ was applied to quantitatively characterize the fiber diameter. For each sample, 10 randomly selected fibres were counted in each image, with a total of 3 images.

Wetting and water-absorption properties of PCL and PCL-PEG hybrid membranes

The wetting property of PCL and PCL-PEG hybrid membranes was studied by measuring the contact angle of water on different membranes through the static sessile drop method using a contact angle goniometer (Kino SL200B, China). Briefly, 1 μL of water was

dropped through the tip of a syringe onto the selected region of a membrane surface. After 1 s equilibrium, the droplet and the surface were imaged by the horizontal microscope connected to the CCD camera. If the droplet were visible on the surface, the contact angle was measured. For each membrane sample, at least three measurements were performed with water dropped on randomly selected spots on the surface.

To study the water-absorption property of the fibrous PCL and PCL-PEG materials, each thoroughly dried mats were weighed on a micobalance and then separately immersed and hydrated in 5mL deionized water for 1 min. The samples were then removed from the water, blotted dry with kimwipes tissue paper (KIMTECH, Roswell, U.S.) before the weights were recorded again. The water uptake capacity of the sample was calculated according to the equation: water uptake (%) = (Wt – W0)/W0 × 100%, where Wt and W0 is the weight of the hydrated and dry mats, respectively.

According to the water contents in the hybrid materials, the PEG composition in the hybrids may be calculated according to the equation:

percent PEG mass in hybrid = percent water content in hybrid/ (1- PEG%) × PEG%.

In this equation, the PEG% theoretically should be the PEG concentration in the hydrogel layer on the fiber surface. One assumption can be made is that the PEG concentration in the hydrated hydrogel layer on the fiber surface was the same as the feed ratio in the surface polymerization. Although the results were estimation, the calculation reflected the approximate PEG composition in the hybrids.

Mechanical analysis

To understand the mechanical property of the hybrid materials, local fiber surface mechanical properties were determined by AFM indentation using atomic force microscopy (AFM) (SPI3800, NSK LTD., Japan) equipped with Budgetsensors tap 300 AI-G AFM tip, which had a spring constant of 40 N/m. PEG-PCL samples were hydrated before testing. Images were scanned through contact mode to locate fibres. AFM tip was then placed on top of a fiber and start indentation. The force-displacement curve of sample was obtained during the indentation of AFM tip on fibers.

To study the tensile strength of the fibrous materials, electrospun PCL and PCL-PEG hybrid membranes of approximated 200 μm thickness were prepared as described above. The fibrous membranes were then cut into rectangular strips of 3×1 cm^2, and fixed on the mechanical tester (AGS-X Series Table-top Precision Testers, Shimadzu, Japan) with two ends clamped. The testing area was 1.5×1 cm^2 and stretched at a speed of 5 mm/min until break. The tensile strength, elongation and elastic modulus were calculated from the stress-strain curve. Four samples were tested for each type of membrane.

Cell adhesion on PCL and 7.5% PEG-PCL membranes

PCL or 7.5% PEG-PCL membranes were cut to 5 mm × 5 mm squares and sterilized via immersion in 75% ethanol for 30 min. The membranes were thoroughly washed three times by DPBS and place on 96-microwell plates (ULAPs, Corning, NY). Human Adipose-derived stem cells (hADSCs) were kind gifts from Dr. Xiumei Wang's lab, Tsinghua University. Each membrane was seeded with 3000 cells and incubated under 37 ℃ and 5% CO2 for 24 h. The supernatants were removed and the membranes gently washed by warm DPBS for three times. The cells were then fixed in 4% paraformaldehyde (Beijing Chemical Works, Beijing, China) and stained with rhodamine-phalloidine and DAPI (Invitrogen,

Carlsbad, CA). The samples were imaged under a laser scanning confocal microscope (A1R-si, Nikon, Tokyo, Japan)

Subcutaneous implantation of PCL and PCL-PEG hybrid materials

Subcutaneous implantation was performed to evaluate the host reaction to the hybrid membrane. All procedures were performed in accordance with the regulations approved by the Institutional Animal Care and Use Committee (IACUC) of Peking University. Modified and non-modified electrospun materials were soaked in 70% aqueous ethanol for 30 min and thoroughly washed with sterilized DPBS three times before implantation. The Sprague Dawley rats (Vitalriver, Beijing, China) weighing 290-320 g were anaesthetized with an intraperitoneal injection of chloral hydrate (400 mg/kg body weight). The abdomen was shaved and swabbed with betadine and a midline incision was made in the skin. Two pockets were created by blunt dissection in the dermal layer on both sides of the midline. One PCL-PEG and one PCL fibrous membranes were then placed into the left and the right side pocket, respectively. Incisions were closed with sutures and the animals were observed until recovery and housed for prescribed time.

Animals were sacrificed post implantation by CO_2 asphyxiation. The implants and the surrounding tissue were harvested from the killed rats, fixed in 4% paraformaldehyde, dehydrated with graded ethanol solutions and embedded in paraffin via standard procedures. The samples were sliced on a microtome at a thickness of 5 μm. The sections were stained with hematoxylin and eosin (H&E) and then imaged by an upright microscope (Olympus DP71, Japan). The presence of inflammatory cells was analyzed by a professional pathologist, Yong-Jian Deng of the Department of Pathology at Southern Medical University (Guangzhou, China).

Statistical analysis

All quantitative measurements were presented as mean ± standard deviation (SD). The one-way analysis of variance followed by Tukey's post hoc analysis was performed to compare the multi-group data. The unpaired t-test was performed when the data was consisted of only two groups. The level of significance was labeled by *, ** and ***, denoting the p value of <0.05, <0.01, and <0.001, respectively.

All results were presented as mean ± standard deviation. Unpaired t-test was performed using SigmaStat statistical software. Differences were statistically significant at $P<0.05$.

2.3 Results and discussion

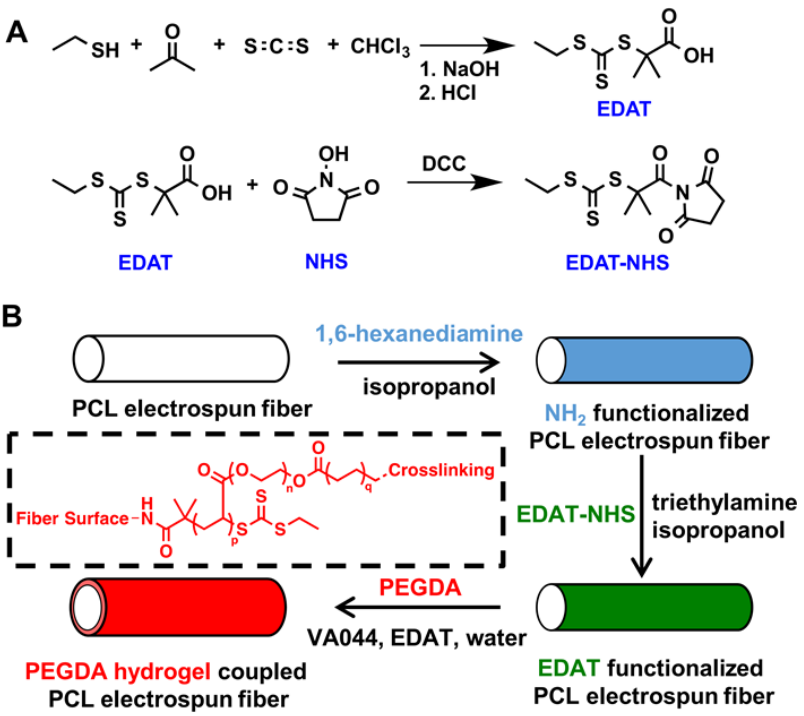

Figure 2.1 (A) Synthesis and functionalization of the chain transfer agent, EDAT. (B) Schematic illustration of the RAFT polymerization of PEG-DA on the PCL electrospun fiber surface. (Wang J Y, et al. ACS Biomaterials Science & Engineering, 2016.)

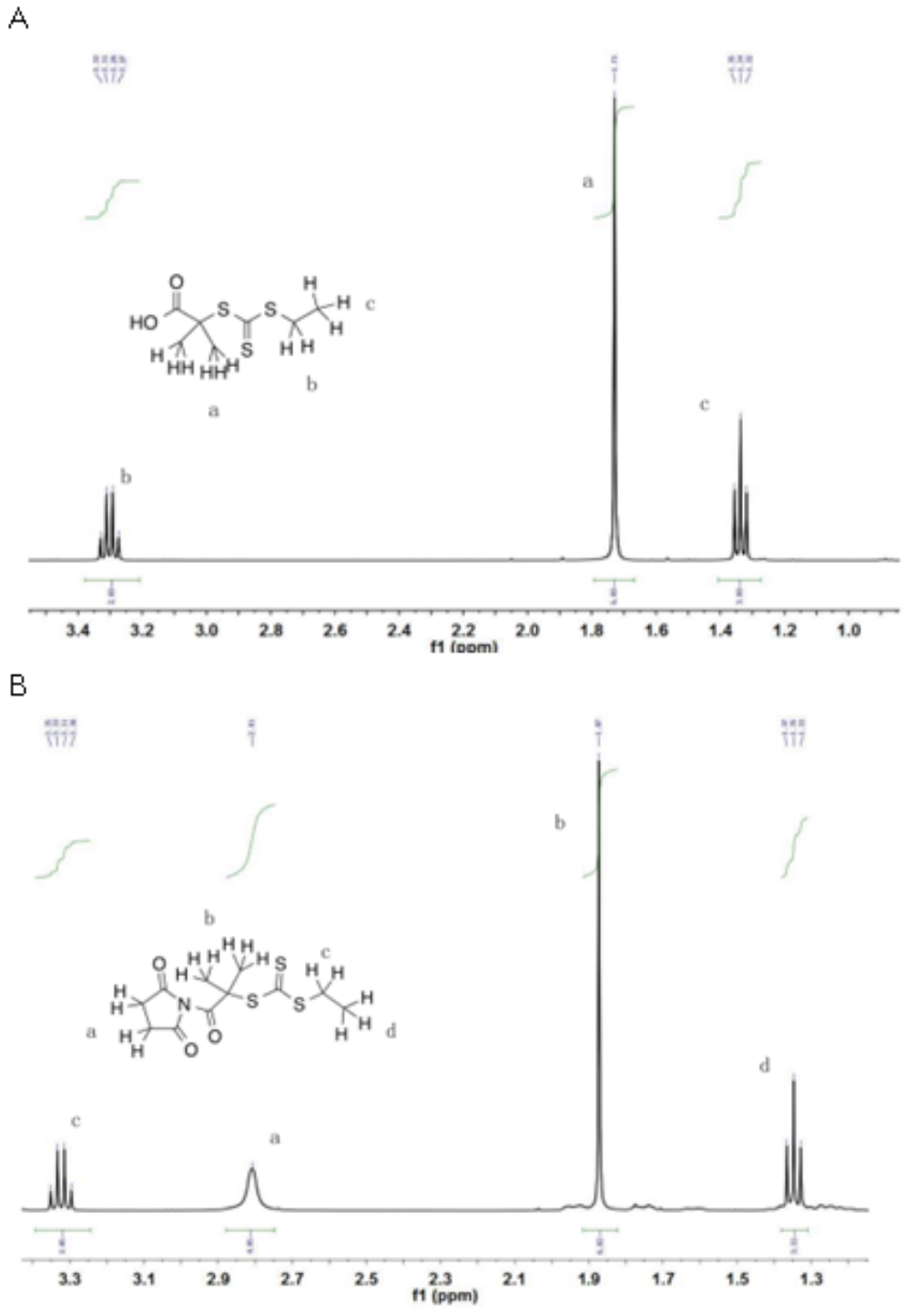

Figure 2.2 (A) ^{1}H-NMR spectrum of EDAT, (B) ^{1}H-NMR spectrum of EDAT-NHS(Wang J Y, et al. ACS Biomaterials Science & Engineering, 2016.)

The reactions and process for fabricating the hybrid PEG-PCL materials is schematically illustrated in **Figure 2.1 A**. The EDAT and EDAT was successfully

synthesized and confirm through ^{1}H-NMR (**Figure 2.2 A** and **B**). The quantity of NH_2 group after aminolysis of PCL fiber was confirmed through ninhydrin assay (**Figure 2.3**). The incorporation of PEG in the electrospun fibers was investigated via FTIR spectroscopy. Given that C–O bonds were more abundant in PEG than in PCL, the absorption peak near 1100 cm^{-1} corresponding to the C–O stretching band was used to identify the PEG component. As shown in **Figure 2.4**, higher peak intensities at 1100 cm^{-1} were observed in the PEG-modified PCL samples and the intensity increased with the initial PEGDA concentration, which may be due to higher amounts of PEG in the hybrid matrices.

The incorporation of PEG was also investigated via imaging the fiber morphology, which was found to vary with the PEG concentration. The pristine PCL electrospun matrices contained the typical non-woven microfibers bearing relatively smooth surfaces, with the fiber diameters around 1.5 μm. (**Figure 2.5 A**) In the 5% PEG-PCL samples, the fibrous morphology was preserved, but the fiber surface became rough with some cornered region filled with gel-like materials; the average fiber diameter increased to 1.9 μm. When the PEG-DA concentration was improved to 7.5%, the fibrous morphology was also clearly maintained, but all the fibers were covered with heavily wrinkled skin layers with the average fiber diameter reaching approximately 3.5 μm. (**Figure 2.5 B**) The fibrous structures were unobservable in the 15% PEG-PCL samples; instead, the matrix exhibited a gel-like morphology containing closed pores with size of around a few micrometers. It was assumed that if the fibers were wrapped homogeneously with PEG hydrogels, the PEG thickness was around 180 nm and 1 μm in the 5% PEG-PCL and 7.5% PEG-PCL matrices, respectively. The morphology suggests that the RAFT polymerization occurred and localized on the fiber surfaces. Interestingly, the wrinkles in the 7.5% PEG-PCL may be caused by the shrinkage of the hydrogel coatings on the PCL surface under the vacuum- drying condition, given that

wrinkling is a characteristic surface behavior of an elastic film when the surface bends over compressed substance (e.g. water) on rigid surfaces.

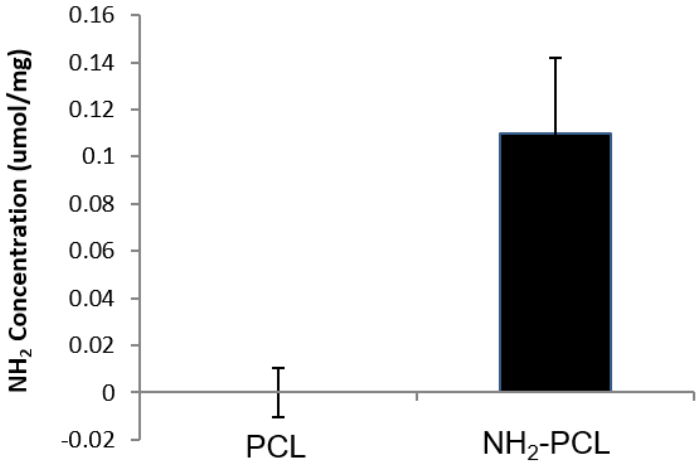

Figure 2.3 Analysis of the amine content in PCL fibers after aminolysis(Wang J Y, et al. ACS Biomaterials Science & Engineering, 2016.)

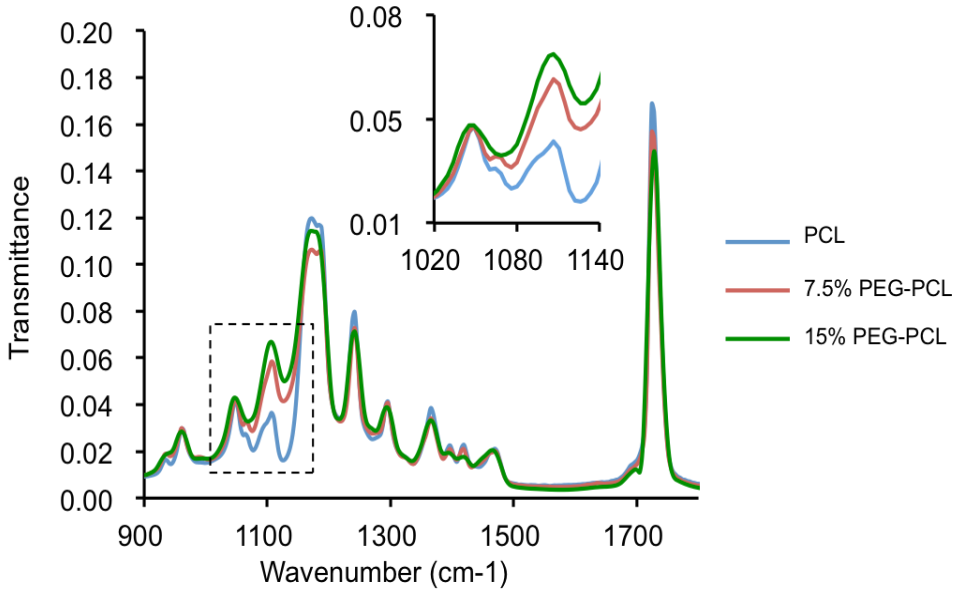

Figure 2.4 FTIR spectra of 15% PEG-PCL (green), 7.5% PEG-PCL (red) and PCL (blue) samples. The enhanced peak at 1100 cm^{-1} corresponding to the C–O bonds in PEG (Wang J Y, et al. ACS Biomaterials Science & Engineering, 2016.)

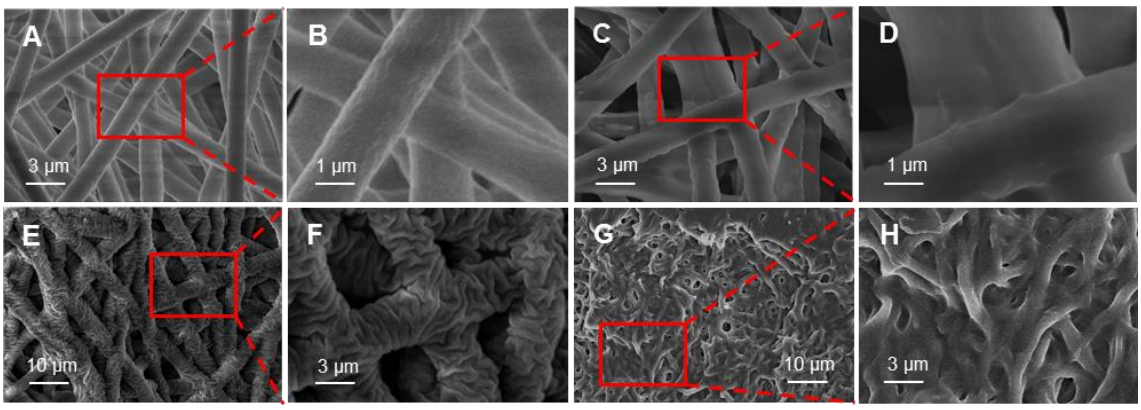

Figure 2.5 SEM images of PCL electrospun fibers and different hybrid matrices. (A and B) pristine PCL fibers, (C and D) 5% PEG-PCL, (E and F) 7.5% PEG-PCL, (G and H) 15% PEG-PCL. The boxed areas in A, C, E and G are magnified in B, D, F and H respectively. (Wang J Y, et al. ACS Biomaterials Science & Engineering, 2016.)

Table 2.2 The average fiber diameter, the water contact angle, water uptake and PEG mass percentage of PCL electrospun fibers and different hybrid matrices. (Wang J Y, et al. ACS Biomaterials Science & Engineering, 2016.)

Sample	Fiber diameter (μm)	Water contact angle (°)	Water uptake (%)	PEG mass in the hybrid (%)
PCL	1.577 ± 0.139	119.3 ± 5.8	0 ± 0	-
5% PEG-PCL	1.935 ± 0.180	-	53.7 ± 4.6	2.83 ± 0.24
7.5% PEG-PCL	3.543 ± 0.375	-	140.2 ± 19.4	11.4 ± 1.6
15% PEG-PCL	-	-	114.6 ± 5.5	20.2 ± 0.97

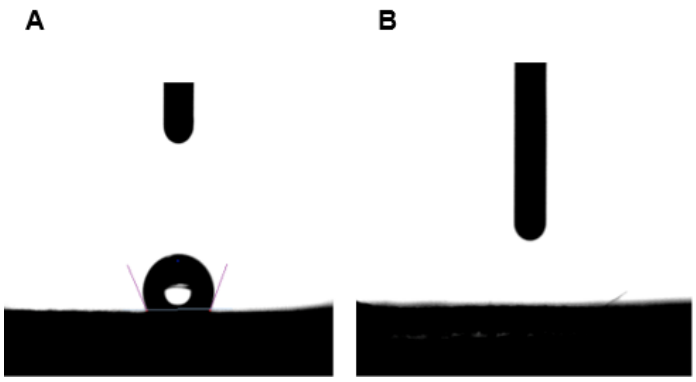

Figure 2.6 Images of measuring water contact angles of (A) PCL electrospun fibers and (B) 7.5% PEG-PCL, with 7.5% PEG-PCL showing a highly hydrophilic surface (Wang J Y, et al. ACS Biomaterials Science & Engineering, 2016.)

The incorporation of PEG also increased hydrophilicity of the original matrices. When in contact with water droplets, the PCL fibers were water-repelling and relatively large contact angles recorded. In all the PEG-PCL composite samples, the water droplets were observed to wet the surface instantly, thus the composite materials are highly hydrophilic. More interestingly, it was noted that the PEG-PCL samples were capable of absorbing water and the amounts of water in the matrices were measured from 50% to 140% of the mass of the dry matrices. Among the three types of composites, 7.5% PEG-PCL seemed to have highest level of water uptake, although no statistical difference between 15% PEG-PCL and 7.5% PEG-PCL was observed. (**Table 2.2**) As the hydrogel layers around the fibers were relatively thin and all matrices were porous, the matrices achieved equilibrium with water within a few seconds and no swelling or deformation was visually noticeable. The resulting composite materials thereby are superior to pure hydrogels in terms of the ability to allow fast-speed water absorption while maintain micro- and macro-scale shapes/structures: the porosity and scaffold-like micro-structure were basically unchanged during the wetting/swelling process.

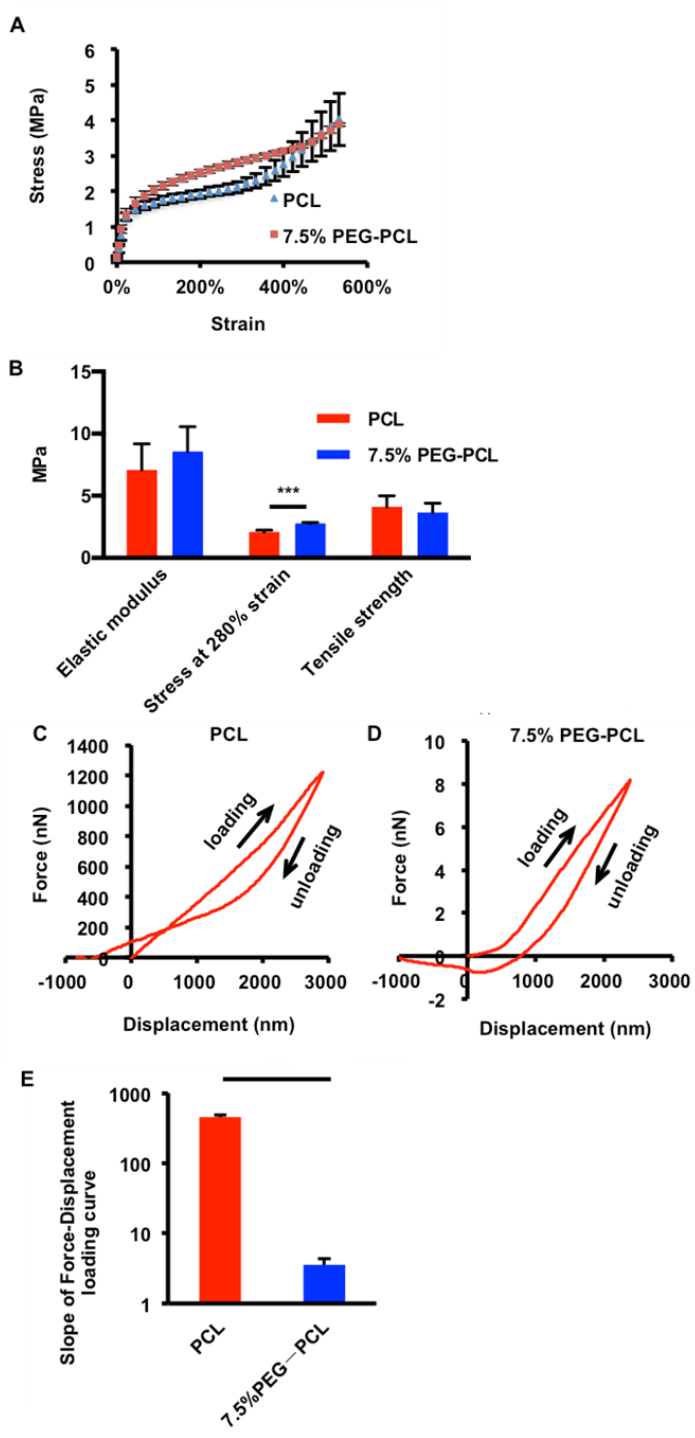

Figure 2.7 (A) Averaged tensile stress–strain curves of 7.5% PEG–PCL and PCL electrospun fibers. (*n* = 4, mean ± STD). (B) Comparison of elastic modulus, stress at 280% strain and tensile strength according to tensile tests in A. (C, D) Representative force–displacement curves obtained from AFM indentation tests on PCL and 7.5% PEG–PCL electrospun fibers, respectively. (E) Comparison of force/displacement ratio in the loading curve in C and D (*n* = 9, mean ± STD; *: *p* < 0.001) (Wang J Y, et al. ACS Biomaterials Science & Engineering, 2016.)**

Mechanical properties are essential to the function/performance of biomaterials *in vitro* and *in vivo*. To understand how the PEG sheath alters the mechanical properties of electrospun fibrous matrices, tensile and AFM indentation tests were performed to characterize the macroscopic and local mechanical properties of the materials, respectively [89,90]. 7.5% PEG-PCL samples, the matrices containing PCL fibers with relatively thick PEG hydrogels, were compared with pristine fibrous PCL. It is seen that the tensile stress-strain curves of PEG-modified or non-modified matrices both show the mechanical characteristics of ductile materials. (**Figure 2.7 A**) At low strain levels, the two types of materials exhibited similar Young's moduli. (**Figure 2.7 B**) After the yield point--approximately at 40% elongation, the stress continued to increase on the account of strain hardening. However, higher stresses were observed in 7.5% PEG-PCL than the pristine PCL samples; in particular, the stress at 280% strain was approximately 33% higher. (**Figure 2.7 B**) It is speculated that the extra stress in stretching the composite matrices may originate from the compressed hydrogels between PCL fibers and were orthogonal of the stretching direction. When the plastic necking started, the curves coincided again and the two types of materials showed approximately the same stress and strain near rupture. (**Figure 2.7 A and B**) These results suggest that the PCL dominates the macroscopic property of the composite materials, and the high moduli and strechability characteristic of plastic materials were maintained in the hybrids.

In contrast to the tensile tests, the AFM indentation applies indentation to a small area on material surfaces and measures the load force and surface displacement. The data thereby reflects the local or surface mechanical properties of materials. **Figure 2.7 B** shows the representative indentation force-displacement curves recorded for 7.5% PEG-PCL and PCL samples. It is noted that within the dis-placement of a few micrometers, the forces indenting

the 7.5% PEG-PCL matrices–at the scale of only a few nano Newtons–were much smaller than the PCL samples. The linear fitting of the loading curves showed that the force-displacement slope of the PCL was over two orders of magnitude greater than 7.5% PEG-PCL. This result indicates that different from the macroscopic behavior, the mechanics at the fiber surface is determined by the hydrogel components.

Hydrogels often demonstrate superior biocompatibility due to the advantage of hydrophilic surfaces in mediating the interactions with proteins and tissues. As the surface is prone to repelling the protein adsorption, hydrogel surfaces often show minimal adhesion to cells and tissues. When cells were seeded on the 7.5% PEG-PCL and PCL matrices, the cells formed aggregates on the former while adhered and spread on the latter, indicative of low cell adhesion on PEG-modified PCL fibers (**Figure 2.8**).

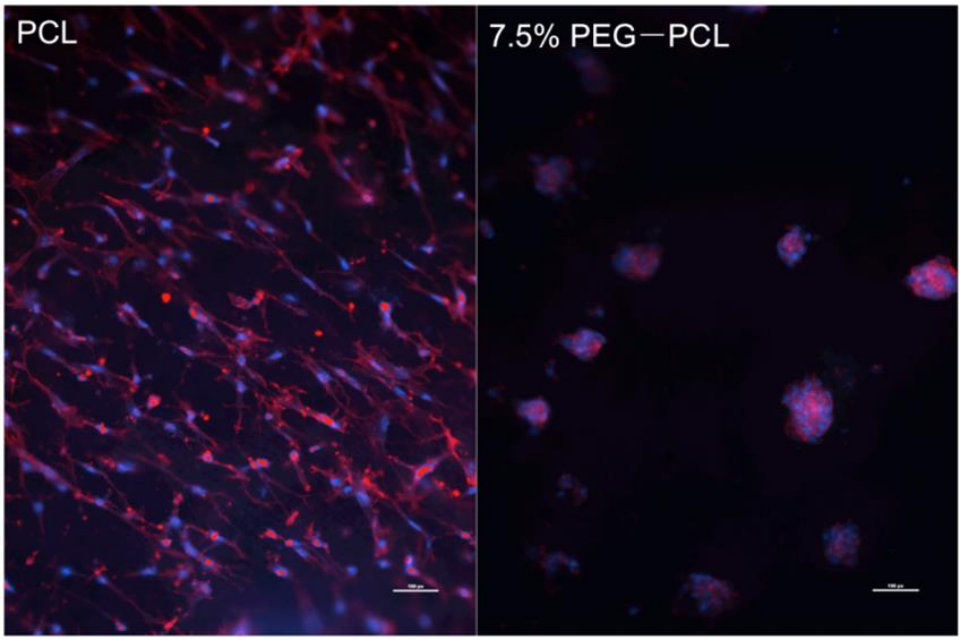

Figure 2.8 Representative images of hADSCs seeded on PCL and 7.5% PEG-PCL membranes. Cells were fixed and stained with rhodamine-phalloidine and DAPI to show F-actin (red) and nucleus (blue), respectively. (Scale bar: 100 μm) (Wang J Y, et al. ACS Biomaterials Science & Engineering, 2016.)

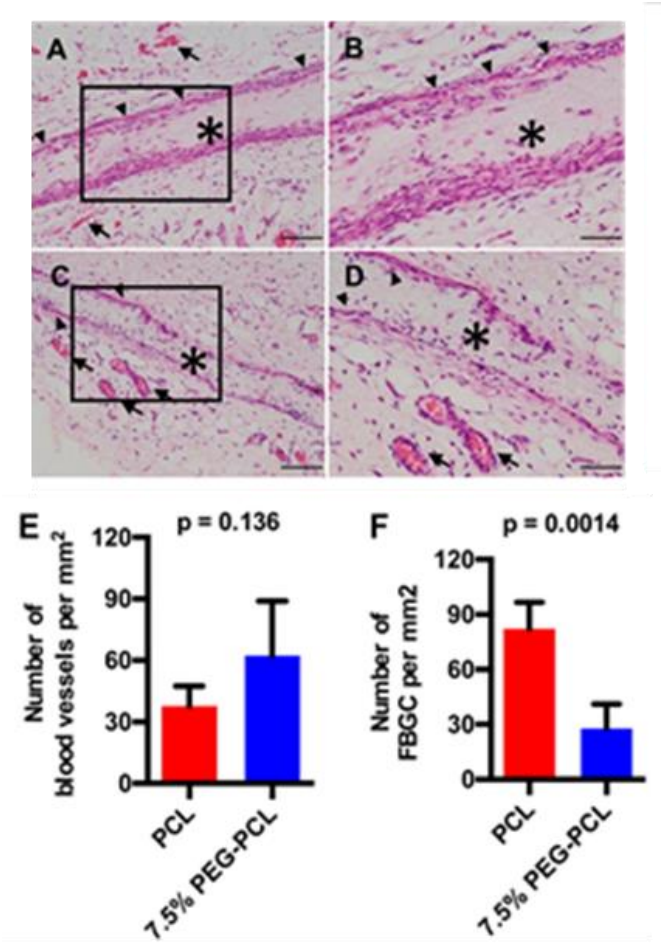

Figure 2.9 Representative H&E stained histological sections of explanted PCL matrices (A, B) and 7.5% PEG-PCL (C, D) after four-week subcutaneous implantation. The boxed areas in (A) and (C) are magnified in (B) and (D), respectively. Asterisks, arrows and arrowheads indicate the area of matrices, blood vessels and foreign body giant cells (FBGCs), respectively. Scale bars: 100 µm (A, C) and 50 µm (B, D). E) and F), quantitative and statistical analysis of the number of FBGCs (E) and blood vessels (F) surrounding the implants, respectively. Data were analyzed using unpaired Stu-dent's t-test. (n = 4, mean ± STD). (Wang J Y, et al. ACS Biomaterials Science & Engineering, 2016.)

The 7.5% PEG-PCL and PCL electrospun membranes were implanted subcutaneously at the abdominal site in rats to further investigate the biocompatibility of the composite materials in vivo. In the micrographs of the histological sections (Figure 2.9 A-D), fewer number of macrophage/foreign-body giant cells (FBGCs) (Figure 2.9 E) were found in 7.5% PEG-PCL PCL in comparison to PCL matrices following the 4-week implantation. Interestingly, like the PCL matrices, the 7.5% PEG-PCL matrices also allowed cell invasion

with small blood vessels observable at the tissue-implant interface. (Figure 2.9 F) The result suggests that the PEG modification did improve the biocompatibility of electrospun fibers without hampering the original porous structure necessary for cell scaffolding.

RAFT polymerization has been investigated for creating various biomaterials such as bioactive polymers/conjugates for drug delivery applications [91-95] and surfaces that prohibiting adhesion of bacteria [96]. Here, it is the first time that RAFT polymerization was performed to synthesize hydrogel coatings on the surface of plastic fibers. Given the low toxicity of the initiator and CTA, the mild polymerization conditions should also be cytocompatible. The methodology thereby is potentially applicable to fabricating materials in presence of biomolecules and cells.

In addition to the methodology, the PEG-modified matrices demonstrate a new type of porous hybrid material. In the literature, the main approaches to fabricate fiber-hydrogel composites include: 1) directly embedding preformed electrospun fibers in hydrogel precursor solutions and crosslinking the hydrogel reagents [97-101] and 2) dual electrospinning/electrospray, in which the polymer and hydrogel precursor solutions were simultaneously electrospun/electrosprayed on the collector and then crosslinked [102-104]. These methods led to materials in which fibers and hydrogels were physically blended together [105-109].

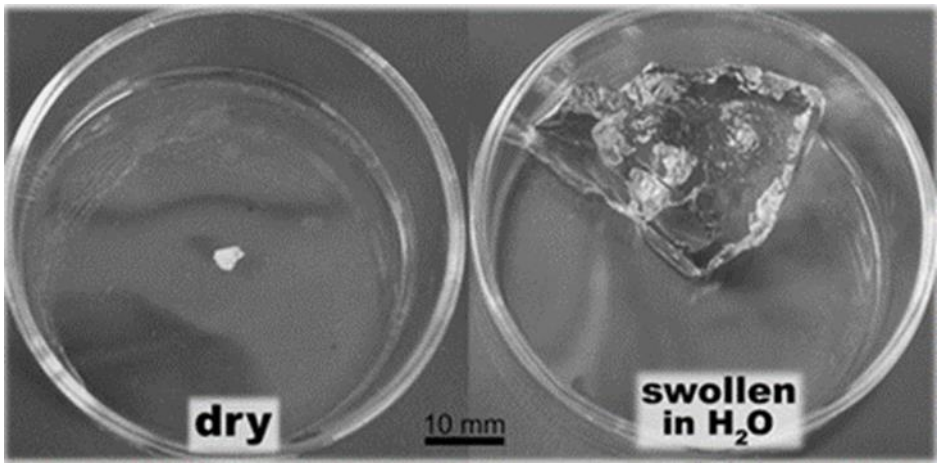

Figure 4.10 Swelling of traditional hydrogels after hydration. (Zhong X, Dehghani F.. Green Chemistry, 2012, 14(9): 2523-2533.)

In our study, hydrogel was chemically bonded to the fiber surface and thereby is relatively stable in the hybrids. More importantly, since the hydrogel coatings on PCL fibers were nanothin, the pores in the original PCL matrices were preserved (5% PEG-PCL and 7.5% PEG-PCL). This allows anchored expansion of the thin hydrogel coating layers, and the process did not cause visible changes to the gross volume, macroscopic structures or the bulk mechanical property of the matrix. In contrast, upon hydration, conventional hydrogel matrices often experience significant expansion of the volume/shape and drop of mechanical properties. The hybrid materials created here therefore present plastic fibers capable of "invisible" hydrogel swelling due to the unique thin coating structure.

The materials developed in this study can be used as scaffolds or to guide specific interactions with cells. The mechanical characterization suggests that PEG-modified PCL matrices exhibit plastic strechability with a low surface elasticity, indicating a composite property that is otherwise non-achievable through plastics and hydrogels alone. The electrospun fibers therefore provide a unique type of cell-invasive scaffolds containing high-strength plastic fibers with the surface hydrogels mimicking soft tissues. The properties of

both the skeleton and the surface hydrogels can be tuned for induction of beneficial cell responses. The CTA remaining on the hydrogel surfaces also have the potential to allow tethering of other molecules for specific biological activities such as adhesiveness toward cells [110]. It is also possible to incorporate therapeutics in the plastic skeleton or the gel layer for designing drug-delivery devices.

2.4 Conclusion

To summarize, a new type of fibrous matrices with microfibers ensheathed with hydrogels of controllable thickness was successfully developed through a RAFT polymerization of PEG oligomers on the surface of PCL electrospun fibers. The hybrid materials exhibit versatile mechanical properties, surface biocompatibility and cell-material interactions that reflect the features of the composite fibrous structure. The facile, water-based methodology is applicable to modifying the surface of other types of porous or non-porous materials to create hybrid materials, and the nondeformable, water-absorbing fibrous materials can find applications in a wide range of biomedical devices.

CHAPTER 3. DEVELOPMENT OF MICRO-WELL ARRAY PATTERNED SCAFFOLDS AND THEIR APPLICATION IN MESENCHYMAL STEM CELL TRANSPLANTATION

3.1 Introduction

To better mimic the natural ECM structure, classic scaffolds such as electrospun fibers and hydrogels are commonly designed to have pores of a few microns in diameter. Such micro-structures usually affect the cells on a cellular/subcellular level by modulating the local biochemical, biomechanical, and mass transport microenvironment to promote cell viability and function. With the rapid advancement in stem cell technologies, different microscale tissues or organoids have been produced through scalable processes. These microtissues often exhibit superior therapeutic functions to single cells. To successfully transplant those microtissues, scaffolds should have the ability to not only control microenvironments on cellular/subcellular level, but also manipulate their spatial distribution on a larger scale (hundreds of microns to a few millimeters) to promote efficient vascularization and prohibit hypoxia and insufficient nutrient supply caused by random cell clumping. In this chapter, the design of a scaffold with control over both microenvironments and spatial distribution by fabrication of microwell patterned electrospun fibers will be demonstrated. The scaffolds' potential in microtissue transplantation by transplanting MSC spheroids in a mouse model of hind limb ischemia is also discussed in this chapter.

Stem cell therapy has gained vast interest recent years as a promising approach for a various of diseases. ES, iPSCs and MSCs are the main candidates in stem cell therapy.

Unlike ES and iPSCs, MSCs have no ethical concerns and no potential for teratoma formation and much less complicated preparation process, which made them the most studied cell source for stem cell therapy [111-117].

However, currently a major challenge in MSCs therapy is the low cell retention and viability. In most studies, MSCs were administered as single cell suspension through systemic or local injection [118,119]. Though MSCs possess the ability to home to pathological tissue after systemic infusion, the efficiency is usually very low and most cells were found trapped in capillaries of organs such as lung, liver and spleen [120,121]. During local injection, in a common case where MSCs are delivered in closed space like muscle, cells suspensions are likely to leak from the injection hole due to backpressure [122]. After injection, large amount, up to 85% of cells were lost by acute wash out into circulation within hours and those retained at injury site had to stand the ischemic and inflammatory environment, which further reduced cell survival [123]. In most studies, injected MSCs disappeared within 7 days.

Cell premodification is a common approach to improve cell viablity after transplantation. There are techniques such as hypoxia preconditioning [124-126], genetic modification through overexpressing prosurvival genes [127-131] or cell surface modification of adhesive peptides [132]. I am particularly interested in exploiting the application of the 3D assembly of MSCs, MSC spheroids. Several studies including ourselves' have found that the three dimensional (3D) MSC spheroids have improved paracrine function as their anti-apoptosis, angiogenic and anti-inflammatory genes are greatly upregulated and higher amounts of corresponding factors are secreted compare to single layer cell culture [133-135]. This functional enhancement is likely due to the increased cell-cell, cell matrix interaction and the mild hypoxic environment inside the spheroid. The upregulated paracrine factors

could benefit both cell survival and therapeutic effect after transplantation. In addition, because of the increased cell density of spheroids, the released paracrine factors would also have a higher local concentration, resulting a more protective local environment [136].

Manipulation on cells alone can hardly ameliorate the low cell retention caused by mechanical dispersion. Therefore, biomaterials based cell delivery strategy was developed to solve this problem. The pre-established cell-material adhesion could provide protection against acute cell loss. In clinical MSC therapies, smaller transplantation volume with higher cell transplantation density is greatly desired due to 1) a smaller transplantation volume could reduce the chance of leaking and mechanical dispersion when cells are injected to a tissue with limited space, which would increase the cell retention in physiological area, 2) higher local cell concentration could generate higher paracrine factor concentration and benefit therapeutic outcome. However, high cell density would inevitably cause random cell clumping that leads to hypoxia and decrease cell viability, especially when multicellular spheroids are applied. In order to achieve both high cell density and good cell viability, spatial regulation of cells is required.

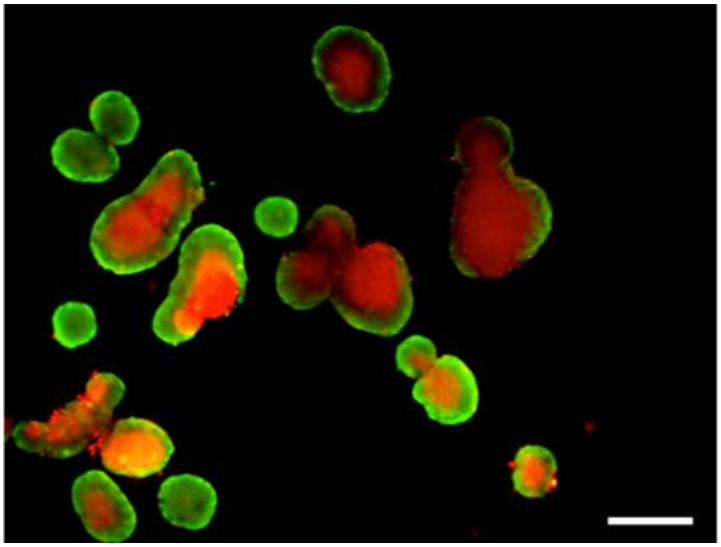

Figure 5.1 Cells death caused by random cell clumping. (Red: dead cells, Green: living cells, Wang X, Wang K, Zhang W, et al. Biomaterials, 2017.)

Conventional foam-like or nonwoven fibrous scaffolds could provide microenvironments on cellular level, however, they may lack control spatial organization of cells/microtissues. Micropatterning technique can regulate the spatial regulation of cells. However, most micropatterning technology were conducted on PDMS or hydrogels. PDMS lacks control of microenvironment and is limited in mass transfer. Hydrogels are weak in mechanical strength, as has been addressed intensively in this dissertation. Therefore, in this study, I seek to develop a scaffold with control of both microenvironment and spatial distribution. To achieve his goal, micropatterning was introduced on electrospun fibers. MSC spheroids together with the micropatterned scaffold were further transplanted in a mouse model of hind limb ischemia with focus on ameliorating cell retention and tissue vascularization.

3.2 Materials and methods

Materials

Polycarbonate-polyurethane copolymer was achieved from DSM biomedical company (Berkeley, CA, USA). Tetrahydrofuran (THF) and dimethyl formamide (DMF) were purchased from Beijing Chemical Works (Beijing, China). The cell culture plates and low-attachment culture plates were from Corning (NY,USA). Dulbecco's phosphate-buffered saline (DPBS) was purchased from Invitrogen (Carlsbad, CA, USA). Bone marrow derived MSC from BALB/C and culture reagents were purchased from Cyagen (Santa Clara, CA, USA). The suppliers of other chemical and biological reagents are specified in the text below.

Fabrication and characterization of microwell-patterned scaffold

The microwell-patterned scaffold was fabricated by a combination of electrospinning and micromolding method. **Figure 1A** illustrates the fabrication of microwell-patterned scaffold. Briefly, conductive PDMS replicas were fabricated by curing the mixture of PDMS prepolymer, crosslinking catalyst and conductive carbon black on microwell patterned master silica wafer. 8% (w/v) CarboSilTM thermoplastic silicone polycarbonate urethane (TPU) solutions were prepared by dissolving the TPU in a 3:2 (v/v) mixture of tetrahydrofunan (THF) and N, N-dimethylformamide (DMF). The TPU solution was electrospun onto the conductive PDMS replica. The flow rate of the syringe pump was set at 0.5 mL/h, the distance between the needle and the PDMS collector was 13 cm and the voltage was 12 kV. The microwell patterned scaffolds were achieved by peeling off the membrane from the PDMS collector. To study the morphology of PU-mw, membrane samples were gold sputter-coated and examined by the scanning electron microscope (SEM) (S-4800, Hitachi, Japan).

Generation and Loading of MSC spheroids

To generate the MSC spheroids, MSCs were seeded on an ultra-low attachment 24-well microplate at 100,000 cells per well. The microplate was placed on an orbital shaker and rotated at 160 rpm for 1 h and placed in incubator for another 23h.

Before loading spheroids, scaffolds were placed on the bottom of a 24-well microplate, with the microwells facing upwards. Then they were washed thoroughly in 75% ethanol and DPBS 3 times each and left to dry. MSC spheroids collected from aspiration from 4 wells were combined together. After centrifugation at 500 rpm for 5 min, spheroids were resuspended in 500 μL medium. The spheroids suspension was added to the scaffold followed by another centrifugation at 500 rpm for 5min. After incubation for 24 h, spheroids seeded scaffold were stained with DAPI and FITC-phalloidin and observed under confocal microscope (Zeiss LSM 510, Oberkochen, Germany).

Real-time PCR assay

The MSC spheroids or monolayers cultured for 24 h were collected and homogenized. The total RNA was extracted from 4×10^5 cells using the RNeasy® Mini kit from Qiagen (Hilden, Germany) according to the manufacturer's instructions. After the determination of RNA concentration by Biophotometer (Eppendorf, Hamburg, Germany), 2 μg of the pure total RNA was transferred and reverse transcribed. The primers are listed in the Supplementary Material. The gene expression levels were then quantified and analyzed using the SYBR Green real-time polymerase chain reaction (PCR) method by the Applied Biosystems StepOnePlus PCR system (Foster City, CA, USA). The primers were all obtained from Qiagen. Copy numbers of each gene were calculated by standard curve method. All gene expression values were normalized to 18S level. Each RNA sample was analyzed in triplicate.

Transplantation of MSC spheroids in mice model of hindlimb ischemia (HLI)

All protocols were approved by the Institutional Animal Care and Use Committee of Emory University. Male 129 mice (Charles River, MA, USA), 8 weeks old were used. The mice were anaesthetized with 1–2% isoflurane. The superficial femoral artery and vein were ligated proximal to the deep femoral artery and tibial arteries, and the portion between the ligation points was excised. Before transplantation of MSC spheroids seeded scaffolds or scaffold alone, each scaffold was cut to 0.4 cm^2 semi-circle to fit the shape of thigh muscle. During transplantation, each scaffold was rinsed in DPBS and placed on top of the thigh muscle with microwells facing towards to the muscle tissue right after the excision of artery. For MSC or MSC spheroids groups, 2×10^5 cells or spheroids with equivalent cell number were suspended in 40 μL DPBS and injected into the ischemic thigh muscle.

Measurements of hindlimb perfusion by laser-Doppler perfusion imaging (LDPI)

LPDI with a laser of 810 nm (MoorLDI, Moor Instruments, Wilmington, DE, USA) was used to evaluate perfusion at various days after HLI. The perfusion ratio was calculated by dividing the mean perfusion of thigh and proximal leg in the ischemic leg by that in the non-ischemic leg for each animal.

Histology and the determine of blood vessel density

Animals were sacrificed by CO_2 inhalation at 7 days after HLI. Sections from ischemic thigh were obtained after fixation in formalin and embedment in paraffin. To stain the blood vessels, sections were deparaffinized and stained with a primary antibody, biotinylated lectin (Vector Laboratories, Burlingame, CA, USA), followed by a second antibody, streptavidin conjugated quantum dot 655 (Invitrogen, Carlsbad, CA, USA). The sections were mounted

with DAPI and observed under fluorescent microscope (Axioskop 2 Plus, Zeiss) using long pass filter.

Bioluminescence imaging

MSCs were transduced with a lentivirus expressing firefly luciferase, GFP and blasticidin resistance under the control of the constitutively active cytomegalovirus and respiratory syncytial virus promoters, respectively (GenTarget, San Diego, CA). 72 h after transduction, MSCs were transferred into standard media containing 10 μg/mL blasticidin (Sigma-Aldrich, St. Louis, MO, USA). Luciferase expression was confirmed with the GFP under fluorescence microscope. Animals were intraperitoneally injected with luciferin 40 mg/kg 30 min before imaged using Bruker in-vivo Xtreme imaging system (Billerica, MA, USA). Luminescence was quantified in the thigh region using Bruker molecular imaging software.

Statistical analysis

All quantitative measurements were presented as mean ± standard deviation (SD). The one-way analysis of variance followed by Tukey's post hoc analysis was performed to compare the multi-group data. The unpaired t-test was performed when the data was consisted of only two groups. The level of significance was labeled by *, ** and ***, denoting the p value of <0.05, <0.01, and <0.001, respectively.

3.3 Results

Fabrication of microwell-patterned scaffold

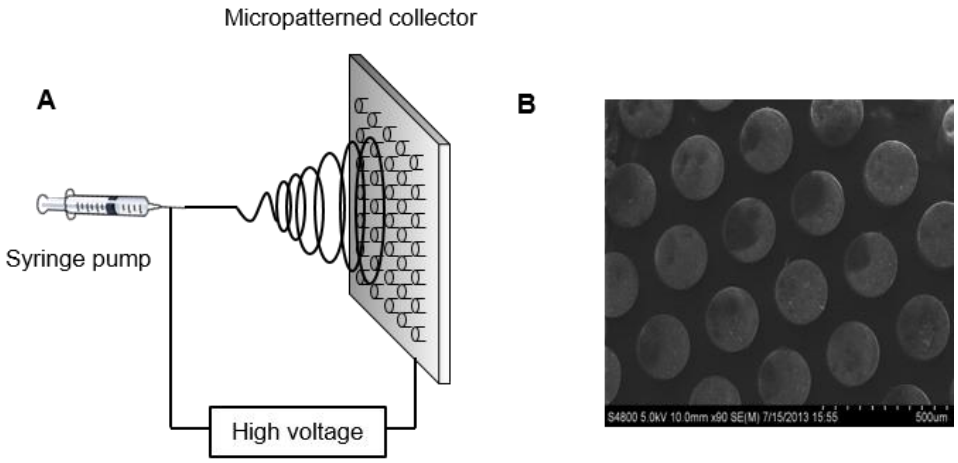

Figure 3.2 (A) Illustration of the electrospinning process. (B) SEM image of micropatterned collector

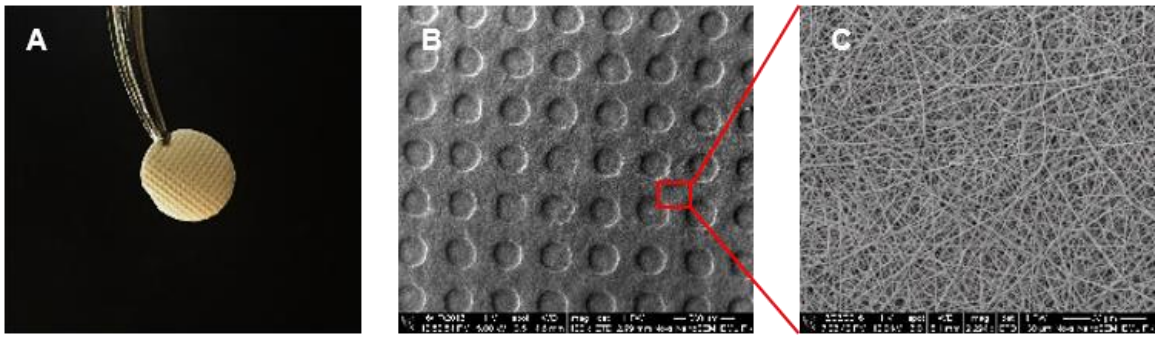

Figure 3.3 Macroscopic (A) and SEM images (B and C) of microwell patterned scaffold.

Figure 3.3 shows the macro and micro structure of the microwell-patterned scaffold. The scaffold is composed of electrospun fibers with diameters of 0.28 ± 0.05 μm. The microwell patterns on scaffold were introduced by micro-molding. Microwells were created as complementary to the micro-pillar patterns on PDMS replica. The microwells were of 200 μm in diameter and 50 μm in depth and were created with a 400-μm center-to-center distance in squared arrays. This scaffold also possesses good mechanical property and can be handled conveniently.

Characterization of MSC spheroids on microwell-patterned scaffold

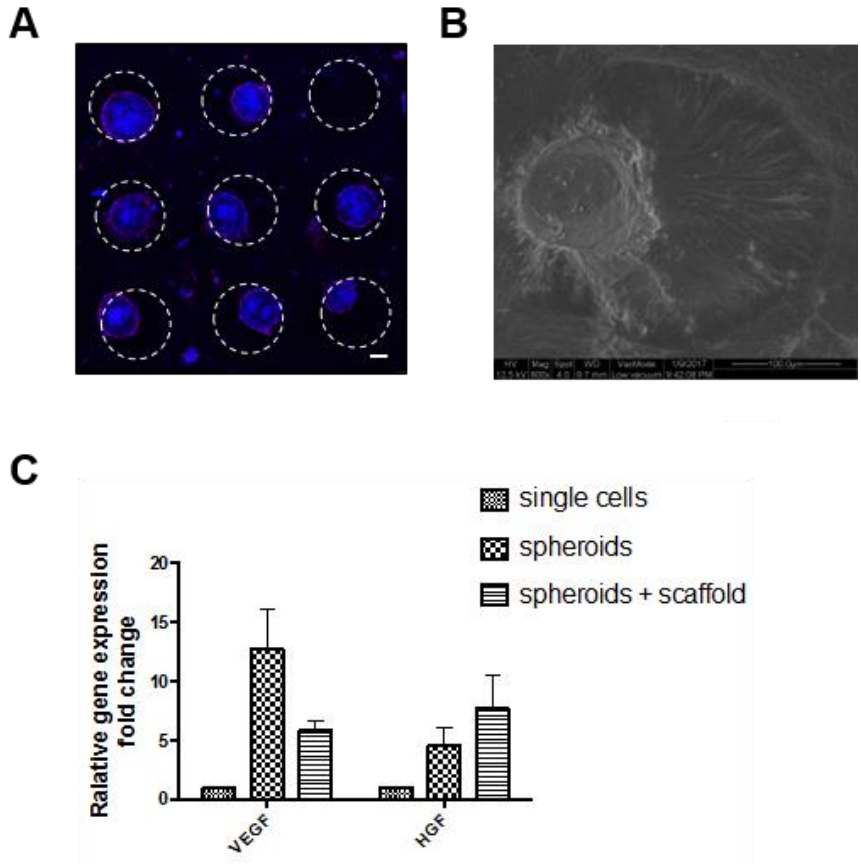

Figure 3.4 Characterization of MSC spheroids on microwell patterned scaffolds. (A) Spheroids were spatially regulated in microwell arrays. (Blue: DAPI Red: Phalloidin) (B) The spherical structure of the MSCs in micro well. (C) MSC spheroids on scaffold had upregulated paracrine gene expression.

Multicellular MSC spheroids were formed after 24 h culture on low-adhesive culture plate. The average size of the spheroids is 150 μm in diameter. After being seeded onto scaffold, the spheroids were found homogeneously distributed in microwells and maintained their spherical structure under fluorescent microscopy (**Figure 3.3 A**). At the bottom of the spheroids, cell spreading on scaffold was observed, indicating the attachment of the spheroids with scaffold. The gene expression of VEGF and HGF was then tested, the two

important factors in angiogenesis and antiapoptosis, in MSC spheroids, MSC spheroids on scaffolds and 2-D cultured MSCs. In expression of VEGF, MSC spheroids on scaffolds showed a 5.9 fold increase over 2-D cultured MSCs and no significant difference with MSC spheroids. In expression of HGF, there is a decrease when spheroids are seeded on scaffolds but they still exhibited a markedly 4.6 fold difference over 2-D cultured MSCs (N = 3, n = 3).

Cell retention of transplanted MSCs in mice model of HLI

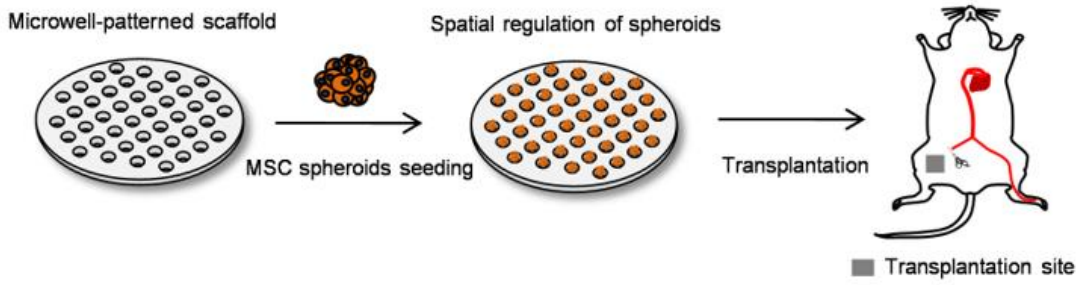

Scheme 3.1 The design of MSC spheroids loaded microwell-patterned scaffold in mice hindlimb ischemia model.

To investigate in vivo cell retention, MSCs transduced with luciferase were transplanted. The intensity of luminescence generated by transduced MSCs positively correlates with the number of cells that express luciferase. It was found that spheroids seeded on scaffold had a significant 6.7 fold higher luciferase intensity over injection of MSC single cells and 6.3 fold higher over injection of MSC spheroids at hours after transplantation. In groups where cells were transplanted without scaffold, no signal can be detected after 7 days. In contrast, the MSC spheroids transplanted with microwell-patterned scaffold survived over 14 days.

Evaluation of the in vivo vascularization efficacy of MSC spheroids loaded microwell patterned scaffold

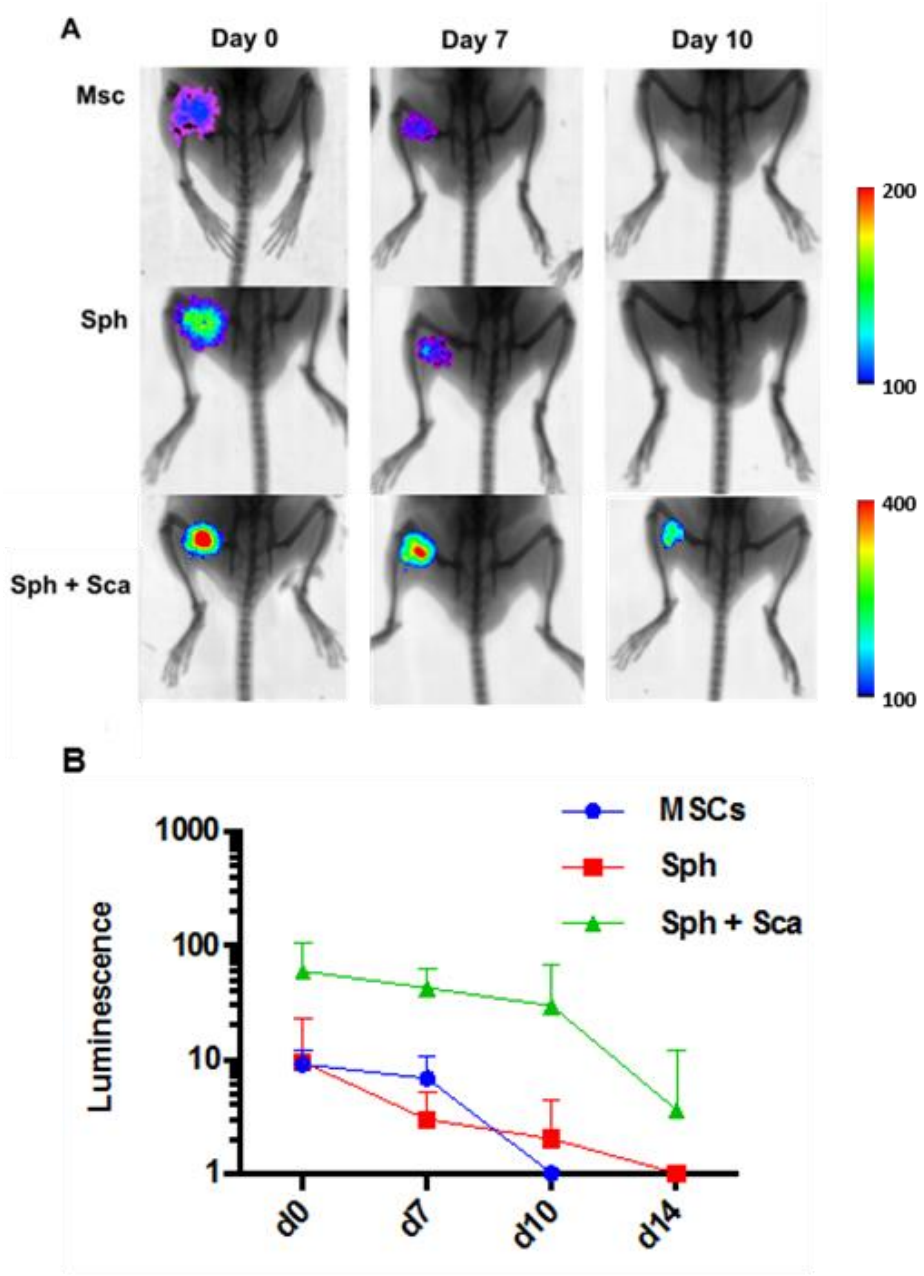

Figure 3.5 In vivo optical bioluminescence imaging (BLI) for determination of cell retention and survival of MSCs. (A) BLI image representative animals from each group at different time point (B) Quantification of BLI signal in regions of interest over the ischemic leg.

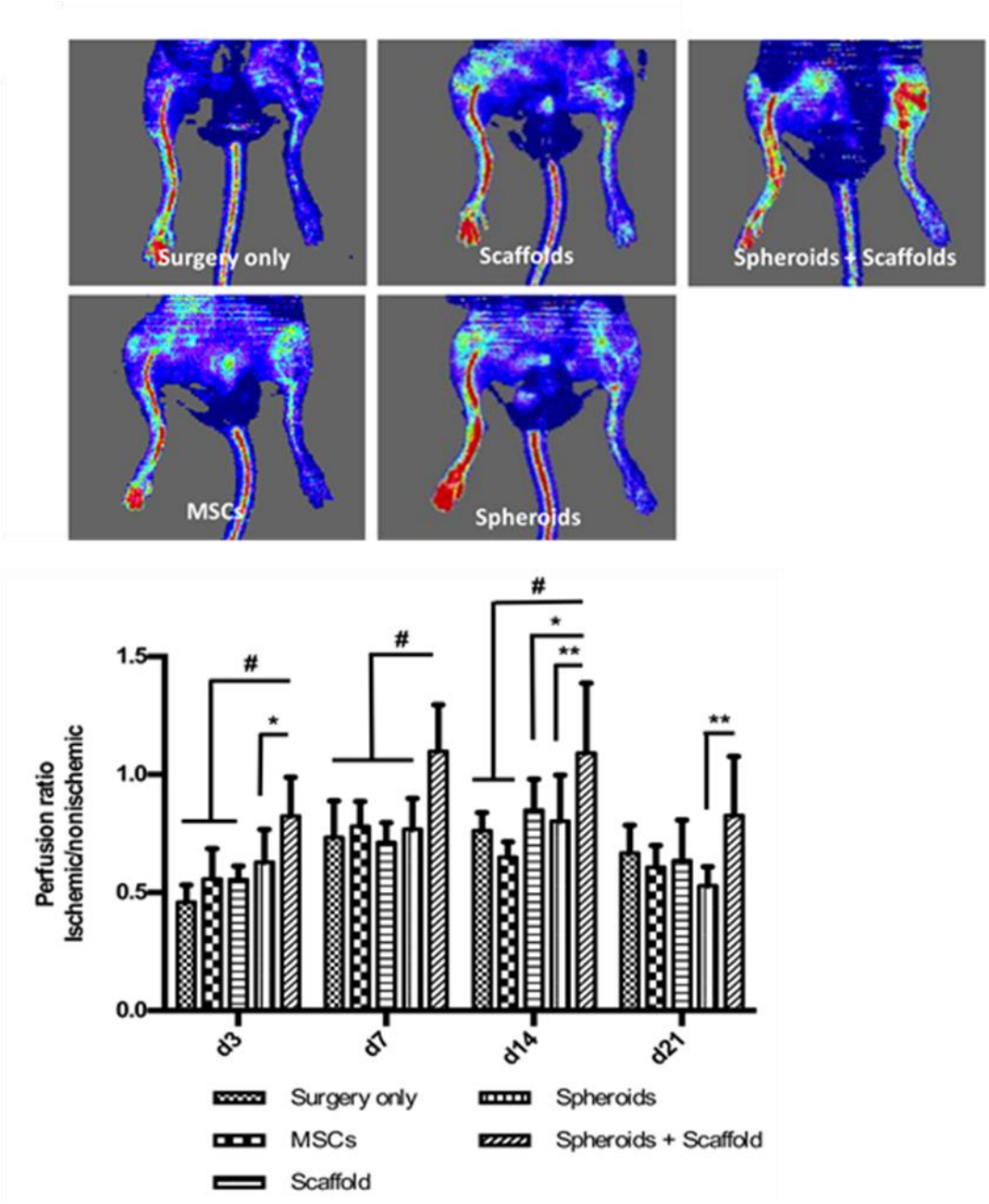

Figure 3.6 Laser Doppler perfusion imaging (LDPI) images from representative animals at different time point and quantification of LDPI signals from area of interests.

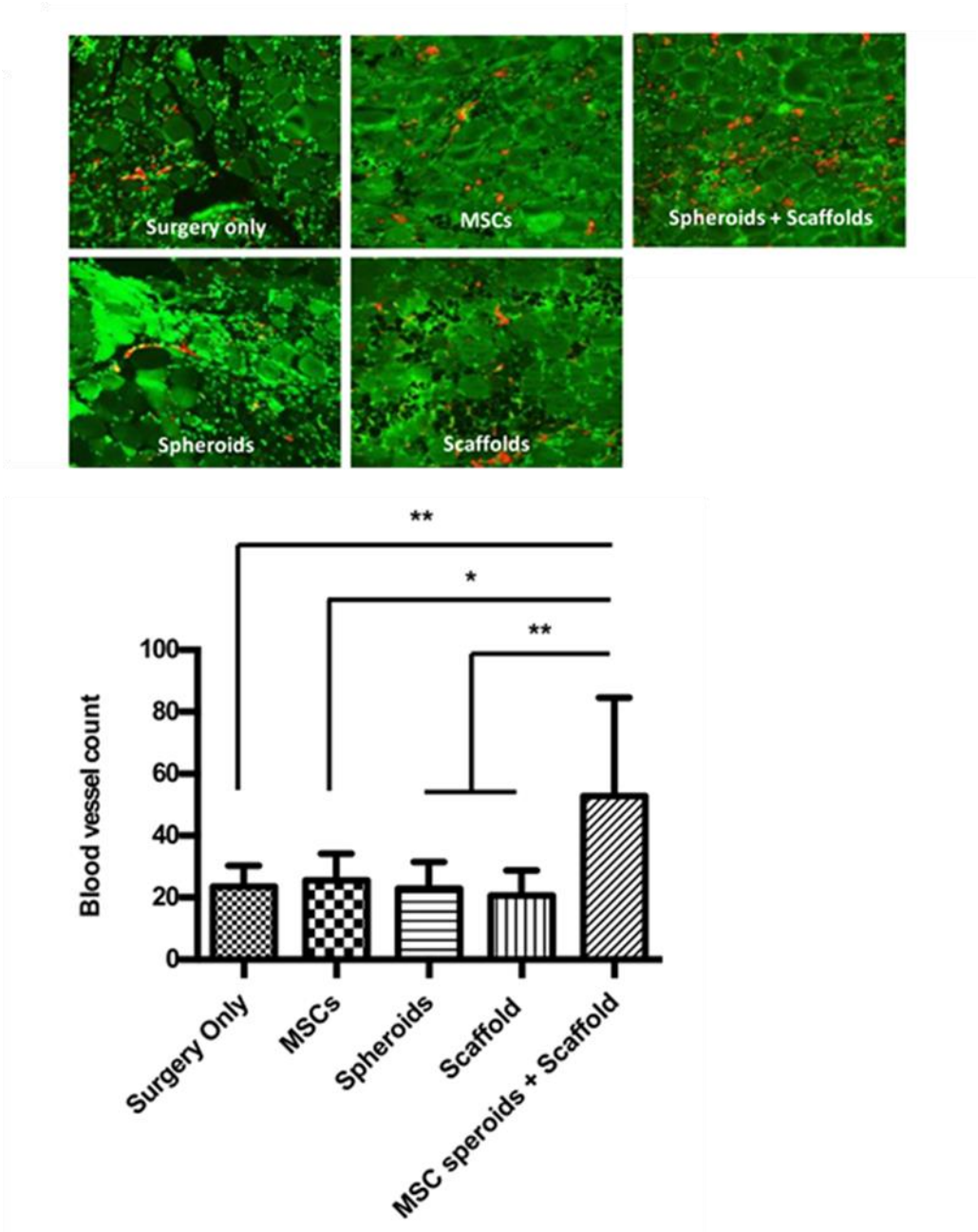

Figure 3.7 Representative images from lectin staining of sections from ischemic tissue at 7 days and quantification of blood vessels for each group.

The therapeutic vascularization efficacy was tested in vivo in a mice model of HLI (**Figure 3.6**). Four control groups (no treatment, MSCs single cells, MSC spheroids and empty scaffold) were included. LDPI was performed to determine the recovery of blood flow. High intensity of blood perfusion was found in areas where MSC spheroids loaded scaffold

were transplanted. Statistical analysis showed that our strategy had a significant increase of blood perfusion over all control groups in the first two weeks (n = 10~15). Immuno-labeling of blood vessels was performed to further investigate the functional recovery (**Figure 3.7**). It was found that at 7 days that the blood vessel density was greatly increased over all control groups after treatment of MSC spheroids, with a 2.2 fold increase over no treatment group. No difference was found among all four control groups (n = 3~4).

The scaffolds and surrounding tissues were harvested and stained withi H&E. It was found that the scaffolds triggered mild foreign body reaction. Blood vessels were found around scaffolds as well.

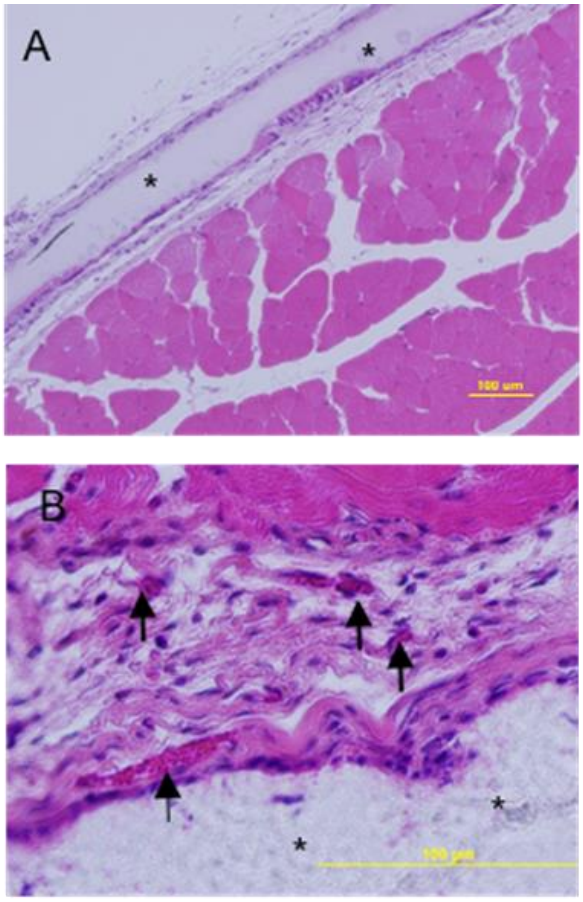

Figure 3.8 H&E staining of implanted scaffold (A) 10x (B) 40x, (*) indicates scaffold and arrows indicates blood vessels

3.4 Discussion

Therapeutic vascularization is greatly desired in many applications, but the problem still remains unsolved. One extensively studied approach for therapeutic vascularization is through the delivery of angiogenic growth factors that were found in the natural process of vascularization [137]. However, such strategies failed to obtain long lasting benefits, probably due to their incapability of recapitulating the natural process where numerous growth factors were involved with specified order and concentration gradient, not to mention the difficulties in preserving bioactivities of these growth factors. An alternative approach, MSC therapy, has potential to overcome these problems. MSCs are able to secrete a broad range of therapeutic growth factors. They also have the ability to sense and respond to ischemic environment with upregulated angiogenic gene expression. In the form of their multicellular 3D spheroids, their therapeutic ability is further enhanced. To translate MSC spheroids into clinical, nevertheless, the key problem is the design of delivery strategy. In direct injections of MSCs, over 90% of cells were lost due to the acute mechanical dispersion. Recently, several studies have applied scaffold-based delivery to address this problem. However, little focus has been put on the delivery of MSC spheroids, which requires specific design to minimize the chance of clumping.

In this study, a microwell-patterned scaffold was fabricated by combination of electrospinning and micromolding. The scaffolds exhibited strong mechanical strength comparing with hydrogels. They could maintain integrity in contracting tissues like muscles and have no potential of cell loss due to dissociation of scaffolds. Microwells were introduced to spatially control the distribution of MSC spheroids. In vitro experiments

confirmed the scaffolds' ability in loading MSC spheroids and maintaining the enhanced paracrine function.

Comparing with other patch-based strategies where most scaffolds were several millimeters thick and cells were seeded inside, our strategy has two advantages in addition to the enhanced paracrine function. First, in our study, cells were seeded only on surface of the scaffold that all cells will be closely attached to injured tissue after transplantation, which minimizes the distance for nutrient diffusion and also enables potential vascular ingrowth and cell integration. The second advantage is the transplantation volume. In our study, the application of MSC spheroids and microwell array enables a high cell density with less transplantation volume and meanwhile reducing the chance of cell clumping. The reduced volume would greatly benefit MSC therapy in human studies.

Results from BLI demonstrated improved cell retention from our strategy. An early cell loss of non-scaffold based delivery was observed, indicating without materials, great amount of cells was lost during injection or by the fast wash out after injection and the protective effect of the scaffolds against the acute mechanical dispersion.

Given the transplanted area was well perfused that cells weren't suffering from ischemia, the disappearance of cells after 14 days was likely due to the clearance by immune cells, which is a limitation of this strategy and need to be taken into consideration in further scaffold design.

LDPI showed that the vascularization effect of spheroids loaded scaffold is localized, which is desired in some cases where off target vascularization is unwanted. It was found that the period where perfusion was significantly increased coincide with the period that

cells can be seen from BLI and after the disappearance of cells at 14 days, the perfusion also started to regress, which might indicate that the perfusion is positively related to cell survival. It is also noted that only 2×10^5 cells were administered in our experiment, which is relatively low comparing with most studies where 1 million cells were given, suggesting an increased efficiency of our strategy. In this research, the mechanism of the MSC contributed to the recovery was not studied that both cell integration and paracrine effect could have possibly occurred in this process, which needs to be further investigated.

The method presented in this study has potential in translation to clinical use. Polycarbonate and polyurethane are both approved materials for medical applications. Other cell types besides MSC can be applied including genetically engineered cells. It may be applied to treat different diseases other than hindlimb ischemia such as myocardial infarction.

3.5 Conclusion

In this study, microwell patterned electrospun fibers were fabricated and characterized. MSC spheroids loaded microwell-patterned scaffold is an effective MSC transplanting strategy with enhanced MSC paracrine function and increased cell retention. This method is capable of improve vascularization in ischemic tissues. These findings indicate that the MSC spheroids loaded microwell-patterned scaffold strategy has great potential for therapeutic vascularization.

CHAPTER 4. DEVELOPMENT OF PORE SIZE CONTROLLABLE SCAFFOLDS FOR MESENCHYMAL STEM CELL TRANSPLANTATION

4.1 Introduction

With the rapid advancement on stem cell and gene technologies, cell based therapy has shown great promise in treating diseases which were once considered incurable, such as myocardial infarction and diabetes. In most preclinical studies and clinical trials, cells suspensions were delivered by direct injection, however, the benefits of cell therapy have been limited by the poor survival and rapid removal of cells [138-142]. So far, there is no convincing evidence that shows the integration of injected cells with host tissue [143]. Therefore, new method for cell delivery with focusing on cell engraftment is demanded. Based on these considerations, researchers are now focusing on the scaffold based cell therapy [144-148]. Scaffolds can provide physical support for cell attachment and create friendly microenvironment of cell growth, as have been describe in the previous chapters of this dissertation.

In applications of scaffold based cell transplantation, cell migration and tissue ingrowth after scaffold implantation is a critical process and should be carefully controlled [149]. For example, some stem cell types may require migration into host tissue and followed by differentiation to perform regeneration [150]; scaffolds with pre-engineered tissue would greatly benefit from the ingrowth of blood vessels to prohibit ischemia [151]; in applications of transplanting scaffold encapsulated allo-or xenogenic islets, complete restriction of cell ingrowth may be preferred in order to prevent immune attack [152].

Pore size is the main character that controls cell migration [153-155]. Studies have shown that large open pores can promote cell migration and vascular infiltration while small pores (usually less than 1um) can restrict the pass of cells [156-158]. However, in most cases, including MSC transplantation, the infiltration of blood vessels and elimination of immune cells are both desired [159]. Therefore, the optimization of pore size need to be studied for improved cell survival.

In this study, a hollow spherical scaffold with controllable pore size was developed. Cells were injected inside the hollow core, therefore transplanted cells will have no direct contact with host tissue. The interaction between host tissue and transplanted cells are solely controlled by the pore size of outer membrane. To demonstrate, scaffolds with three different pore sizes were fabricated and their morphology, mechanical property and mass transfer efficiency were characterized. MSC loaded scaffolds were further transplanted *in vivo* and characterized biocompatibility and cell survival in scaffolds with different pore sizes.

4.2 Materials and methods

Materials

DMAC and Span85 was purchased Sinopharm (Shanghai, China). PES (Mw 40000) was purchased from JUSEP (Changchun, China). PVP (Mw 40000), LiCl, PEG 400 and FITC-Dextran (Mw 2,000,000) were purchased from Sigma-Aldrich (Milwaukee, WI, USA). The cell culture plates and low-attachment culture plates were from Corning (NY, USA). Dulbecco's phosphate-buffered saline (DPBS) was purchased from Invitrogen (Carlsbad, CA, USA). Bone marrow derived MSC from BALB/C and culture reagents were purchased from

Cyagen (Santa Clara, CA, USA). The suppliers of other chemical and biological reagents are specified in the text below.

Preparation of the pore sized controllable spherical scaffold

Scaffolds were prepared by a gel–sol phase-inversion method. The polymer solution was made by dissolving PES, LiCl, PVP and PEG 400 in DMAC, followed by dropwised into a Span85 solution with assist of a syringe pump. Different pore size of scaffolds was fabricated by immersing the resulted PES scaffold in DMAC solvent with a predetermined time. Then the scaffolds were washed thoroughly with kerosene and rinsed in water for 7 days to remove trace of organic solvent. The scaffolds were then sterilized with high pressure steam and dried for further characterization.

Microscopic spectroscopic characterization

To obtain the morphological characteristics of different scaffoldss, different samples were gold sputter-coated and examined by the scanning electron microscope (SEM) (S-4800, Hitachi, Japan) under acceleration voltage of 15 kV. ImageJ was applied to quantitatively characterize the scaffold pore size. For each sample, all pores were selected and measured in each image at magnification of 20000x, and a total of 5 images were counted.

Mechanical analysis

The mechanical resistance of scaffolds were determined using a texture analyzer (CT3 4500, Brookfield,USA). The mechanical deformation tests were performed at a mobile probe (TA44) speed of 0.5 mm/s until the bead matrix was observed to burst.

Release profile

FITC-Dextran (Mw 2,000,000) was dissolved in DPBS to make a final concentration of 1 mg/mL. 10 μL of the solution was injected in to each scaffold by microsyringe. 3 scaffolds were then immersed in 5 mL DPBS in each well of 6 well plate. The plate was placed on rotary shaker at speed of 80 rpm in room temperature. 200 μL of solution was taken at predetermined time point to read fluorescence under emission wavelength of 490 nm. 200 μL fresh DPBS was added immediately after the removal of sample solution each time after to make a constant total volume of 5 mL.

Florescent staining of MSCs in scaffold

Scaffolds with 3 x 10^5 MSCs were culture for 24 h before embedded in optimal cutting temperature compound (Sakura, Alphen aan den Rijn, Nederland). The scaffolds were frozen sectioned followed by staining with DAPI and Phalloidin-rhodamine.

MSC function in scaffolds *in vitro*

The total RNA was extracted using the TRIzol kit (Invitrogen, Carlsbad, CA, USA) according to the manufacturer's instructions, and the RNA concentration determined by NanoDrop (Thermo Scientific, Wilmington, DE, USA). 2 μg of the pure total RNA was transferred and reverse transcribed with the TransScript First-Strand cDNA Synthesis SuperMix (Transgen, Beijing, PR China). The gene expression levels were then analyzed using the SYBR Green real-time polymerase chain reaction (PCR) method and quantified using the Bio-Rad CFX96 real-time PCR system (Bio-Rad, Hercules, CA, USA). The primers were all obtained from Sangon (Shanghai, China). The relative gene expression data was analyzed using the $2^{-\Delta\Delta CT}$ method. All gene expression values were normalized to the β-actin level. Each RNA sample was analyzed in triplicate.

In vivo implantation of scaffolds

All protocols were approved by the Institutional Animal Care and Use Committee of Peking University. Male 129 mice (Vital River, Beijing, China), 8-10 weeks' old were used. Scaffolds were loaded with MSCs by injection (3 x 10^5 in 10 μL cell culture medium) one day before implantation. Scaffolds were then replaced in 24 well plate with 1 mL complete medium for further use. The mice were anaesthetized with anaesthetized with an intraperitoneal injection of chloral hydrate (400 mg/kg body weight). The implantation cite was shaved and swabbed twice with betadine and DPBS. An incision of 3mm was made near groin. A pocket was carefully created by forceps, followed by the insertion of scaffold.

In vivo tracking of MSC viability

MSCs were transduced with a lentivirus expressing firefly luciferase, GFP and puromycin resistance under the control of the constitutively active cytomegalovirus and respiratory syncytial virus promoters, respectively (Hanbio, Shanghai, China). 72 h after transduction, MSCs were transferred into standard media containing 1 μg/mL puromycin (Solarbio, Beijing, China). Luciferase expression was confirmed with the GFP under fluorescence microscope. Animals were intraperitoneally injected with luciferin 40 mg/kg 30 min before imaged using Kodak In-Vivo Imaging Systems (Billerica, MA, USA). Luminescence was quantified in the thigh region using Bruker molecular imaging software.

Histology

Animals were sacrificed by CO_2 inhalation at 15 or 30 days after implantation. Mini-scaffolds and the surrounding tissues were obtained after fixation in formalin and embedment in paraffin. The samples were sliced on a microtome at a thickness of 5 μm. The

sections were stained with H&E and then imaged by an upright microscope (Olympus DP71, Japan).

4.3 Results and discussion

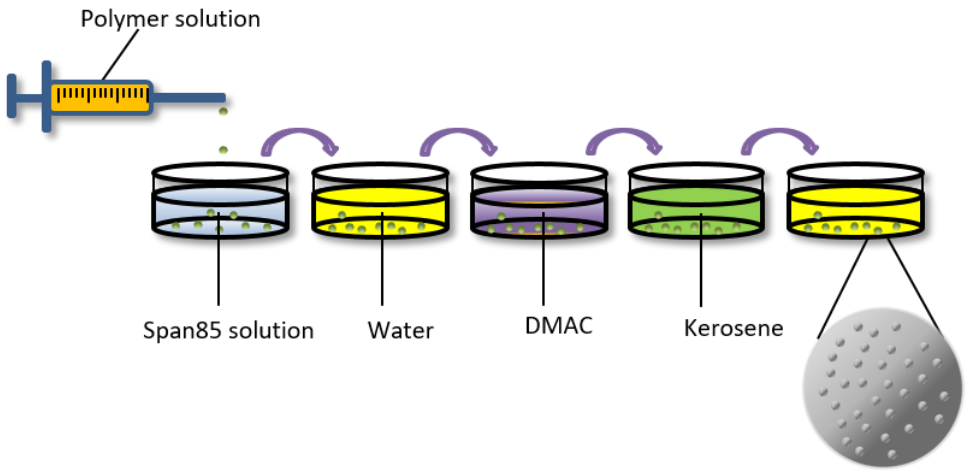

Figure 4.1 Illustration of scaffold preparation

The scaffold preparation procedure is illustrated in **Figure 4.1**. The fabrication procedure of the scaffold is simple, prolific and highly reproducible. With our experiment settings, about 2400 scaffolds can be produced in one hour. The diameter of the scaffold can be adjusted by changing the flow rate of polymer solution. The pore size of the scaffold is controlled by simply adjusting the immersing time of scaffolds in DMAC. In our study, three immersing time, 0 s, 20 s and 40 s were selected to fabricate scaffolds with dense surface, nano-pore surface and micro pore surface, respectively.

Figure 4.2 shows the macro- and micro-view of the scaffolds' surface morphology and inner structure. The scaffold displayed a highly monodispersed macro morphology of hollow sphere, with an average diameter of 3 mm. SEM revealed that it has straight channel micro

structure near surface like the classic structure of flat membranes prepared by the well-known gel–sol phase-inversion method. The samples without immersing in DMAC exhibits a dense layer at surface (**Figure 4.2 C**), with no visible pores under SEM. The dense layer is formed by the increase of polymer concentration caused by the initial rapid diffusion of DMAC into water. After the formation of dense layer, the solvent exchange decreased and porous structures were formed under the surface, as showed in **Figure 4.2 B**.

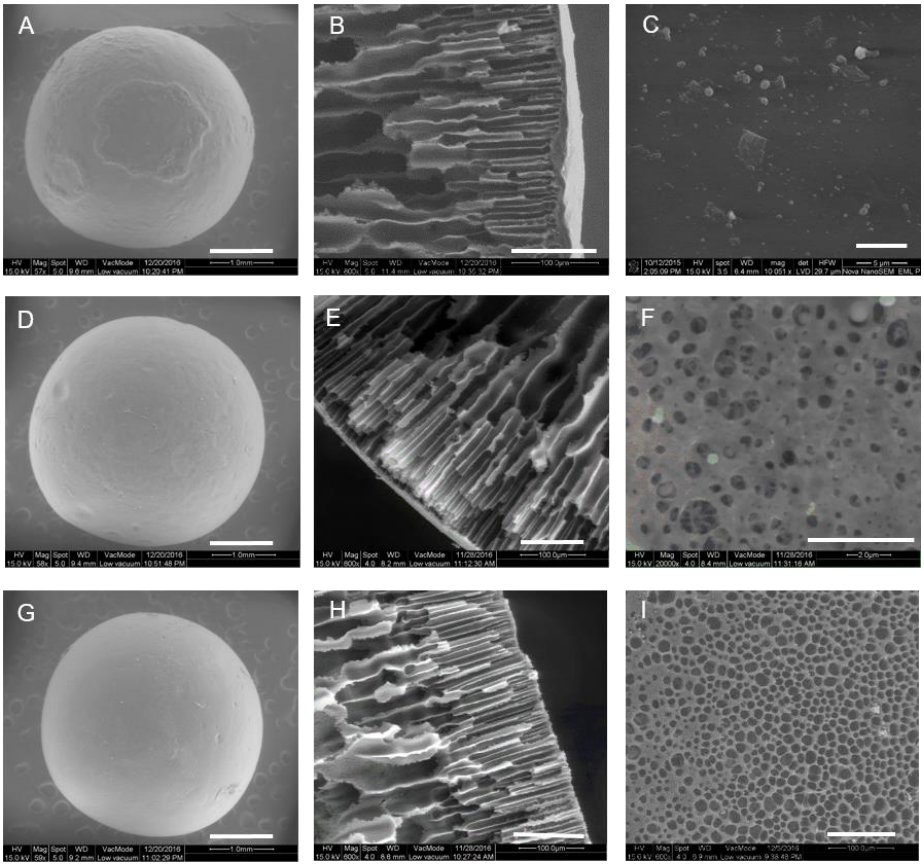

Figure 4.2 Representative SEM images of scaffolds. (A-C) dense layer scaffold (D-F) nanopore scaffold (G-I) micropore scaffold, scale bar in (A, D and G): 1 mm, (B, E, H and I)： 100 μ m, (C and F): 5 μ m

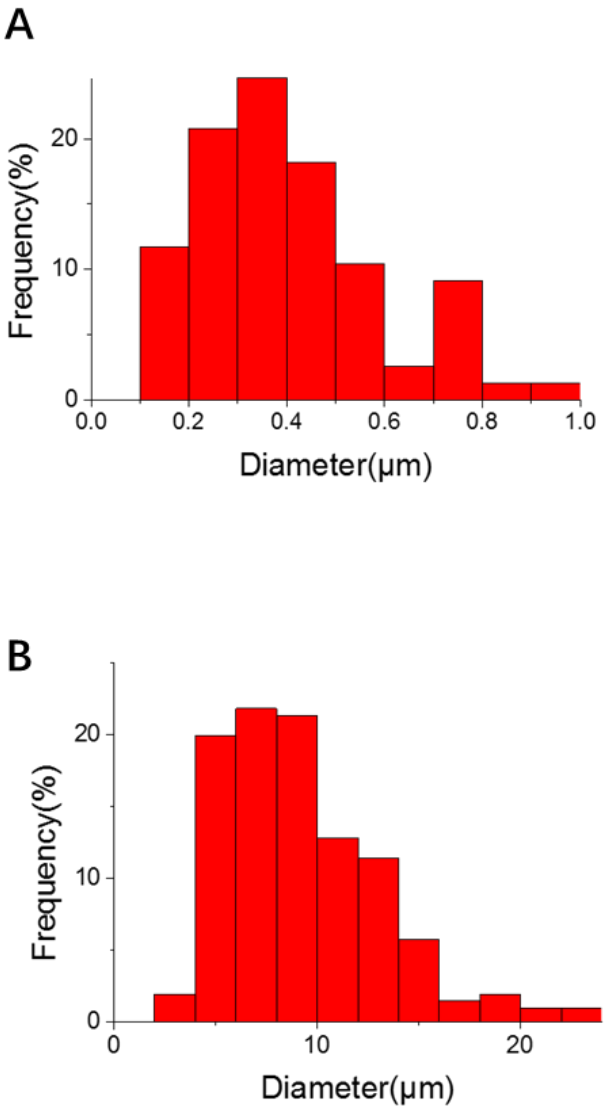

Figure 4.3 Statistical analysis of pore size distribution. (A) nanopore scaffolds (B) micropore scaffolds

SEM images and the following statistical analysis **Figure 4.3** clearly confirmed our method of controlling the surface pore size. While no visible pores were found on dense layer samples, under SEM the pore size has increased to 0.401±0.187 μm and 9.22 ±3.83 μm after immersing in DMAC for 20 s and 40 s, respectively. The increase of surface pore size is due to the removal of the dense surface layer while immersing in DMAC. When immersed in DMAC, the pores of inner straight channel gradually appear. Therefore, the

pore size of the surface in theory should be controllable from 0 to the pore size of inner straight channel which in this case is around 10 μm.

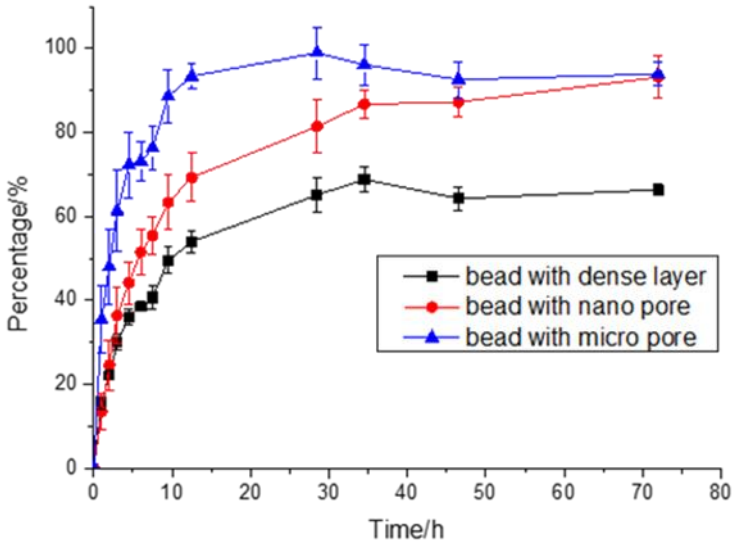

Figure 4.4 Release profile of scaffolds with different pore size.

Mass transfer efficiency is an important character of scaffolds. It determines the accessibility of the seeded cell to nutrient and oxygen. Here the mass transfer efficiency of three samples with different pore size were compared by testing the release profile of FITC-Dextran, which is a fluorescent labelled high molecule weight polymer, mimicks the diffusion of nutrient. The release curve in **Figure 4.4** shows that scaffolds with micropores have the fastest release of FITC-Dextran, which reached nearly 100% at 15 hours, while scaffolds with nanopores took nearly 72 hours. It is interesting to find that though no pores were found on scaffolds with dense layer, there were some release of FITC-Dextran from these samples as well. It is possible that the pore size of dense layer scaffolds is too small to be observed under SEM. If so, their pore size should be less than 50 nm.

The fluorescent staining of MSCs showed that after being loaded cells were attached to the inner surface of scaffold **(Figure 4.5)**. The distribution of MSCs on inner surface is relatively homogeneous, no obvious cell aggregation was observed.

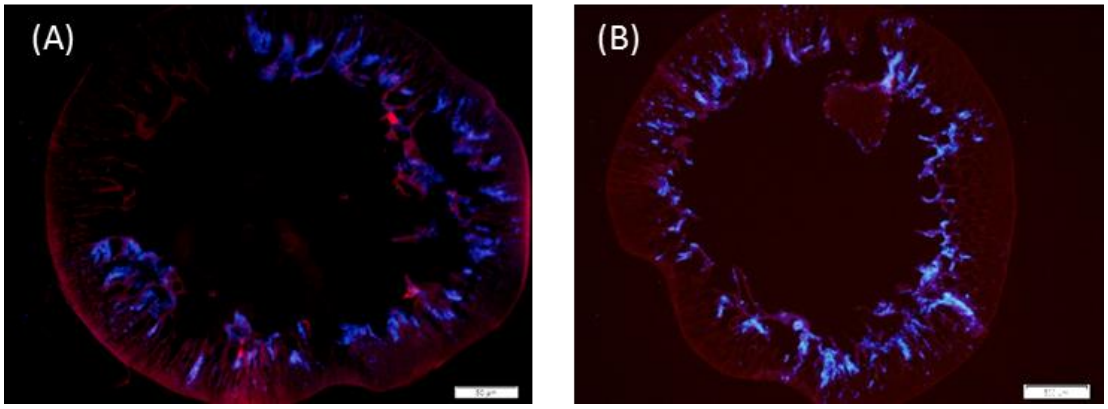

Figure 4.5 Fluorescent staining of MSCs in scaffolds. (A) nanopore scaffolds, (B) micropore scaffolds. (Blue: DAPI, Red: Phalloidin-Rhodamine, bar indicates 500 µm)

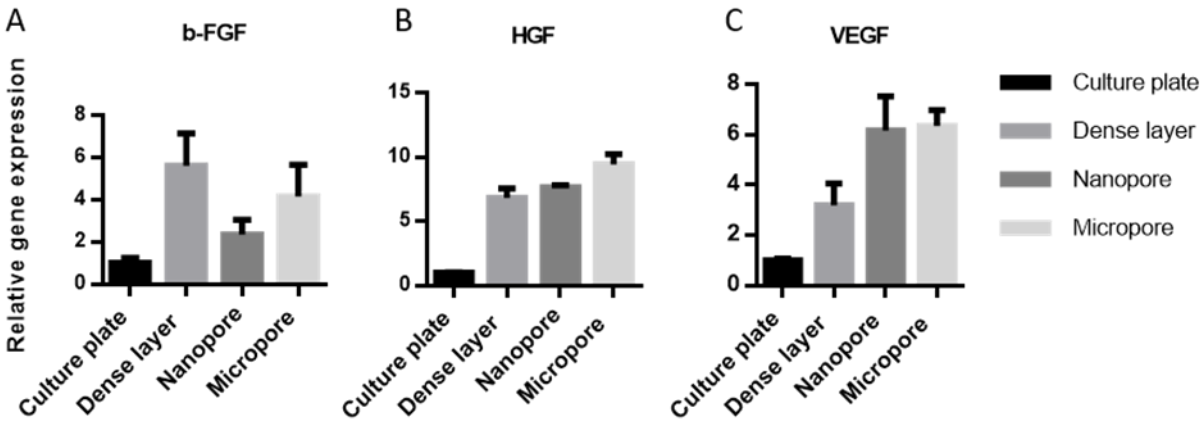

Figure 4.6 Gene expression of MSCs in scaffold. (A) b-FGF (B) HGF (C) VEGF

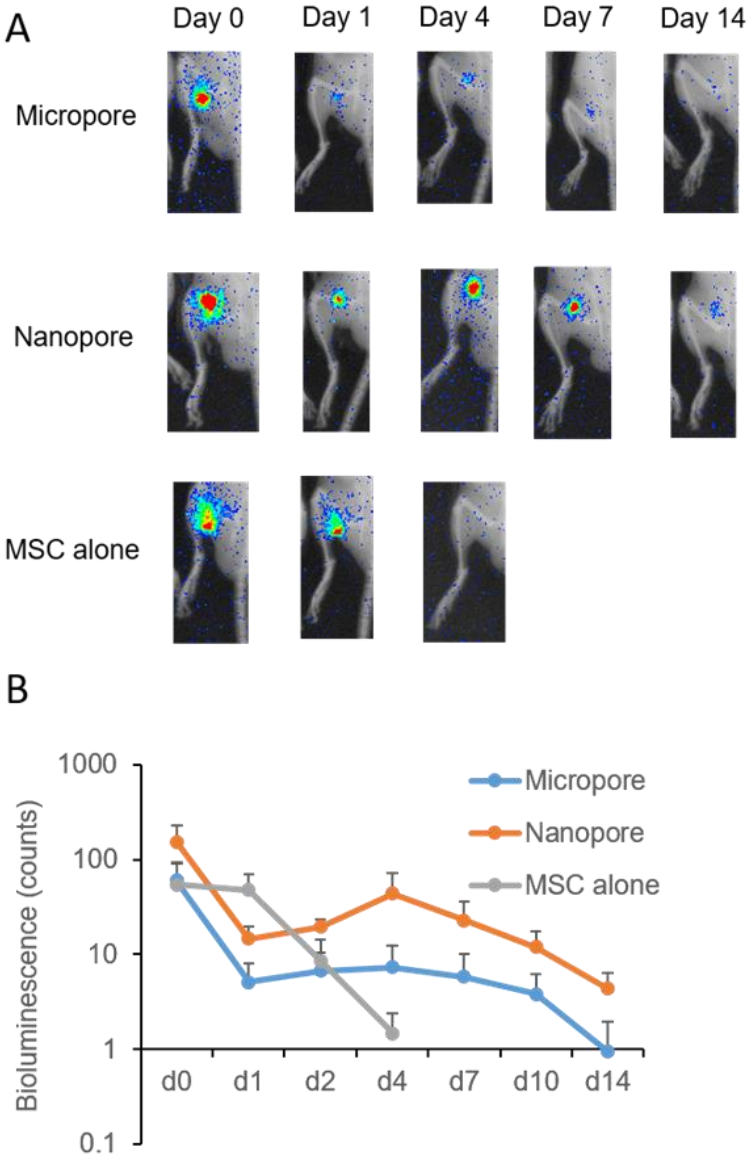

Figure 4.7 MSC in vivo survival characterized by bioluminescence (A) representative bioluminescence images from scaffolds with different pore size at different time points. (B) statistical analysis of MSC survival from bioluminescence test

Cell function in the three scaffolds were characterized by examine their gene expressions. b-FGF, HGF and VEGF are paracrine factor secreted by MSC. They were found to have angiogenic, antiapoptosis and antiscarring functions. The gene expression of MSCs encapsulated in three scaffolds were compared while MSCs cultured on normal

plastic plate being control group. It was found that all three paracrine genes upregulated significantly (2-10 times) in all three samples. It was believed that this upregulation may be due to the hypoxic environment caused by limited space inside the scaffold.

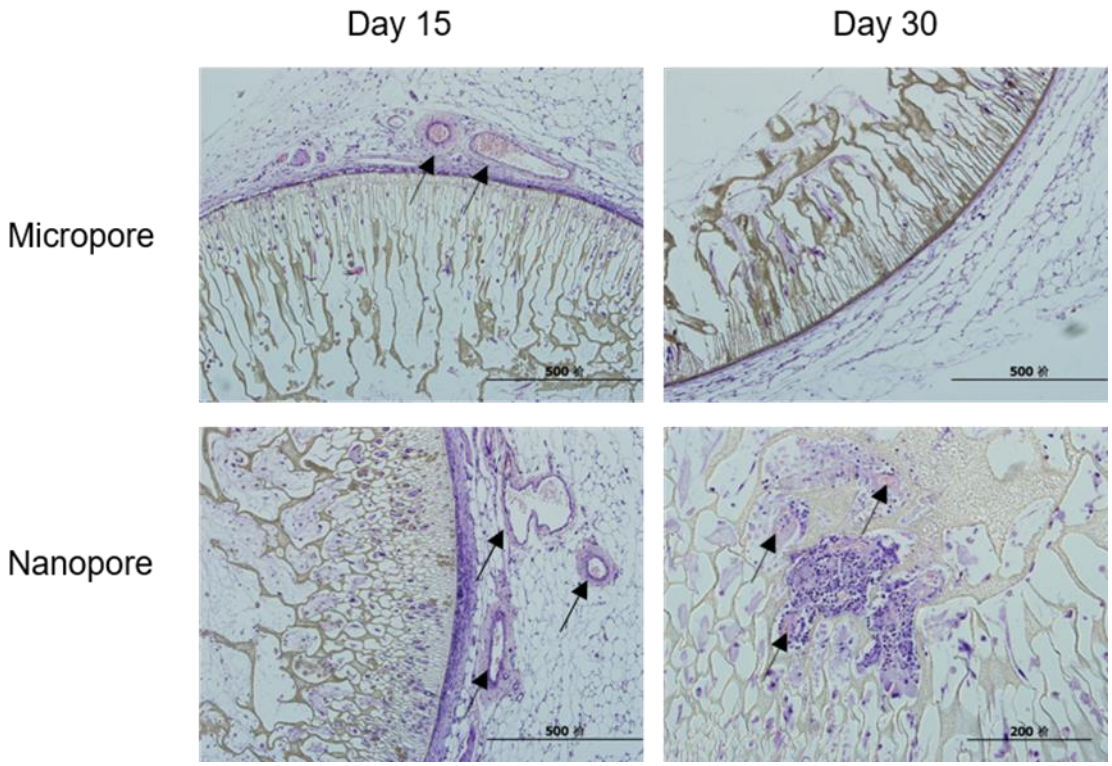

Figure 4.8 Representative H&E staining of scaffolds and surrounding tissue. Arrows indicates blood vessels.

Finally, the *in vivo* performance of scaffolds was tested by subcutaneous implantation of MSCs loaded scaffold in mice. Dense layer scaffolds were not selected in this experiment due to concerns of the limited permeability. The viability of MSCs were track by bioluminescence. **Figure 4.7** shows the retention transplanted MSCs. It was found that directly injected MSCs completely disappeared within 4 days, which is consistent with results from others [160]. It is interesting to see that the nanopore scaffold had better cell survival over micropore scaffold at all 7 time points, indicating that in our experiment settings a more limited interaction between host tissue and transplanted cells is better for cell

survival. It would also be interesting to investigate scaffolds with even smaller pores in further work to see how far this trend will go on. There was a huge decrease of MSCs in both scaffolds within 24 hours. It was thought that the rapid cell death is due to the hypoxic environment before sufficient vascular system is developed around the scaffold. There was an increase of MSCs in nanopore scaffold at 4 days. It was assumed this is time point where vascularization occurred and cells had enough nutrient to proliferate. Most MSCs in scaffolds disappeared 14 days after transplantation.

HE staining of scaffolds shows that both of the scaffolds triggered mild fibrosis (**Figure 4.8**). Fibrotic tissues of 10 to 50 μm in thickness were found surrounding each scaffold. Blood vessels can be found within 100 μm range from surface of all scaffolds. It is observed that the blood vessels grew inside nanopore scaffolds at 30 days, which suggests that the nano pores are the sufficient to allow ingrowth of vessels so that the final disappearance of MSC should not due to insufficient nutrient or oxygen supply but because of the clearance of immune cells. Cell can still be found inside scaffolds at 15 and 30 days post transplantation. However, with HE staining alone their cell type can hardly be identified. They could be MSCs with very low cell number that couldn't be detected in bioluminescence test or they could be infiltrated immune cells.

Spherical scaffolds have been investigated for cell transplantation. So far, almost all spherical scaffolds are based on hydrogels materials such as alginate [161, 162], agarose [163] and PEG gels [164]. However, hydrogel beads are mechanically weak and the pore size of hydrogels are usually so small that cells can only be loaded at same time with the formation of hydrogels. Here, it is the first time that a plastic hollow spherical scaffold with controllable pore size has been developed for cell transplantation. This novel scaffold has

several advantages that benefit practical application. First, the PES plastic scaffold shows superior mechanical property over hydrogels. They are easy to maneuver. Second, PES is known for its stability, which enables the storage and transportation of the premade scaffold.

Unlike traditional scaffolds, the mini scaffolds have two porous layers and their pore sizes can be controlled independently. For the purpose of this study, which is to control interaction between host tissues and transplanted cells, the control of pore size of the outer membrane was demonstrated. It was shown that the change of out pore size did not affect pore size of inner membrane. In addition, in theory the pore size of inner membrane can also be regulated by adjusting the formula of polymer solution. It would be an interesting work in the future to study scaffold with different inner pore size as well because the inner pore size could regulate the microenvironment and distribution of transplanted cells.

In this study, I demonstrated the mini-scaffold's application in cell transplantation, where they showed ability of improve cell function and controlled cell retention with different outer pore size. Meanwhile, this type of scaffold also has potential in a wide range of biomedical applications. For example, it can be used for sustained release of drugs. The hollow core can be used for drug loading and different pore size can be applied to control release rate. There are limitations as well. Firstly, the pore size distribution is relatively broad in our technique. The scaffold can serve well as cell delivery vehicle but may not be the best candidate for complete immunoisolation applications. Secondly, due to the depth of this study, I didn't go further in analyzing infiltrated cells, which may be investigated in future work.

4.4 Conclusion

In this study, a pore size controllable hollow spherical scaffold was developed. The scaffold has a hollow spherical shape and straight pores in inner surface. The pore size can be easily controlled during preparation. In this study, three types of scaffold with different pore size were developed. Their structure, secretion profile and mechanical property were characterized. It was found that the paracrine gene of MSCs were upregulated after being seeded in scaffolds. The MSCs survival in scaffold was evaluated *in vivo.* It was found that MSCs survival can be improved and controlled by different pore size of scaffolds. This novel scaffold has great potential in biomedical applications

CHAPTER 5. SUMMARY AND FUTURE DIRECTIONS

This dissertation focused on the development of scaffolds with integrated properties and functions for cell transplantation applications. In this dissertation, three types of novel scaffolds with integrated properties were developed and characterized both *in vitro* and *in vivo.*

The first scaffold was developed through an integration of hydrophobic polyesters with hydrogels. Surface RAFT polymerization technique was adopted to polymerize nanothin layer of PEG hydrogels on surface of PCL micro fibers. It is the first time such structure was reported. In this way, the composite materials could remain the fibrous and porous nano-morphology. The introduction of hydrogel is "invisible" from macro view, but after hydrogel coating, the material changed from hydrophobic to water absorbable and showed improved biocompatibility *in vivo*. The method developed here is applicable to all polyester scaffolds and radical polymerized hydrogels, therefore has wide biomedical applications.

The second scaffold was developed for transplantation of microtissues. In this work, micropatterning was introduced on electrospun fibers so that the scaffolds could not only provide ECM like microenvironment, but also gain regulation on a larger scale, the spatial distribution of microtissues. For the first time it was demonstrated that this micropatterned scaffold is able to improve cell retention of MSC spheroids after transplantation and achieve better tissue vascularization. With the rapid advancement of *in vitro* microtissue fabrication technique, this scaffold will find increasing importance in cell transplantation applications.

In my third work, a hollow spherical scaffold with controllable pore size developed for cell transplantation. With controllable permeability, the balance between vascularization and

immune reaction could be optimized. For the first time, MSCs transplanted with the mini-capsules were demonstrated to improve cell function and retention. The *in vivo* cell retention could be controlled be different pore size of the scaffold surface. It was found that vascularization may have greater effect on acute cell survival while immune reactions determine the length of cell retention. In the future it would be interesting to fabricate scaffolds with smaller pore size to seek optimized cell retention.

Currently, vascularization is still a major challenge in scaffold based cell transplantation. A fast vascularization of the scaffold is strongly preferred to improve early survival of the transplanted cells. So far, most of the tissue engineering products are limited to tissues such as bones, cartilages and skins where blood vessels are not rich. The sized of engineered tissues are also limited by poor vascularization. In our study, I think cell survival was greatly hampered by vascularization as well. Therefore, one future focus of my study could be the improvements of scaffold vascularization. Studies have shown that one solution for improving vascularization is through prevascularization (**Figure 5.1**). In my case, the mini-capsule developed in this dissertation could be implanted alone in advance for prevascularization. Then cells could be injected in capsules after the establish of sufficient vascular system. I consider this method could greatly improve the early loss of cells.

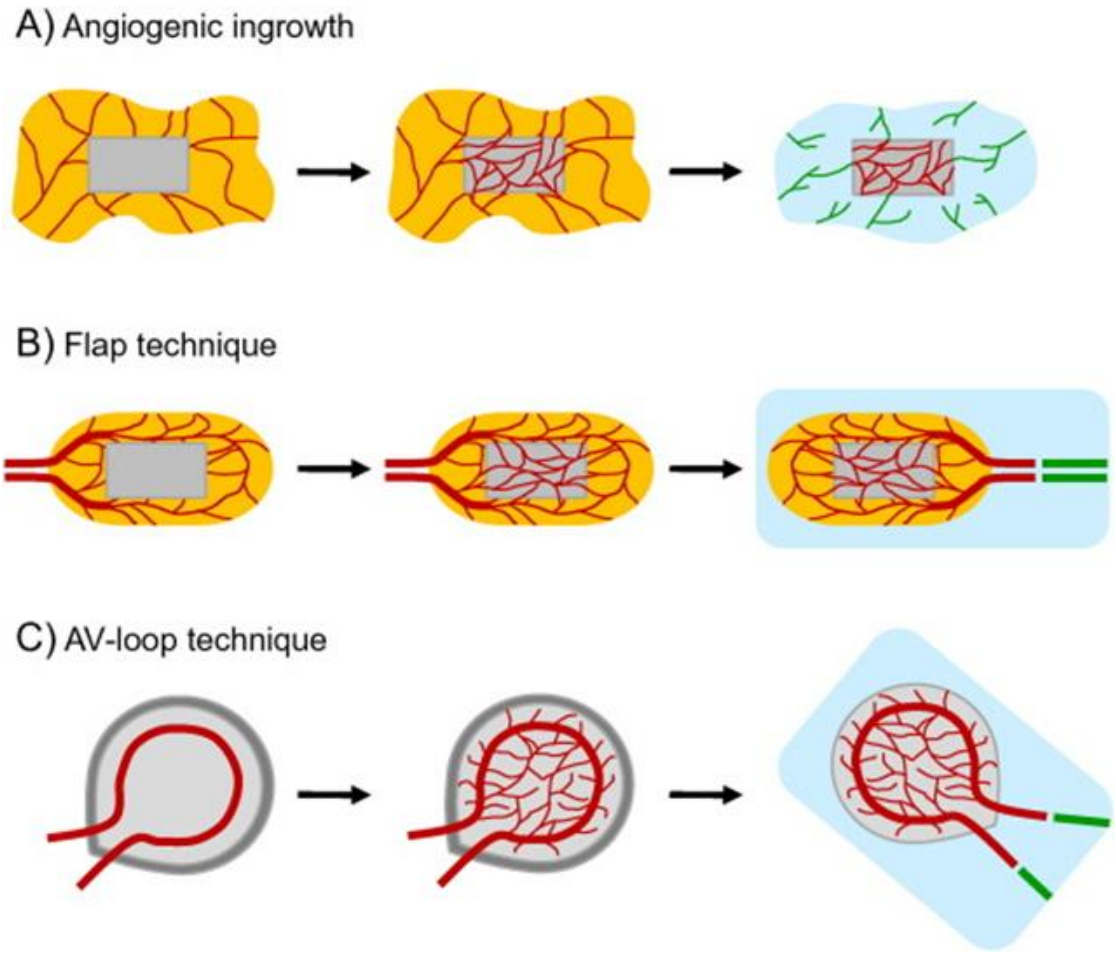

Figure 5.1 Current *in situ* prevascularization approaches, including angiogenic ingrowth (A), flap technique (B) and AV-loop technique (C). A: Implantation of a scaffold (gray) into a well-vascularized tissue (orange) induces random ingrowth of newly developing microvessels (red). After complete vascularization, the implant is transferred to the defect site (blue), where the preformed microvessels develop interconnections to the microvessels of the host tissue (green) by inosculation. B: A scaffold is implanted into a muscle flap (orange) to allow the random ingrowth of newly developing microvessels (red). After prevascularization, the entire flap with the incorporated implant is freely transferred to the defect site (blue), where the vascular pedicle of the flap is surgically anastomosed to host vessels (green). C: Inside a protected growth chamber (dark gray), an AV-loop is incorporated into a scaffold (gray) to generate a prevascularized tissue construct by spontaneous sprouting of vessels out of the loop (red). The prevascularized tissue construct is then transferred and surgically anastomosed to the blood vessels (green) of the defect site (blue) (Laschke M W, et al. Biotechnology advances, 2016, 34(2): 112-121.)

In this dissertation, scaffolds' applications in cells transplantation were demonstrated the by transplanting scaffolds with MSCs or MSCs spheroids, since MSCs are the most

studied and promising cell types. In fact, these scaffolds with integrated properties also have the potential for transplantation of other cell types. For example, islets have a similar size of MSC spheroids, which would also prefer spatial regulation during transplantation to avoid hypoxia. Therefore, the micropatterned fiber scaffold would greatly benefit the transplantation of islets as well.

However, far more had to be done before cell therapy could finally move from benchside to bedside. I hope this dissertation could facilitate a little bit of this process.

APPENDIX

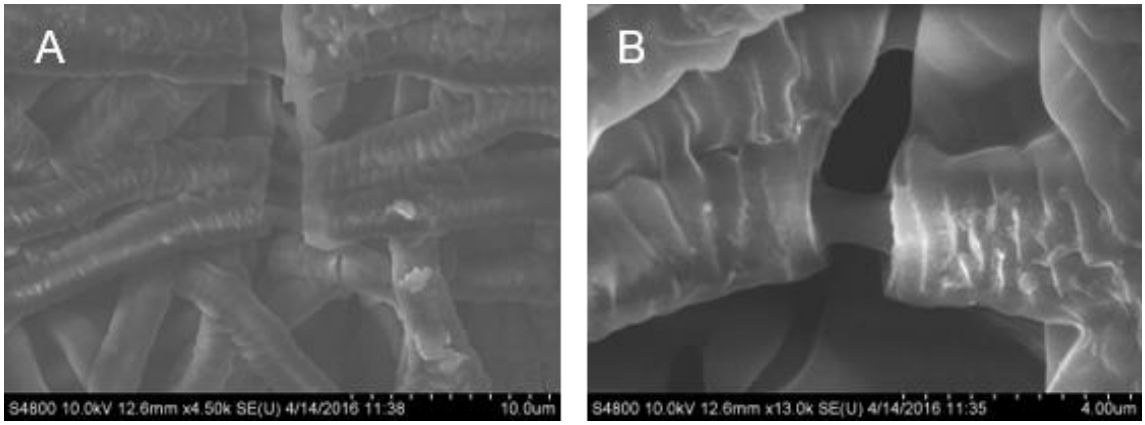

Figure A-1 7.5% PEG-PCL reveals the inner PCL core after frozen in liquid nitrogen. (A) 4500 x, (B) 13000 x

Figure A-2 General appearance of mini-capsule

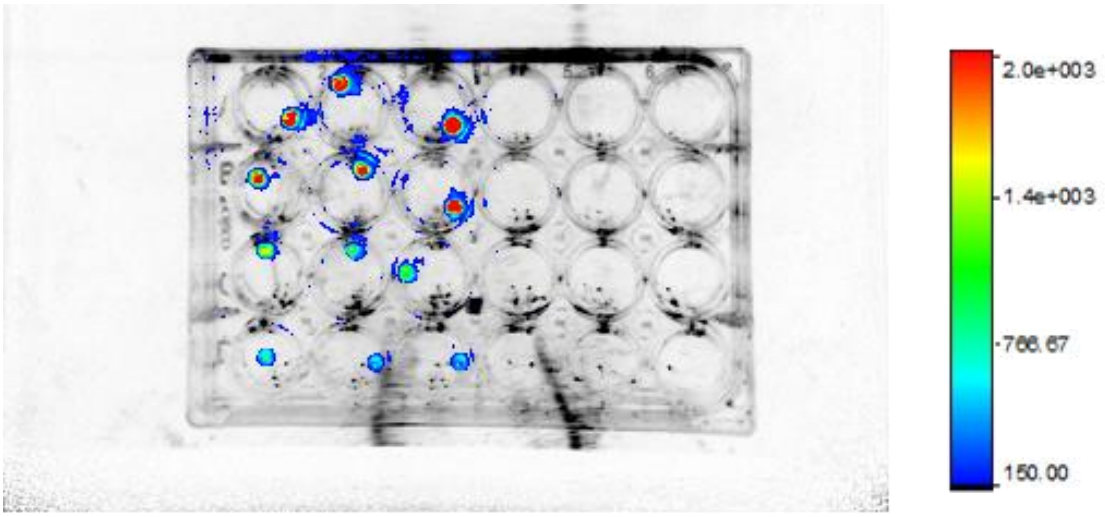

Figure A-3 BLI image of *in vitro* cultured MSCs in mini-capsule. Scaffolds loaded with $6x10^5$, $3\ x10^5$, $1.5\ x10^5$ and $7.5\ x\ 10^4$ MSCs (from up to bottom, respectively) were cultured and imaged in triplicates (lateral).

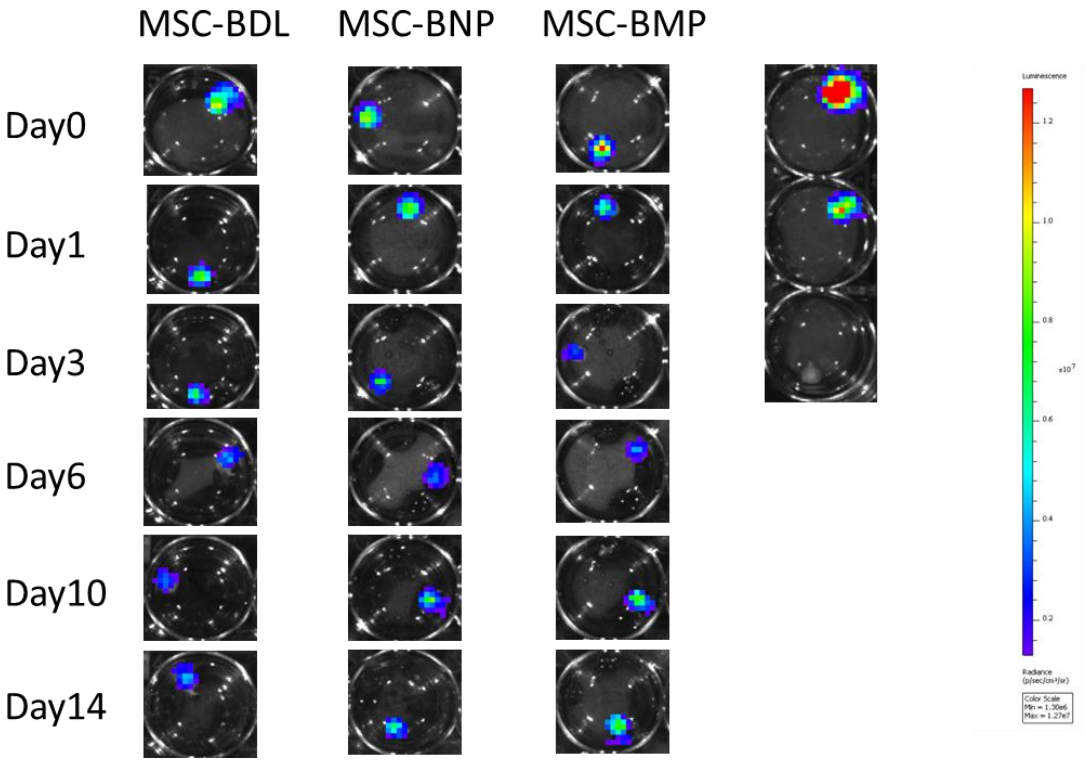

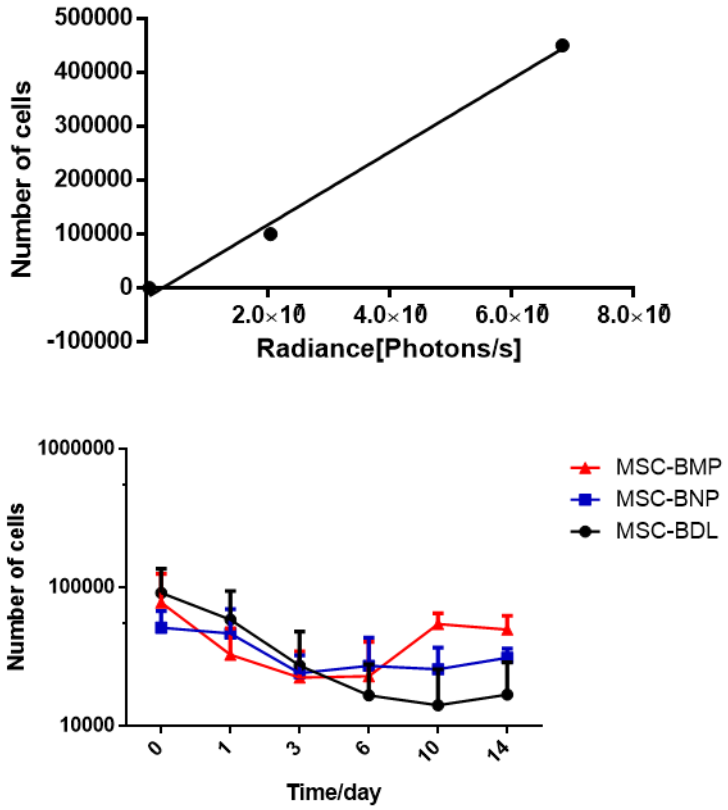

Figure A-4 In vitro cell survival tested by bioluminescence assay.

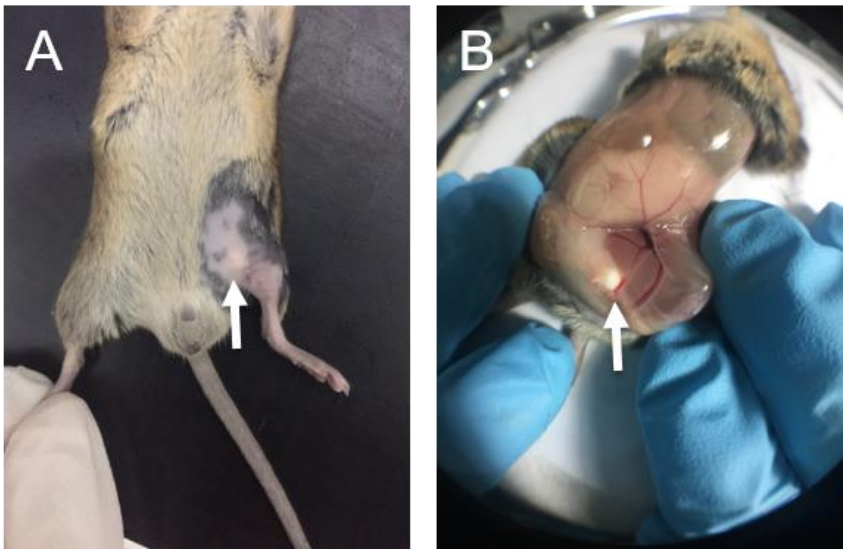

Figure A-5 Images of mice with implanted mini-capsules. (A) exterior appearance (B) subcutaneous appearance (arrow indicates scaffold)

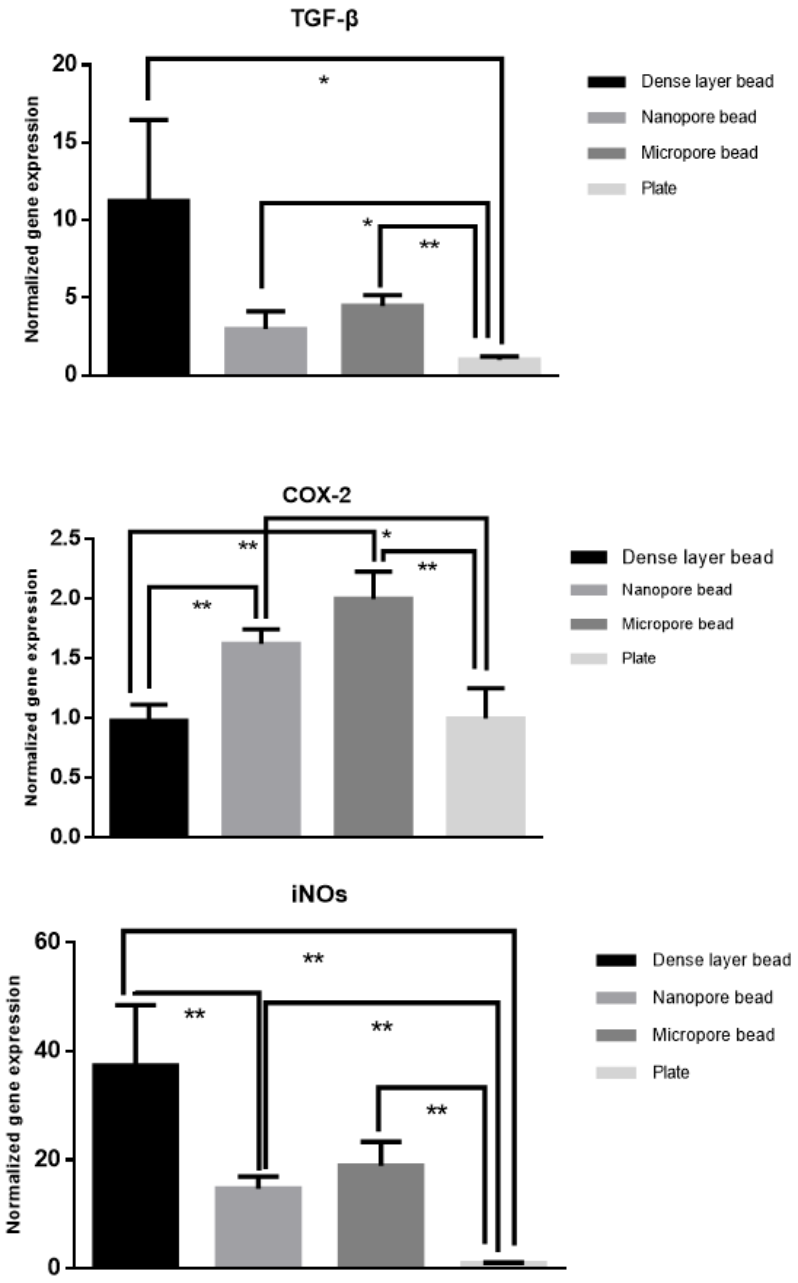

Figure A-6 Anti-inflammatory gene expression of MSCs loaded in scaffolds with different pore size

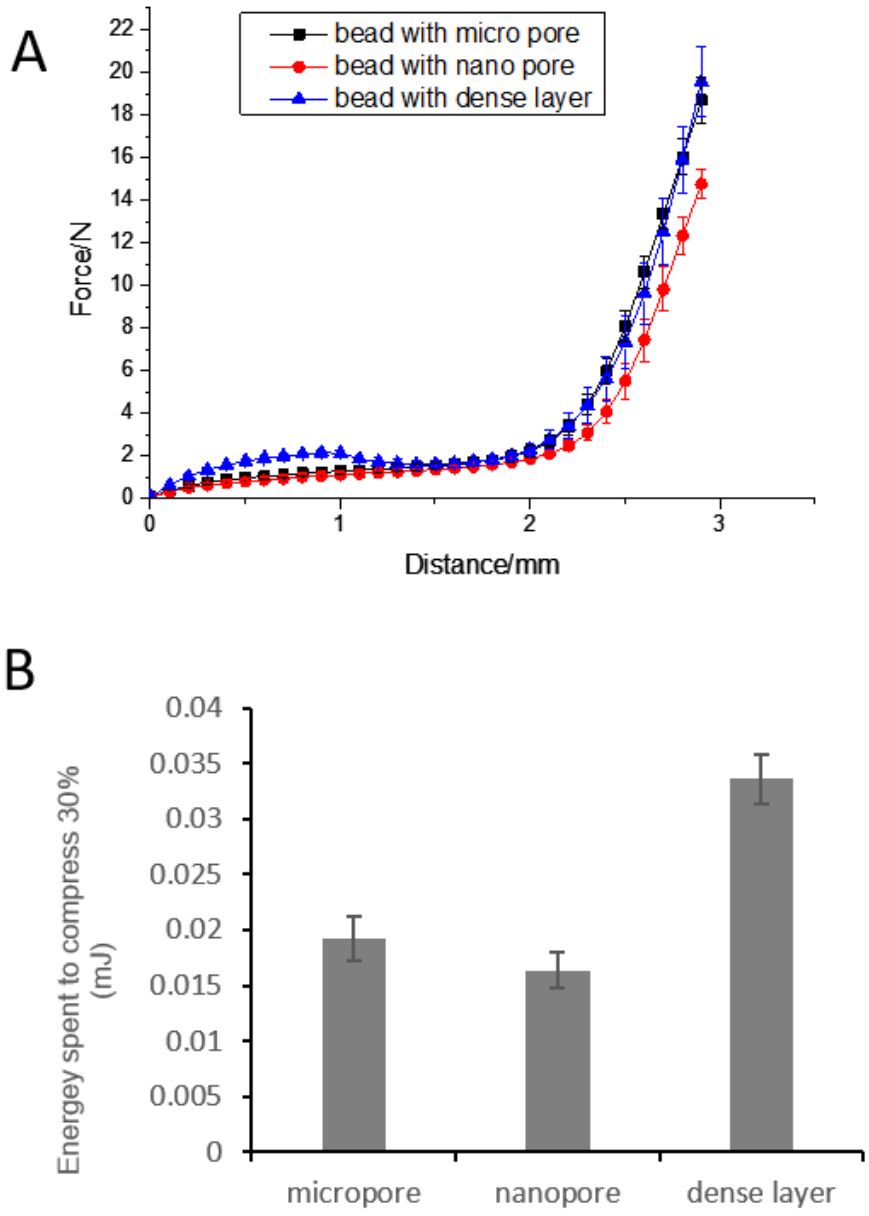

Figure A-7 Mechanical properties of scaffolds with different pore size from compression experiments, (A) force – displacement curve (B) energy spent to compress scaffold to 30% strain

Calculation of proper loading cell number in mini-capsule

As the mini-capsule has a diameter of 3 mm, it raised concerns of the insufficient oxygen supply for cells seeded inside. It is known that the oxygen supply is related to rate

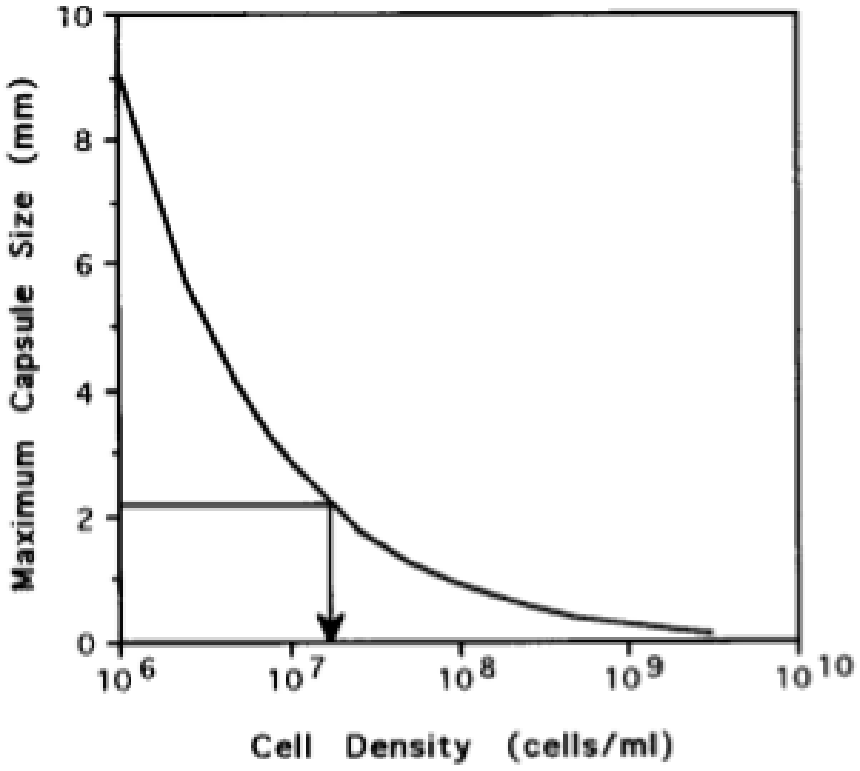

Figure A-8 The relation between diameter of spherical scaffold and seeding cell density (Kim, SK., Yu, SH., Son, JH. et al. Biotechnology Letters (1998) 20: 549.)

of oxygen consumption, which is proportional to number of cells (**Figure A-5)**. Therefore, the maximum cell number was calculated in our capsule in order to avoid hypoxia. The equation is listed below:

$\phi = (r_s \times r_c^2) / (9D_s \times S_o)$

ϕ: Thiele modulus, the ratio of the rate of oxygen consumption and the rate of oxygen diffusion, (0.3 is considered well supplied of oxygen and is adopted in this calculation)

r_s: the rate of oxygen consumption of cells = **cell density** x oxygen consumption of single cell (here 98 fmol/cell/h is adopted as median number being reported for MSC oxygen consumption [1])

r_c: radius of scaffold, which is 1.5 mm

D_s: diffusion coefficient of oxygen, as the pores are too big to affect free diffusion of oxygen, the coefficient remains the same as oxygen diffusion in water which is 2.5 x 10^{-5} cm^2/s

S_o: the solubility of oxygen in water, which is 7 mg/L at room temperature

Therefore, with all given parameters, the proper cell density is this system is 2.42 x 10^7 cells/mL. Given the volume of the scaffold is 14 mm^3, the total cell number should be about 3 x 10^5. This cell number is further applied in following *in vitro* and *in vivo* studies.

The limitation of this calculation is obvious. This calculation is based on assumptions that cells are well – distributed, therefore it is just a rough estimation. Still, it is enough to point out the order of magnitude for appropriate cell number.

References

[1] Pattappa G, Heywood HK, De Bruijn JD, Lee DA. The metabolism of human mesenchymal stem cells during proliferation and differentiation. Journal of cellular physiology. 2011;226(10):2562-70

REFERENCES

[1] J.A. Hubbell. Biomaterials in tissue engineering. Nature Biotechnology, 1995, 13(6): 565-576.

[2] Q.P. Pham, U. Sharma, A.G. Mikos. Electrospinning of polymeric nanofibers for tissue engineering applications: a review. Tissue Engineering, 2006, 12(5) :1197-1211.

[3] S. Van Vlierberghe, P. Dubruel, E. Schacht. Biopolymer-based hydrogels as scaffolds for tissue engineering applications: a review. Biomacromolecules, 2011,12(5): 1387-1408.

[4] A.F. Godier-Furnémont, T.P. Martens, M.S. Koeckert, L. Wan, J. Parks, K. Arai, G. Zhang, B. Hudson, S. Homma, G. Vunjak-Novakovic. Composite scaffold provides a cell delivery platform for cardiovascular repair. Proceedings of the National Academy of Sciences, 2011:108(19): 7974-7979.

[5] M.J. Caicco, T. Zahir, A.J. Mothe, B.G. Ballios, A.J. Kihm, C.H. Tator, M.S. Shoichet. Characterization of hyaluronan–methylcellulose hydrogels for cell delivery to the injured spinal cord. Journal of Biomedical Materials Research, 2013, 101(5): 1472-1477.

[6] S. Yang, K.-F. Leong, Z. Du, C.-K. Chua. The design of scaffolds for use in tissue engineering. Tissue Engineering, 2001,7(6): 679-689.

[7] Bhardwaj.N, Kundu, S. C. Electrospinning: A fascinating fiber fabrication technique. Biotechnology Advances, 2010, 325-347.

[8] kada.Y, Tsuji, H. Biodegradable polyesters for medical and ecological applications. Macromolecular Rapid Communications, 2000, 117-132.

[9] Annabi, N, Tamayol, A, Uquillas, J. A, Akbari, M, Bertassoni, L. E, Cha, C,Camci-Unal, G, Dokmeci, M. R, Peppas, N. A, Khademhosseini. A. 25th anniversary article: rational design and applications of hydrogels in regenerative medicine. Advanced Materials, 2014, 85-124.

[10] Khademhosseini, A, Langer, R. Microengineered hydrogels for tissue engineering. Biomaterials, 2007, 5087-5092.

[11] S.V. Murphy. A. Atala. 3D bioprinting of tissues and organs. Nature Biotechnology, 2014, 32(8): 773-785.

[12] X. Yin, B.E. Mead, H. Safaee, R. Langer, J.M. Karp, O. Levy. Engineering stem cell organoids. Cell Stem Cell, 2016, 18(1): 25-38.

[13] K. Matsubayashi, P.W. Fedak, D.A. Mickle, R.D. Weisel, T. Ozawa, R.-K. Li. Improved left ventricular aneurysm repair with bioengineered vascular smooth muscle grafts. Circulation,2003,108(10 suppl 1): II-219-II-225.

[14] J.S. Park, J.S. Chu, A.D. Tsou, R. Diop, Z. Tang, A. Wang, S. Li. The effect of matrix stiffness on the differentiation of mesenchymal stem cells in response to TGF-β.Biomaterials, 2011, 32(16) :3921-3930.

[15] K. Wang, W.-D. Hou, X. Wang, C. Han, I. Vuletic, N. Su, W.-X. Zhang, Q.-S. Ren, L. Chen,Y.Luo. Overcoming foreign-body reaction through nanotopography: Biocompatibility and immunoisolation properties of a nanofibrous membrane. Biomaterials, 2016, 249-258.

[16] S.-J. Liu, Y.-C. Kau, C.-Y. Chou, J.-K. Chen, R.-C. Wu, W.-L. Yeh. Electrospun PLGA/collagen nanofibrous membrane as early-stage wound dressing. Journal of Membrane Science,2010 ,355(1) :53-59.

[17] Z. Chen, P. Wang, B. Wei, X. Mo, F. Cui. Electrospun collagen–chitosan nanofiber: A biomimetic extracellular matrix for endothelial cell and smooth muscle cell.Acta Biomaterialia, 2010 ,6(2): 372-382.

[18] N. Bhardwaj, S.C. Kundu. Electrospinning: a fascinating fiber fabrication technique. Biotechnology Advances, 2010, 28(3): 325-347.

[19] R.O. Hynes. The extracellular matrix: not just pretty fibrils.Science,2009, 326(5957): 1216-1219.

[20] R. Flemming, C.J. Murphy, G. Abrams, S. Goodman, P. Nealey. Effects of synthetic micro-and nano-structured surfaces on cell behavior. Biomaterials, 1999, 20(6) : 573-588.

[21] T.G. Kim, T.G. Park. Biomimicking extracellular matrix: cell adhesive RGD peptide modified electrospun poly (D, L-lactic-co-glycolic acid) nanofiber mesh. Tissue Engineering, 2006, 12(2): 221-233.

[22] H.G.Ş. Ayaz, A. Perets, H. Ayaz, K.D. Gilroy, M. Govindaraj, D. Brookstein, P.I. Lelkes. Textile-templated electrospun anisotropic scaffolds for regenerative cardiac tissue engineering. Biomaterials, 2014, 35(30): 8540-8552.

[23] H. Yoshimoto, Y. Shin, H. Terai, J. Vacanti. A biodegradable nanofiber scaffold by electrospinning and its potential for bone tissue engineering. Biomaterials, 2003, 24(12) :2077-2082.

[24] M. Zhou, W. Qiao, Z. Liu, T. Shang, T. Qiao, C. Mao, C. Liu. Development and in vivo evaluation of small-diameter vascular grafts engineered by outgrowth endothelial cells and electrospun chitosan/poly (ε-caprolactone) nanofibrous scaffolds. Tissue Engineering , 2013, 20(1-2) :79-91.

[25] M. Ochsner, M.R. Dusseiller, H.M. Grandin, S. Luna-Morris, M. Textor, V. Vogel, M.L. Smith. Micro-well arrays for 3D shape control and high resolution analysis of single cells. Lab on a Chip, 2007, 7(8) :1074-1077.

[26] A.P. Napolitano, P. Chai, D.M. Dean, J.R. Morgan. Dynamics of the self-assembly of complex cellular aggregates on micromolded nonadhesive hydrogels. Tissue Engineering, 2007,13(8) :2087-2094.

[27] P.R. Baraniak, T.C. McDevitt. Scaffold-free culture of mesenchymal stem cell spheroids in suspension preserves multilineage potential. Cell and Tissue Research, 2012, 347(3): 701-711.

[28] Robey TE, Saiget MK, Reinecke H, Murry CE. Systems approaches to preventing transplanted cell death in cardiac repair. Journal of Molecular and Cellular Cardiology, 2008, 567-81.

[29] M. Owen. Marrow stromal stem cells. J Cell Sci, 1988, 63-76.

[30] Roche ET, Hastings CL, Lewin SA, Shvartsman DE, Brudno Y, Vasilyev NV, et.al. Comparison of biomaterial delivery vehicles for improving acute retention of stem cells in the infarcted heart. Biomaterials, 2014, 6850-6858.

[31] Orive G, Santos E, Pedraz JL, Hernandez RM. Application of cell encapsulation for controlled delivery of biological therapeutics. Advanced Drug Delivery Reviews, 2014, 67-68:3-14.

[32] O'Cearbhaill, Eoin D, et.al. Mayo Clinic Proceedings. 2014,

[33] X. Wang, C. Liu, S. Li, Y. Xu, P. Chen, Y. Liu, Q. Ding, W. Wahafu, B. Hong, M. Yang. Hypoxia precondition promotes adipose-derived mesenchymal stem cells based repair of diabetic erectile dysfunction via augmenting angiogenesis and neuroprotection. PloS One, 2015, 10(3):e0118951.

[34] L. Wei, J.L. Fraser, Z.-Y. Lu, X. Hu, S.P. Yu. Transplantation of hypoxia preconditioned bone marrow mesenchymal stem cells enhances angiogenesis and neurogenesis after cerebral ischemia in rats. Neurobiology of Disease, 2012, 46(3) :635-645.

[35] D. Mu, X.-L. Zhang, J. Xie, H.-H. Yuan, K. Wang, W. Huang, G.-N. Li, J.-R. Lu, L.-J. Mao, L. Wang. Intracoronary transplantation of mesenchymal stem cells with overexpressed integrin-linked kinase improves cardiac function in porcine myocardial infarction.scientific reports ,2016,6

[36] C.Y. Lo, B.R. Weil, B.A. Palka, A. Momeni, J.M. Canty, S. Neelamegham.Cell surface glycoengineering improves selectin-mediated adhesion of mesenchymal stem cells (MSCs) and cardiosphere-derived cells (CDCs): pilot validation in porcine ischemia-reperfusion model. Biomaterials, 2016, 19-30.

[37] J. Yu, K.T. Du, Q. Fang, Y. Gu, S.S. Mihardja, R.E. Sievers, J.C. Wu, R.J. Lee. The use of human mesenchymal stem cells encapsulated in RGD modified alginate microspheres in the repair of myocardial infarction in the rat. Biomaterials, 2010, 31(27): 7012-7020.

[38] Y. Li, W. Liu, F. Liu, Y. Zeng, S. Zuo, S. Feng, C. Qi, B. Wang, X. Yan, A. Khademhosseini. Primed 3D injectable microniches enabling low-dosage cell therapy for critical limb ischemia. Proceedings of the National Academy of Sciences, 2014,111(37) :13511-13516.

[39] E. Mathieu, G. Lamirault, C. Toquet, P. Lhommet, E. Rederstorff, S. Sourice, K. Biteau, P. Hulin, V. Forest, P. Weiss. Intramyocardial delivery of mesenchymal stem cell-seeded hydrogel preserves cardiac function and attenuates ventricular remodeling after myocardial infarction. PLoS One ,2012, 7(12): e51991.

[40] D. Kai, Q.-L. Wang, H.-J. Wang, M.P. Prabhakaran, Y. Zhang, Y.-Z. Tan, S. Ramakrishna. Stem cell-loaded nanofibrous patch promotes the regeneration of infarcted myocardium with functional improvement in rat model.Acta Biomaterialia ,2014,10(6) :2727-2738.

[41] J.R. Bagó, G.J. Pegna, O. Okolie, M. Mohiti-Asli, E.G. Loboa, S.D. Hingtgen. Electrospun nanofibrous scaffolds increase the efficacy of stem cell-mediated therapy of surgically resected glioblastoma. Biomaterials, 2016, 116-125.

[42] B.-J. Kang, H. Kim, S.K. Lee, J. Kim, Y. Shen, S. Jung, K.-S. Kang, S.G. Im, S.Y. Lee, M. Choi. Umbilical-cord-blood-derived mesenchymal stem cells seeded onto fibronectin-immobilized polycaprolactone nanofiber improve cardiac function. Acta Biomaterialia, 2014,10(7): 3007-3017.

[43] J. Jin, S.I. Jeong, Y.M. Shin, K.S. Lim, Y.M. Lee, H.C. Koh, K.S. Kim . Transplantation of mesenchymal stem cells within a poly (lactide - co - ε - caprolactone) scaffold improves cardiac function in a rat myocardial infarction model.European Journal of Heart Failure, 2009,11(2) :147-153.

[44] R. Gaetani, D.A. Feyen, V. Verhage, R. Slaats, E. Messina, K.L. Christman, A. Giacomello, P.A. Doevendans, J.P. Sluijter, Epicardial application of cardiac progenitor cells in a 3D-printed gelatin/hyaluronic acid patch preserves cardiac function after myocardial infarction. Biomaterials ,2015,339-348.

[45] P. Ayala, J. Caves, E. Dai, L. Siraj, L. Liu, O. Chaudhuri, C.A. Haller, D.J. Mooney, E.L. Chaikof. Engineered composite fascia for stem cell therapy in tissue repair applications, Acta Biomaterialia, 2015, 1-12.

[46] J.R. Bagó, G.J. Pegna, O. Okolie, S.D. Hingtgen. Fibrin matrices enhance the transplant and efficacy of cytotoxic stem cell therapy for post-surgical cancer. Biomaterials, 2016,42-53.

[47] L. Zhang, Z. Cao, T. Bai, L. Carr, J.-R. Ella-Menye, C. Irvin, B.D. Ratner, S. Jiang, Zwitterionic. hydrogels implanted in mice resist the foreign-body reaction. Nature Biotechnology, 2013, 31(6) :553-556.

[48] K. Bjugstad, D. Redmond Jr, K. Lampe, D. Kern, J. Sladek Jr, M. Mahoney. Biocompatibility of PEG-based hydrogels in primate brain. Cell Transplantation, 2008, 17(4) :409-415.

[49] Bhardwaj, N, Kundu, S. C. Electrospinning, A fascinating fiber fabrication technique. Biotechnology Advances, 2010, 325-347.

[50] Ikada, Y, Tsuji, H. Biodegradable polyesters for medical and ecological applications. Macromolecular Rapid Communications, 2000, 117-132.

[51] Annabi, N, Tamayol, A, Uquillas, J. A, Akbari, M, Bertassoni, L. E, Cha, C, Camci-Unal, G, Dokmeci, M. R, Peppas, N. A, Khademhosseini, A. 25th Anniversary Article: Rational Design and Applications of Hydrogels in Regenerative Medicine.Advanced Materials, 2014, 85-124.

[52] Khademhosseini, A, Langer, R. Microengineered hydrogels for tissue engineering. Biomaterials, 2007, 5087-5092.

[53] Wade, R, Burdick, J. A. Advances in nanofibrous scaffolds for biomedical applications: From electrospinning to self-assembly. Nano Today, 2014, 722-742.

[54] Ghobril, C, Grinstaff, M. W. The chemistry and engineering of polymeric hydrogel adhesives for wound closure: a tutorial. Chemical Society Reviews, 2015, 1820-1835.

[55] Place, E. S, George, J. H, Williams, C. K, Stevens, M. M. Complexity in biomaterials for tissue engineering. Chemical Society Reviews, 2009, 1139-1151.

[56] Mahler, A, Reches, M, Rechter, M, Cohen, S, Gazit, E. Rigid. Self-Assembled Hydrogel Composed of a Modified Aromatic Dipeptide. Advanced Materials, 2006, 1365-1370.

[57] Chen, Q, Liang, S, Thouas, G. A. Elastomeric biomaterials for tissue engineering. Progress in Polymer Science, 2013, 584-671.

[58] Hoare, T. R, Kohane, D. S. Hydrogels in drug delivery: Progress and challenges. Polymer 2008, 1993-2007.

[59] Bosworth, L. A, Turner, L. A, Cartmell, S. H. State of the art composites comprising electrospun fibres coupled with hydrogels: a review. Nanomedicine : Nanotechnology, Biology, and Medicine, 2013, 322-335.

[60] Moutos, F. T, Guilak, F. Composite scaffolds for cartilage tissue engineering. Biorheology, 2008, 501-512.

[61] Visser, J, Melchels, F. P, Jeon, J. E, van Bussel, E. M, Kimpton, L. S, Byrne, H. M, Dhert, W. J, Dalton, P. D, Hutmacher, D. W, Malda, J. Reinforcement of hydrogels using three-dimensionally printed microfibres. Nature Communications ,2015, 6933.

[62] Kim, S, Jordan A, Korley J, et al. Drawing in poly (ε-caprolactone) fibers: tuning mechanics, fiber dimensions and surface-modification density. Journal of Materials Chemistry B, 2017,

[63] Aguirre-Chagala E, Altuzar V, León-Sarabia E, et al. Physicochemical properties of polycaprolactone/collagen/elastin nanofibers fabricated by electrospinning. Materials Science and Engineering: C, 2017, 76: 897.

[64] Beachley, V, Wen, X. Polymer nanofibrous structures: Fabrication, biofunctionalization, and cell interactions. Prog Polym Sci ,2010, 868-892.

[65] Rocco, K. A, Maxfield, M. W, Best, C. A, Dean, E. W, Breuer, C. K. In vivo applications of electrospun tissue-engineered vascular grafts: a review. Tissue Engineering, 2014, 628-640.

[66] Szentivanyi, A, Chakradeo, T, Zernetsch, H, Glasmacher, B. Electrospun cellular microenvironments: Understanding controlled release and scaffold structure. Advanced Drug Delivery Reviews, 2011, 209-220.

[67] Shapiro, J. M, Oyen, M. L. Hydrogel composite materials for tissue engineering ,Scaffolds Jom, 2013, 505-516.

[68] McMahon, R. E, Qu, X, Jimenez-Vergara, A. C, Bashur, C. A, Guelcher, S. A, Goldstein, A. S, Hahn, M. S. Hydrogel-electrospun mesh composites for coronary artery bypass grafts. Tissue Engineering, 2011, 451-461.

[69] Feingold-Leitman, D, Zussman, E, Seliktar, D. Evaluation of a composite scaffold made from electrospun nanofibers and a hydrogel for tissue engineering. Journal of Bionanoscience ,2009,45-47.

[70] Jang, J, Lee, J, Seol, Y, Jeong, Y. H, Cho, D. Improving mechanical properties of alginate hydrogel by reinforcement with ethanol treated polycaprolactone nanofibers. Engineering, 2013, 1216-1221.

[71] Eslami, M, Vrana, N. E, Zorlutuna, P, Sant, S, Jung, S, Masoumi, N, Khavari-Nejad, R. A, Javadi, G, Khademhosseini, A. Fiber-reinforced hydrogel scaffolds for heart valve tissue engineering. Journal of Biomaterials Applications, 2014, 399-410.

[72] Freeman, J. W, Woods, M. D, Cromer, D. A, Ekwueme, E. C, Andric, T, Atiemo, E. A, Bijoux, C. H, Laurencin, C. T. Evaluation of a hydrogel-fiber composite for ACL tissue engineering. Journal of Biomechanics, 2011, 694-699.

[73] Cho, K, Lee, H. J, Han, S. W, Min, J. H, Park, H, Koh, W. G. Multi-compartmental hydrogel microparticles fabricated by combination of sequential electrospinning and photopatterning. Angewandte Chemie, 2015, 11511-11515.

[74] An, D, Ji, Y, Chiu, A, Lu, Y. C, Song, W, Zhai, L, Qi, L, Luo, D, Ma, M. Developing robust, hydrogel-based, nanofiber-enabled encapsulation devices (NEEDs) for cell therapies. Biomaterials, 2015, 40-48.

[75] Hong, Y, Huber, A, Takanari, K, Amoroso, N. J, Hashizume, R, Badylak, S. F, Wagner, W. R. Mechanical properties and in vivo behavior of a biodegradable synthetic polymer microfiber-extracellular matrix hydrogel biohybrid scaffold. Biomaterials, 2011,3387-3394.

[76] Ekaputra, A. K, Prestwich, G. D, Cool, S. M, Hutmacher, D. W. Combining Electrospun Scaffolds with Electrosprayed Hydrogels Leads to Three-Dimensional Cellularization of Hybrid Constructs. Biomacromolecules, 2008, 2097-2103.

[77] Thayer, P. S, Dimling, A. F, Plessl, D. S, Hahn, M. R, Guelcher, S. A, Dahlgren, L. A, Goldstein, A. S. Cellularized cylindrical fiber/hydrogel composites for ligament tissue engineering. Biomacromolecules, 2014, 75-83.

[78] Croisier, F, Duwez, A. S, Jerome, C, Leonard, A. F, van der Werf, K. O, Dijkstra, P. J, Bennink, M. L. Mechanical testing of electrospun PCL fibers. Acta Biomaterialia ,2012, 218.

[79] Wang, W, Barber, A. H. Measurement of size-dependent glass transition temperature in electrospun polymer fibers using AFM nanomechanical testing. Journal of Polymer Science Part B: Polymer Physics ,2012, 546-551.

[80] Li, Y, Lokitz, B. S, McCormick, C. L. RAFT Synthesis of a Thermally Responsive ABC Triblock Copolymer Incorporating N-Acryloxysuccinimide for Facile in Situ Formation of Shell Cross-Linked Micelles in Aqueous Media. Macromolecules, 2006, 2726-2728.

[81] Fairbanks, B. D, Gunatillake, P. A, Meagher, L. Biomedical applications of polymers derived by reversible addition - fragmentation chain-transfer (RAFT). Advanced Drug Delivery Reviews ,2015,141-152.

[82] Liu, J, Bulmus, V, Barner-Kowollik, C, Stenzel, M. H, Davis, T. P. Direct synthesis of pyridyl disulfide-terminated polymers by raft polymerization. Macromolecular Rapid Communications ,2007,305-314.

[83] Boyer, C, Bulmus, V, Liu, J, Davis, T. P, Stenzel, M. H, Barner-Kowollik, C. Well-Defined protein−polymer conjugates via in situ raft polymerization. Journal of the American Chemical Society, 2007, 7145-7154.

[84] Boyer, C, Bulmus, V, Davis, T. P, Ladmiral, V, Liu, J, Perrier, S. Bioapplications of RAFT polymerization. Chemical Reviews, 2009, 5402-5436.

[85] Roy, D, Knapp, J. S, Guthrie, J. T, Perrier, S. Antibacterial cellulose fiber via RAFT surface graft polymerization. Biomacromolecules, 2007, 91-99.

[86] Willcock, H, O'Reilly, R. K. End group removal and modification of RAFT polymers. Polym. Chem, 2010, 149-157.

[87] Phelps EA, Garcia AJ. Engineering more than a cell: vascularization strategies in tissue engineering. Current Opinion in Biotechnology, 2010, 704-709.

[88] Schaper W. Collateral circulation: past and present. Basic Research in Cardiology,2009, 5-21.

[89] Potente M, Gerhardt H, Carmeliet P. Basic and therapeutic aspects of angiogenesis. Cell,2011,873-87.

[90] Carmeliet P, Jain RK. Molecular mechanisms and clinical applications of angiogenesis. Nature, 2011,298-307.

[91] Novosel EC, Kleinhans C, Kluger PJ. Vascularization is the key challenge in tissue engineering. Advanced Drug Delivery Reviews, 2011, 300-11.

[92] Briquez PS, Clegg LE, Martino MM, Gabhann FM, Hubbell JA. Design principles for therapeutic angiogenic materials. Nature Reviews Materials, 2016, 1:15006.

[93] Liew A, O'Brien T. Therapeutic potential for mesenchymal stem cell transplantation in critical limb ischemia. Stem Cell Research & Therapy, 2012, 3:28.

[94] Russo V, Young S, Hamilton A, Amsden BG, Flynn LE. Mesenchymal stem cell delivery strategies to promote cardiac regeneration following ischemic injury. Biomaterials, 2014,3956-3974.

[95] Karp JM, Leng Teo GS. Mesenchymal stem cell homing: the devil is in the details. Cell Stem Cell, 2009, 206-216.

[96] Kean TJ, Lin P, Caplan AI, Dennis JE. MSCs: Delivery routes and engraftment, cell-targeting strategies, and immune modulation. Stem Cells International, 2013,732742.

[97] O'Cearbhaill ED, Ng KS, Karp JM. Emerging medical devices for minimally invasive cell therapy. Mayo Clinic Proceedings, 2014,259-273.

[98] Feyen DA, Gaetani R, Doevendans PA, Sluijter JP. Stem cell-based therapy: Improving myocardial cell delivery. Advanced Drug Delivery Reviews, 2016.

[99] Wei L, Fraser JL, Lu ZY, Hu X, Yu SP. Transplantation of hypoxia preconditioned bone marrow mesenchymal stem cells enhances angiogenesis and neurogenesis after cerebral ischemia in rats. Neurobiology of Disease, 2012,4635-4645.

[100] Wang X, Liu C, Li S, Xu Y, Chen P, Liu Y et.al. Hypoxia precondition promotes adipose-derived mesenchymal stem cells based repair of diabetic erectile dysfunction via augmenting angiogenesis and neuroprotection. Plos One, 2015, e0118951.

[101] Kuster GM, Liao R. Fortune Favors the Prepared: Safety and Efficacy of Allogeneic Hypoxia Preconditioned Mesenchymal Stromal Cells in Primates. Circulation Research. 2016, 908-910.

[102] Mu D, Zhang XL, Xie J, Yuan HH, Wang K, Huang W, et al. Intracoronary Transplantation of Mesenchymal Stem Cells with Overexpressed Integrin-Linked Kinase Improves Cardiac Function in Porcine Myocardial Infarction. Scientific Reports, 2016, 19155.

[103] Wang WW, Li ZZ, Wang W, Jiang Y, Cheng J, Lu S, et al. Enhanced renoprotective effect of HIF-1alpha modified human adipose-derived stem cells on cisplatin-induced acute kidney injury in vivo. Scientific Reports, 2015, 10851.

[104] Locatelli P, Olea FD, Hnatiuk A, De Lorenzi A, Cerda M, Gimenez CS, et al. Mesenchymal stromal cells overexpressing vascular endothelial growth factor in ovine myocardial infarction. Gene Therapy, 2015, 449-457.

[105] Ding Y, Zhang RY, He B, Liu Z, Zhang K, Ruan JW, et al. Combination of electroacupuncture and grafted mesenchymal stem cells overexpressing TrkC improves remyelination and function in demyelinated spinal cord of rats. Scientific Reports, 2015,9133.

[106] Zhao L, Liu X, Zhang Y, Liang X, Ding Y, Xu Y, et al. Enhanced cell survival and paracrine effects of mesenchymal stem cells overexpressing hepatocyte growth factor promote cardioprotection in myocardial infarction. Experimental Cell Research,2016,

[107] Lo CY, Weil BR, Palka BA, Momeni A, Canty JM, Jr., Neelamegham S. Cell surface glycoengineering improves selectin-mediated adhesion of mesenchymal stem cells (MSCs) and cardiosphere-derived cells (CDCs): Pilot validation in porcine ischemia-reperfusion model. Biomaterials, 2016,19-30.

[108] Uchida S, Itaka K, Nomoto T, Endo T, Matsumoto Y, Ishii T, et al. An injectable spheroid system with genetic modification for cell transplantation therapy. Biomaterials. 2014,2499-2506.

[109] Laschke MW, Schank TE, Scheuer C, Kleer S, Schuler S, Metzger W, et al. Three-dimensional spheroids of adipose-derived mesenchymal stem cells are potent initiators of blood vessel formation in porous polyurethane scaffolds. Acta Biomaterialia. 2013,6876-6884.

[110] Wang K, Yu L-Y, Jiang L-Y, Wang H-B, Wang C-Y, Luo Y. The paracrine effects of adipose-derived stem cells on neovascularization and biocompatibility of a macroencapsulation device. Acta Biomaterialia, 2015,65-76.

[111] Sart S, Tsai AC, Li Y, Ma T. Three-dimensional aggregates of mesenchymal stem cells: cellular mechanisms, biological properties, and applications. Tissue Engineering Part B, Reviews, 2014,365-380.

[112] Chen S, Shi J, Zhang M, Chen Y, Wang X, Zhang L, et al. Mesenchymal stem cell-laden anti-inflammatory hydrogel enhances diabetic wound healing. Scientific Reports. 2015, 5:18104.

[113] Blocki A, Beyer S, Dewavrin JY, Goralczyk A, Wang Y, Peh P, et al. Microcapsules engineered to support mesenchymal stem cell (MSC) survival and proliferation enable long-term retention of MSCs in infarcted myocardium. Biomaterials,2015,12-24.

[114] Robinson ST, Douglas AM, Chadid T, Kuo K, Rajabalan A, Li H, et al. A novel platelet lysate hydrogel for endothelial cell and mesenchymal stem cell-directed neovascularization, Acta Biomaterialia, 2016,86-98.

[115] Yao X, Liu Y, Gao J, Yang L, Mao D, Stefanitsch C, et al. Nitric oxide releasing hydrogel enhances the therapeutic efficacy of mesenchymal stem cells for myocardial infarction. Biomaterials. 2015,130-140.

[116] Parisi-Amon A, Mulyasasmita W, Chung C, Heilshorn SC. Protein-engineered injectable hydrogel to improve retention of transplanted adipose-derived stem cells. Advanced Healthcare Materials, 2013,428-432.

[117] Yeom J, Kim SJ, Jung H, Namkoong H, Yang J, Hwang BW, et al. Supramolecular hydrogels for long-term bioengineered stem cell therapy. Advanced Healthcare Materials, 2015, 237-244.

[118] Levit RD, Landazuri N, Phelps EA, Brown ME, Garcia AJ, Davis ME, et al. Cellular encapsulation enhances cardiac repair. Journal of the American Heart Association.2013, e000367.

[119] Bago JR, Pegna GJ, Okolie O, Mohiti-Asli M, Loboa EG, Hingtgen SD. Electrospun nanofibrous scaffolds increase the efficacy of stem cell-mediated therapy of surgically resected glioblastoma, Biomaterials, 2016,116-125.

[120] [34] Kang BJ, Kim H, Lee SK, Kim J, Shen Y, Jung S, et al. Umbilical-cord-blood-derived mesenchymal stem cells seeded onto fibronectin-immobilized polycaprolactone nanofiber improve cardiac function. Acta Biomaterialia, 2014,3007-3017.

[121] Jin J, Jeong SI, Shin YM, Lim KS, Shin H, Lee YM, et al. Transplantation of mesenchymal stem cells within a poly(lactide-co-epsilon-caprolactone) scaffold improves cardiac function in a rat myocardial infarction model. European Journal of Heart Failure. 2009,147-153.

[122] Gaetani R, Feyen DA, Verhage V, Slaats R, Messina E, Christman KL, et al. Epicardial application of cardiac progenitor cells in a 3D-printed gelatin/hyaluronic acid patch preserves cardiac function after myocardial infarction. Biomaterials. 2015,339-348.

[123] Ayala P, Caves J, Dai E, Siraj L, Liu L, Chaudhuri O, et al. Engineered composite fascia for stem cell therapy in tissue repair applications. Acta Biomaterialia. 2015, 1-12.

[124] Bago JR, Pegna GJ, Okolie O, Hingtgen SD. Fibrin matrices enhance the transplant and efficacy of cytotoxic stem cell therapy for post-surgical cancer. Biomaterials, 2016, 42-53.

[125] Roche ET, Hastings CL, Lewin SA, Shvartsman DE, Brudno Y, Vasilyev NV, et al. Comparison of biomaterial delivery vehicles for improving acute retention of stem cells in the infarcted heart. Biomaterials, 2014, 6850-6858.

[126] Wang K, Hou W-D, Wang X, Han C, Vuletic I, Su N, et al. Overcoming foreign-body reaction through nanotopography: Biocompatibility and immunoisolation properties of a nanofibrous membrane. Biomaterials,2016, 249-258.

[127] Ko SH, Bandyk DF. Therapeutic angiogenesis for critical limb ischemia. Seminars in Vascular Surgery, 2014, 23-31.

[128] Asahara T, Kawamoto A, Masuda H. Concise review: Circulating endothelial progenitor cells for vascular medicine. Stem Cells,1650-1655.

[129] Raval Z, Losordo DW. Cell therapy of peripheral arterial disease: from experimental findings to clinical trials. Circulation Research, 2013,1288-1302.

[130] Cooke JP, Losordo DW. Modulating the vascular response to limb ischemia: angiogenic and cell therapies. Circulation Research, 2015,1561-1578.

[131] Asahara T, Murohara T, Sullivan A, Silver M, van der Zee R, Li T, et al. Isolation of Putative Progenitor Endothelial Cells for Angiogenesis. Science. 1997,964-966.

[132] Yeh ET, Zhang S, Wu HD, Korbling M, Willerson JT, Estrov Z. Transdifferentiation of human peripheral blood CD34+-enriched cell population into cardiomyocytes, endothelial cells, and smooth muscle cells in vivo. Circulation, 2003,2070-2073.

[133] Ziegelhoeffer T, Fernandez B, Kostin S, Heil M, Voswinckel R, Helisch A, et al. Bone marrow-derived cells do not incorporate into the adult growing vasculature. Circulation Research. 2004,230-238.

[134] Zentilin L, Tafuro S, Zacchigna S, Arsic N, Pattarini L, Sinigaglia M, et al. Bone marrow mononuclear cells are recruited to the sites of VEGF-induced neovascularization but are not incorporated into the newly formed vessels. Blood, 2006,3546-3554.

[135] Sil AK, Maeda S, Sano Y, Roop DR, Karin M. IkappaB kinase-alpha acts in the epidermis to control skeletal and craniofacial morphogenesis. Nature, 2004,660-664.

[136] Mirotsou M, Jayawardena TM, Schmeckpeper J, Gnecchi M, Dzau VJ. Paracrine mechanisms of stem cell reparative and regenerative actions in the heart. Journal of Molecular and Cellular Cardiology. 2011, 280-289.

[137] J. Huang, Z. Zhang, J. Guo, A. Ni, A. Deb, L. Zhang, M. Mirotsou, R.E. Pratt, V.J. Dzau, Genetic modification of mesenchymal stem cells overexpressing CCR1 increases cell viability, migration, engraftment, and capillary density in the injured myocardium, Circulation Research, 2010, 106(11):1753-1762.

[138] P. Menasché, Stem cell therapy for heart failure. Circulation ,2009,119(20) :2735-2740.

[139] J. Ankrum, J.M. Karp, Mesenchymal stem cell therapy: two steps forward, one step back, Trends in Molecular Medicine , 2010, 16(5) :203-209.

[140] J. Terrovitis, R. Lautamäki, M. Bonios, J. Fox, J.M. Engles, J. Yu, M.K. Leppo, M.G. Pomper, R.L. Wahl, J. Seidel.Noninvasive quantification and optimization of acute cell retention by in vivo positron emission tomography after intramyocardial cardiac-derived stem cell delivery. Journal of the American College of Cardiology,2009,54(17):1619-1626.

[141] N.K. Satija, V.K. Singh, Y.K. Verma, P. Gupta, S. Sharma, F. Afrin, M. Sharma, P. Sharma, R. Tripathi, G. Gurudutta, Mesenchymal stem cell‐based therapy: a new paradigm in regenerative medicine. Journal of Cellular and Molecular Medicine, 2009, 13(11‐12):4385-4402.

[142] A.F. Godier-Furnémont, T.P. Martens, M.S. Koeckert, L. Wan, J. Parks, K. Arai, G. Zhang, B. Hudson, S. Homma, G. Vunjak-Novakovic, Composite scaffold provides a cell delivery platform for cardiovascular repair.Proceedings of the National Academy of Sciences ,2011,108(19) :7974-7979.

[143] T. Garg, O. Singh, S. Arora, R. Murthy, Scaffold: a novel carrier for cell and drug delivery, Critical Reviews™ in Therapeutic Drug Carrier Systems 2012:29(1)

[144] C. Le Visage, O. Gournay, N. Benguirat, S. Hamidi, L. Chaussumier, N. Mougenot, J.A. Flanders, R. Isnard, J.-B. Michel, S. Hatem. Mesenchymal stem cell delivery into rat infarcted myocardium using a porous polysaccharide-based scaffold: a quantitative comparison with endocardial injection. Tissue Engineering, 2011, 18(1-2):35-44.

[145] X. Zhao, J. Kim, C.A. Cezar, N. Huebsch, K. Lee, K. Bouhadir, D.J. Mooney. Active scaffolds for on-demand drug and cell delivery, Proceedings of the National Academy of Sciences,2011, 108(1):67-72.

[146] R.M. Hernández, G. Orive, A. Murua, J.L. Pedraz, Microcapsules and microcarriers for in situ cell delivery. Advanced Drug Delivery Reviews, 2010,62(7) :711-730.

[147] E. Avolio, V.V. Alvino, M.T. Ghorbel, P. Campagnolo, Perivascular cells and tissue engineering: Current applications and untapped potential, Pharmacology& Therapeutics,2017, 83-92.

[148] M.M. Lalu, L. McIntyre, C. Pugliese, D. Fergusson, B.W. Winston, J.C. Marshall, J. Granton, D.J. Stewart, Safe ty of Cell Therapy with Mesenchymal Stromal Cells (SafeCell): A Systematic Review and Meta-Analysis of Clinical Trials, Plos One, 2012, 7(10):e47559.

[149] C.M. Murphy, M.G. Haugh, F.J. O'Brien, The effect of mean pore size on cell attachment, proliferation and migration in collagen–glycosaminoglycan scaffolds for bone tissue engineering. Biomaterials, 2010,31(3):461-466.

[150] M.P. Prabhakaran, J.R. Venugopal, S. Ramakrishna, Mesenchymal stem cell differentiation to neuronal cells on electrospun nanofibrous substrates for nerve tissue engineering. Biomaterials , 2009, 30(28):4996-5003.

[151] H. Bramfeld, G. Sabra, V. Centis, P. Vermette. Scaffold vascularization: a challenge for three-dimensional tissue engineering, Current Medicinal Chemistry 2010,17(33):3944-3967.

[152] L.M. Weber, C.G. Lopez, K.S. Anseth, Effects of PEG hydrogel crosslinking density on protein diffusion and encapsulated islet survival and function. Journal of Biomedical Materials Research Part A, 2009, 90(3):720-729.

[153] J.M. Sobral, S.G. Caridade, R.A. Sousa, J.F. Mano, R.L. Reis, Three-dimensional plotted scaffolds with controlled pore size gradients: effect of scaffold geometry on mechanical performance and cell seeding efficiency. Acta Biomaterialia, 2011,7(3):1009-1018.

[154] S.-M. Lien, L.-Y. Ko, T.-J. Huang. Effect of pore size on ECM secretion and cell growth in gelatin scaffold for articular cartilage tissue engineering. Acta Biomaterialia 2009,5(2): 670-679.

[155] C.M. Murphy, F.J. O'Brien. Understanding the effect of mean pore size on cell activity in collagen-glycosaminoglycan scaffolds. Cell Adhesion & Migration, 2010,4(3) :377-381.

[156] F.J. O'Brien, B. Harley, I.V. Yannas, L.J. Gibson, The effect of pore size on cell adhesion in collagen-GAG scaffolds, Biomaterials, 2005,26(4) :433-441.

[157] J.J. Lee, S.-G. Lee, J.C. Park, Y.I. Yang, J.K. Kim, Investigation on biodegradable PLGA scaffold with various pore size structure for skin tissue engineering, Current Applied Physics 7 ,2007, e37-e40.

[158] P. de Vos, M.M. Faas, B. Strand, R. Calafiore. Alginate-based microcapsules for immunoisolation of pancreatic islets. Biomaterials ,2006,27(32):5603-5617.

[159] W. Dai, S.L. Hale, B.J. Martin, J.-Q. Kuang, J.S. Dow, L.E. Wold, R.A. Kloner, Allogeneic mesenchymal stem cell transplantation in postinfarcted rat myocardium, Circulation 2005,112(2):214-223.

[160] M.C. Collins, J.L. Moore Jr, B.J. Burrows, A.P. Kypson, B.J. Muller-Borer. Early cell loss associated with mesenchymal stem cell cardiomyoplasty, Open Tissue Eng Regen Med J 5 ,2012,17-24.

[161] L. Bian, D.Y. Zhai, E. Tous, R. Rai, R.L. Mauck, J.A. Burdick, Enhanced MSC chondrogenesis following delivery of TGF-β3 from alginate microspheres within hyaluronic acid hydrogels in vitro and in vivo. Biomaterials ,2011,32(27):6425-6434.

[162] E. Trouche, S. Girod Fullana, C. Mias, C. Ceccaldi, F. Tortosa, M.-H. Seguelas, D. Calise, A. Parini, D. Cussac, B. Sallerin, Evaluation of alginate microspheres for mesenchymal stem cell engraftment on solid organ. Cell Transplantation, 2010, 19(12) :1623-1633.

[163] A. Paul, D. Shum-Tim, S. Prakash, Investigation on PEG integrated alginate–chitosan microcapsules for myocardial therapy using marrow stem cells genetically modified by recombinant baculovirus. Cardiovascular Engineering and Technology,2010,1(2):154-164.

[164] A. Batorsky, J. Liao, A.W. Lund, G.E. Plopper, J.P. Stegemann, Encapsulation of adult human mesenchymal stem cells within collagen ‐ agarose microenvironments, Biotechnology and Bioengineering, 2005,92(4):492-500.

VITA

Wang Jinyang

Jinyang Wang was born in Beijing, China, and moved to Shanghai in 2000. He received a B.A. in Chemistry from Fudan University. In 2011, he started pursuing a doctorate in Biomedical Engineering (Georgia Tech/Emory/Peking University joint Ph.D. program). He spent one year on Emory campus to conduct research in a collaborative lab in 2014. Outside the lab he likes traveling, sports and playing guitar.